PALEOMAGNETISM AND TECTONICS OF MANDA HARARO RIFT OF NORTH AFAR, ETHIOPIA

By:

AMEHA ATNAFU MULUNEH

A Thesis submitted to School of Graduate studies of Addis Ababa University in partial fulfillment for the requirements of the Degree of Master of Science in Earth Sciences (Structural Geology and Tectonics).

January, 2010G.C

ADDIS ABABA UNIVERSITY

SCHOOL OF GRADUATE STUDIES

PALEOMAGNETISM AND TECTONICS OF MANDA HARARO RIFT OF NORTH AFAR, ETHIOPIA

BY:

AMEHA ATNAFU MULUNEH

DEPARTMENT OF EARTH SCIENCES

APPROVED BY:

Dr. Balemwal Atnafu ……

Chairperson

Dr. Tesfaye Kidane……

Advisor

Dr. Bekele Abebe……

Examiner

Dr. Girma W/Tinsae……

Examiner

Geological map of Manda Hararo rift

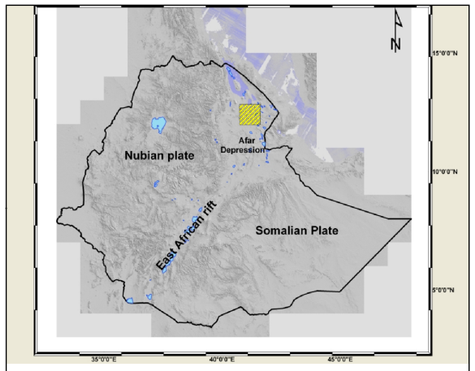

Location of the Study area (Shaded region)

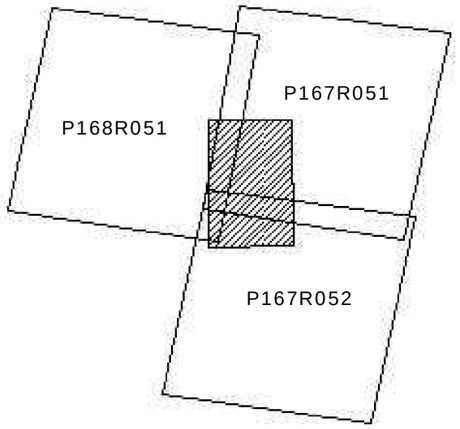

Landsat Scene index

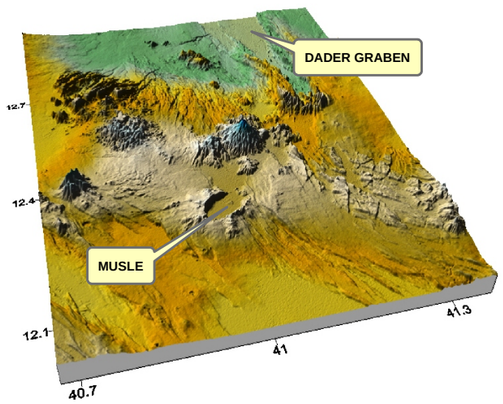

Physiography of study area

Coordinate system
Black number: Latitude and Longitude
Blue number: UTM-Zone 37-Northern Hemisphere- WGS 84

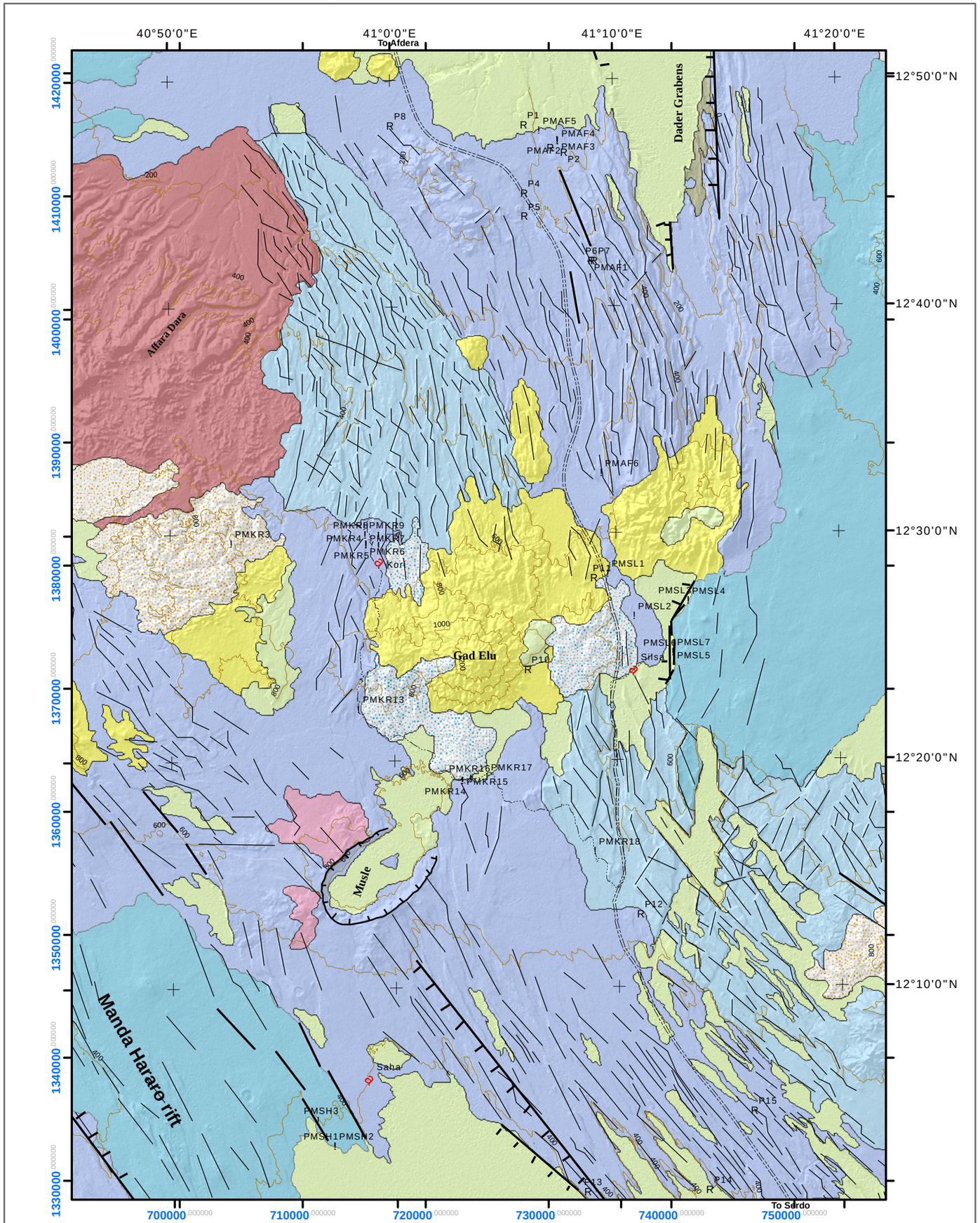

Legend

- Silts, Clay and Sand (Mud Flats)
- Evaporites
- Continental Conglomerate
- Plagioclase, Phyric Basalt (0.1Ma)
- Recent Basalt (0.6-1.0Ma)
- Upper stratoid basalt (1-2Ma)
- Lithic Tuff
- Lavas of intermediate composition
- Silicic Massifs, mostly of Rhyolitic composition
- Alkaline and peralkaline Granite (26-22Ma)

Symbols

- ! Paleomagnetic sampling sites
- R Available age data
- Major Faults
- Minor faults
- Topographic contours (m)
- Villages
- Asphalt road (under construction)
- Dry weather road
- Caldera

®

Scale

1:350,000

0 7.5 15 22.5 km

Data Sources and referances
1. CNR-CNRS (Afar team), 1973
2. J. Varet. 1975
3. Kidane et al., 2003
4. P. Lahitte et al., 2003
5. Present study; widely spaced traverses and image interpretation

Table of Contents

List of Appendices iii

List of figures iv

List of Tables v

List of Symbols and abbreviations v

Abstract vi

Chapter 1 1

1.1 Introduction 1

1.2 Objective of the study 2

1.3 Location, Physiography and environment of the study area 4

1.4 Overview of the study 4

Chapter 2 6

2.1 Magmatism in Afar 6

2.2 Major Tectonic elements of the Afar Depression 8

Chapter 3 11

3.1 Geology of the Afar Depression 11

3.1.1 Neoproterozoic Basement, Mesozoic sedimentary rocks and Eocene-Miocene basalts 11

3.1.2 Miocene igneous rocks 13

3.1.3 Pliocene-Pleistocene volcanic rocks 14

3.1.4 Quaternary volcanic and sedimentary formations 14

3.2 Evolution of the Afar Depression 16

3.3 Rifting models for the evolution of Afar Depression 17

Chapter 4 21

Structure of Red Sea Rift 21

Chapter 5 27

Paleomagnetism-application to tectonics 27

5.1 Overview 27

5.1.1 The earth's magnetic field 27

5.1.2 Magnetism in Rocks 27

5.1.3 Paleomagnetic sampling and Analysis 29

5.2. Methodology and approach of the study 32

5.2.1 Pre-field work 32

5.2.2 Field work 33

5.2.3 Laboratory analysis 33

5.3 Sampling 36

5.4 Laboratory treatment 38

5.5 Data Analysis 42

5.6. Paleomagnetic Direction 46

5.7. Tectonic rotation 50

5.8. Paleosecular variation (PSV) and Virtual Geomagnetic Polarity (VGP) 52

5.9 Discussion 55

5.10. Conclusion 57

5.11. Recommendation 58

References 59

List of Appendices

Detail geological map of the Manda Hararo rift 68

Data arranged for Paleomac software package 69

List of figures

1.1. Topographic **classification of Afar depression**.....**3**

1.2. Tectonic frame work of rift propagation and overlap.....**5**

3.1. Simplified geological map of Afar.....**12**

3.2. Sedimentary deposits and high angle normal faults in Saha.....**15**

4.1. Evolutionary model of Manda Hararo rift.....**22**

4.2. Landsat ETM+ mosaic of Manda Hararo rift.....**23**

4.3. Topographic profile across Tendaho graben.....**24**

4.4. Physiographic setting of Manda Hararo rift and Tendaho graben.....**26**

5.1. Generalized paleomagnetic sampling scheme.....**30**

5.2. Laboratory facility in Earth sciences department of AAU.....**34**

5.3. Normal faults and flow sequences in Saha area.....**36**

5.4. Available age data in the study area.....**38**

5.5. Landsat ETM+ mosaic of sampling sites.....**40**

5.6. Representative intensity curve of samples.....**41**

5.7. Histogram of NRM **41**

5.8. Vector component diagram with intensity decay curve.....**44**

5.9. Paleomagnetic polarity of samples plotted with GPTS.....**45**

5.10. Stereographic projection of all sites.....**47**

5.11. Paleomagnetic polarity of 3 flows from Afdera site.....**49**

5.12. Site mean paleomagnetic polarity of all sites.....**51**

5.13. Stereographic projections from Kori and Saha.....**52**

5.14. Stereogram of mean ChRM from kori and saha.....**53**

5.15. Stereographic projection showing VGP scatter.....**55**

5.16. Rift propagation and overlap of Erta'ale-Manda Hararo and Erta'ale-Dader trends..56

List of Tables

1. **Corrected data for sun angle.....32**
2. **Summary of sampling sites and paleomagnetic results.....48**
3. **Site mean Virtual paleomagnetic poles (VGP) for all analyzed sites.....54**

List of Symbols and abbreviations

AF= Alternating Field

APWP= Apparent Polar Wander Path

ChRM= Characteristics Remnant Magnetization

ETM+= Enhanced Thematic Mapper

GAD= Geocentric Axial Dipole

GPTS= Geomagnetic Polarity Time Scale

MDF= Median Destructive Curve

mT= mili Tesla

NRM= Natural Remnant Magnetization

PCA= Principal Component Analysis

Abstract

This study explains tectonics and Paleomagnetism of Manda Hararo rift in north afar. The field trip which was organized by scientists from New Zealand, Ethiopia and UK was made to study the Dabbahu magmatic segment in northern part of Manda Hararo rift. A total of 271 oriented core samples were collected for paleomagnetic study from 34 sites within Manda Hararo rift. Available age data of Basalts from the sampled localities show that the age ranges between 0.09Ma to 1.11Ma. 175 specimens were subjected to progressive Alternating Field (AF) demagnetization after routine sample preparation in the laboratory. Almost all specimens show fairly simple demagnetization behavior. AF between 0 to 30mT often isolates the first component. Median Destructive Field for most specimens ranges between 20 and 35mT, suggesting that Pseudo single domain grains as remnant magnetization carriers. Among 34 sites, 30 sites show normal polarities and four sites show reversed polarities. The normal and reversed polarities are 180^0 apart, showing that the ChRM are free of secondary NRM components. Magnetic polarities were found to be coincident with Geomagnetic Polarity Time Scale (GPTS) of Cande and Kent (1995). Geomagnetic Polarity Time Scale of Langeries et al., (1997), Lund et al., (1998) and Nowaczyk & Frederichs (1999) were used to explain and determine age of the reversed polarity site PMAF04 from Afdera. The overall mean direction for 33 sites is $D=357.1^0$, $I=10.6^0$ ($k=32.6$ and $\alpha_{95}=4.4^0$). Comparison of observed mean direction with predicted direction of Kidane *et al*., 2003 for stable Africa for ~2Ma ($\mathbf{D}=359.7^0$, $\mathbf{I}=16.4^0$, $\boldsymbol{\alpha_{95}}=5.7^0$), indicates no statistically significant vertical axis rotation has occurred in Manda Hararo rift. Comparison of mean direction from Kori and Saha with the predicted direction of Kidane *et al*., 2003 indicates that significant amount of counter clock wise rotation ($\sim 5.9^0 \pm 8.6^0$) has occurred. Further comparison of mean values from the two sites with the Apparent Polar Wander Path curve of Besse and Courtillot, 1991, shows a counter clock wise rotation of $7.1^0 \pm 6.7^0$. This local rotation is due to the overlap of Red Sea propagators, Erta'ale-Dader in the east and Erta'ale-Manda Hararo in the west. A reference pole is determined based on 33 sites. It is located at $\lambda=83.1^0$N, $\phi=238.8^0$E($\alpha_{95}=4.0^0$).

Chapter 1

Introduction, Objectives and Location of the Study area

1.1 Introduction

The East African rift system in the Afar depression is one of the few places worldwide where the processes of sea floor spreading is occurring on land, affording an opportunity to directly observe and quantify the plate separation processes. Large tracts of the depression lie at or below sea level, attesting to a long history of stretching and magma intrusion. Another unique feature of this rift system is its position above or near a large deep seated zone of anomalously hot mantle rocks that both heat the overlying plates and provide a long lived supply of melt.

The triangular shaped Afar depression covers an area of about 200,000km^3 and is bounded by marginal escarpments, which close at narrow axial rift zones and ranges. It is flanked by the Ethiopian plateau in the west and the Somalian plateau to the south east. The Ali-sabieh and Danakil blocks bound the eastern and northeastern sides of the Afar depression, respectively. Further south, the northeastern segment of the Main Ethiopian rift separates the Ethiopian and Somalian plateau. The Ethiopian escarpment extends north into Eritrea and closes the Afar depression against the Danakil at the Gulf of Zula, which is re-entrant from the Red Sea.

The Afar depression is divided into north, central and south sectors on the basis of its geology and geography (Tesfaye *et al*., 2003). The northern part of the depression is dominated by axial volcanic ranges (e.g. Erta'ale). The <1m.a. old shield volcanoes of the axial ranges are typically produced by basaltic fissures eruptions aligned in NW to SE belt, parallel to the regional tectonic trend of the Red Sea (Barberi and Varet, 1977; Varet and Gasse, 1978).

The central sector dominated by graben and horst structures and bounded to the west and east by axial volcanic ranges, is occupied by Pliocene flood basalts and quaternary sedimentary rocks. The Tendaho graben is one of the biggest in this part of the Afar depression.

In central Afar, the Aden ridge spurred the development of minor rift segments (Manighetti *et al*., 1998). The area is characterized by the intersection of the N-S faults marking the western

escarpment, the NE-SW faults of MER, and the NW-SE and E-W faults of the propagating rifts (Manda Hararo-Goba'ad and Manda Inakir-Asal-Ghoubbet rifts).

Southern Afar, like central Afar, is dominated by horst and graben structures. Unlike central Afar, however, the grabens strike north-north east, and the topography has a mean elevation of 700m. The Tendaho-Gobbad discontinuity separates central Afar from southern Afar (Ebinger and Hayward, 1996). The prominent N-NE trending grabens in centre of southern Afar are the continuation of Wonji Fault Belt, the axial rift zone of Main Ethiopian Rift (MER) (Tesfaye *et al.*, 2003).

The Red Sea and Gulf of Aden oceanic rifts have been propagating towards one another for sometime but not yet directly connected and both have penetrated in to Afar where they are now actively opening and propagating via the development of a series of disconnected, propagating rift segments (e.g. Manighetti *et al.*,1997). The Red Sea is spreading and propagating in to the Afar depression along SE (Manda Hararo-Gobbat) and Gulf of Aden along NW (Asal-Manda Inakir) paths that consist of disconnected rifts defined by a series of Quaternary Shield volcano (Manighetti *et al.*, 2001). Large scale, Southwest ward propagation of the Aden ridge was an episodic processes with stages of rapid propagation, mostly at rates >10cm/yr, interrupted by million year pauses on transverse discontinuities coinciding with the rheological boundaries between different crustal provinces of the Arabian-Somalian plate. The propagation of the two rift segments caused large scale block rotation about a vertical axis in central Afar.

1.2 Objective of the study

Numerous tectonic models have been proposed for the evolution of the afar triple junction. The overlapping rift localization or ''Book shelf'' model was first proposed by Tapponier *et al.*, (1990) and has been revised by Sigmudsson (1992) and Manighetti et al., (2001). Tapponnier *et al.*, (1990) suggests that wherever rift boundaries overlap and are disconnected, the transfer of the strain is accommodated by a bookshelf faulting mechanism. This mechanism requires the rotation of small rigid blocks about a vertical axis that is compensated by strike slip displacement along faults that are parallel to the rift. The overlapping and propagating rifts are believed to have induced dextral shearing that has caused clockwise rotation of the Central Block about a

vertical axis due to differential spreading rates. This study aims in explaining the tectonics, kinematics and block motion studies linked to rift overlap and propagation in the Manda Hararo rift, which is located on the NW part of the overlap, of the North central Afar using paleomagnetic technique and principles and a thesis will be submitted to the school of graduate studies of Addis Ababa university as a partial fulfillment of Master of Science degree in Earth Sciences (Structural geology and Tectonics).

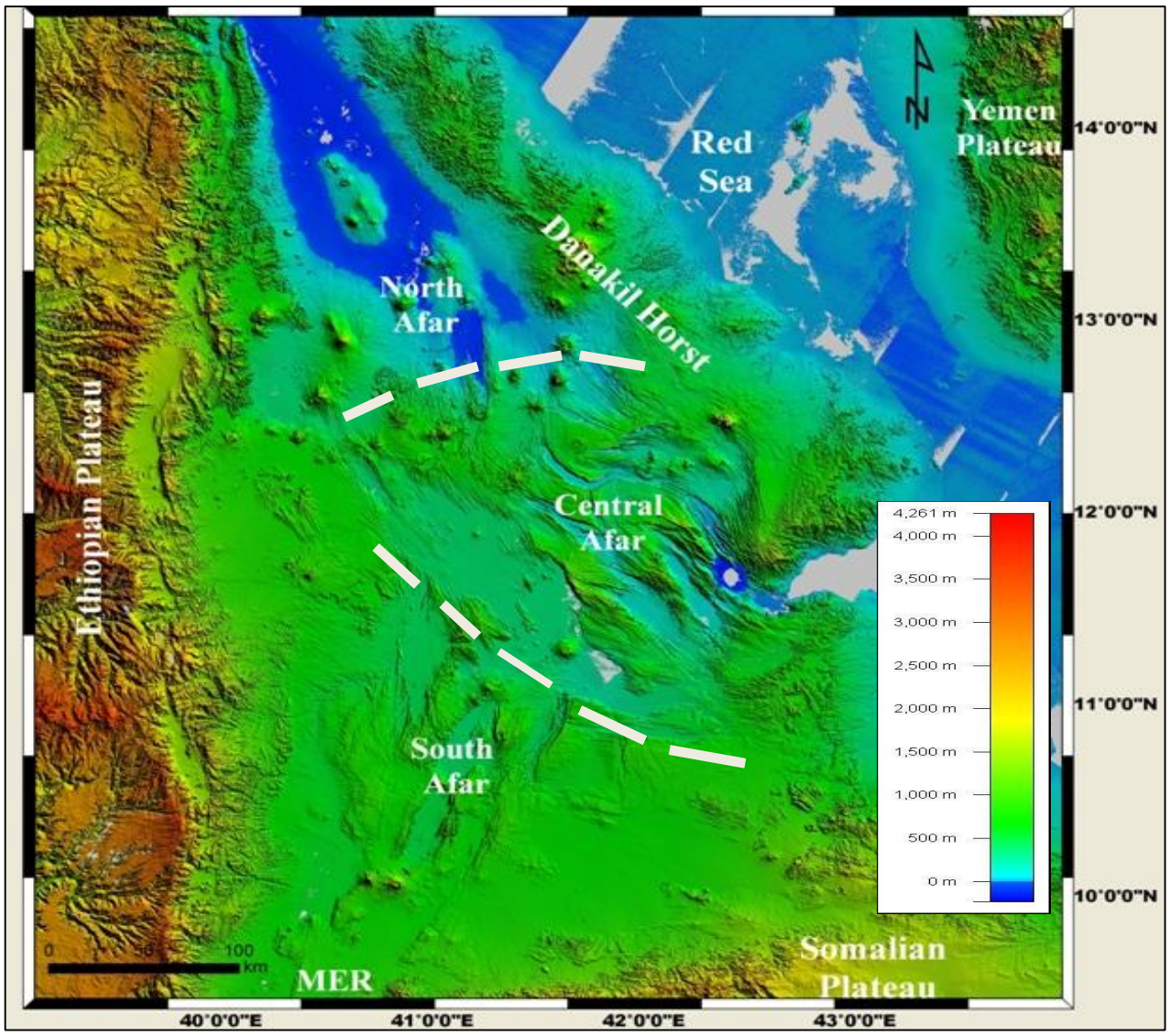

Fig. 1.1. A 90m resolution digital elevation model showing the physiographic setting and rough classification of the afar depression (modified after Tesfaye, S. *et al.*, 2003).

1.3 Location, Physiography and environment of the study area

The study area is located in the Afar depression, North Eastern part of Ethiopia enclosed between the geographic coordinates of $40^0$30'E to $41^0$15'E longitude and 12^0N to 13^0N of latitude. Some part of the study area can be accessed via all weather asphalt surfaced Serdo-Afdera road which is under construction, and via dry weather gravel road from Silsa to Kori village. The elevation in the study area varies from 400m above sea level to 20m below sea level (fig.1.1).

The lowlands of Afar depression are dominated by heat. There is no rain for most of the year and yearly rainfall average ranges from 100 to 200mm. The Awash River flowing North-Eastward via southern Afar provides a narrow green belt and enables life for the flora and fauna and for the inhabitants as well. About 128km from Red Sea, Awash ends in a chain of salt lakes, where its water evaporates as quickly as it is supplied. About 1200km^2 of Afar depression is covered by salt, and salt mining is still a major source of income for many Afar people.

1.4 Overview of the study

In the thesis that follows, Chapter 2 outlines the magmatism and tectonics of the Afar depression. Geology and tectonic evolution of the Afar depression will be discussed in Chapter 3. Chapter 4 mainly focuses on the structural evolution of the Manda Hararo rift and Dabbahu magmatic segment. The core of this study, Paleomagnetism, will be presented in detail in Chapter 5. This chapter also includes overview of Paleomagnetism, methodology of the study, field sampling, laboratory treatment and data analysis and discussion of the results.

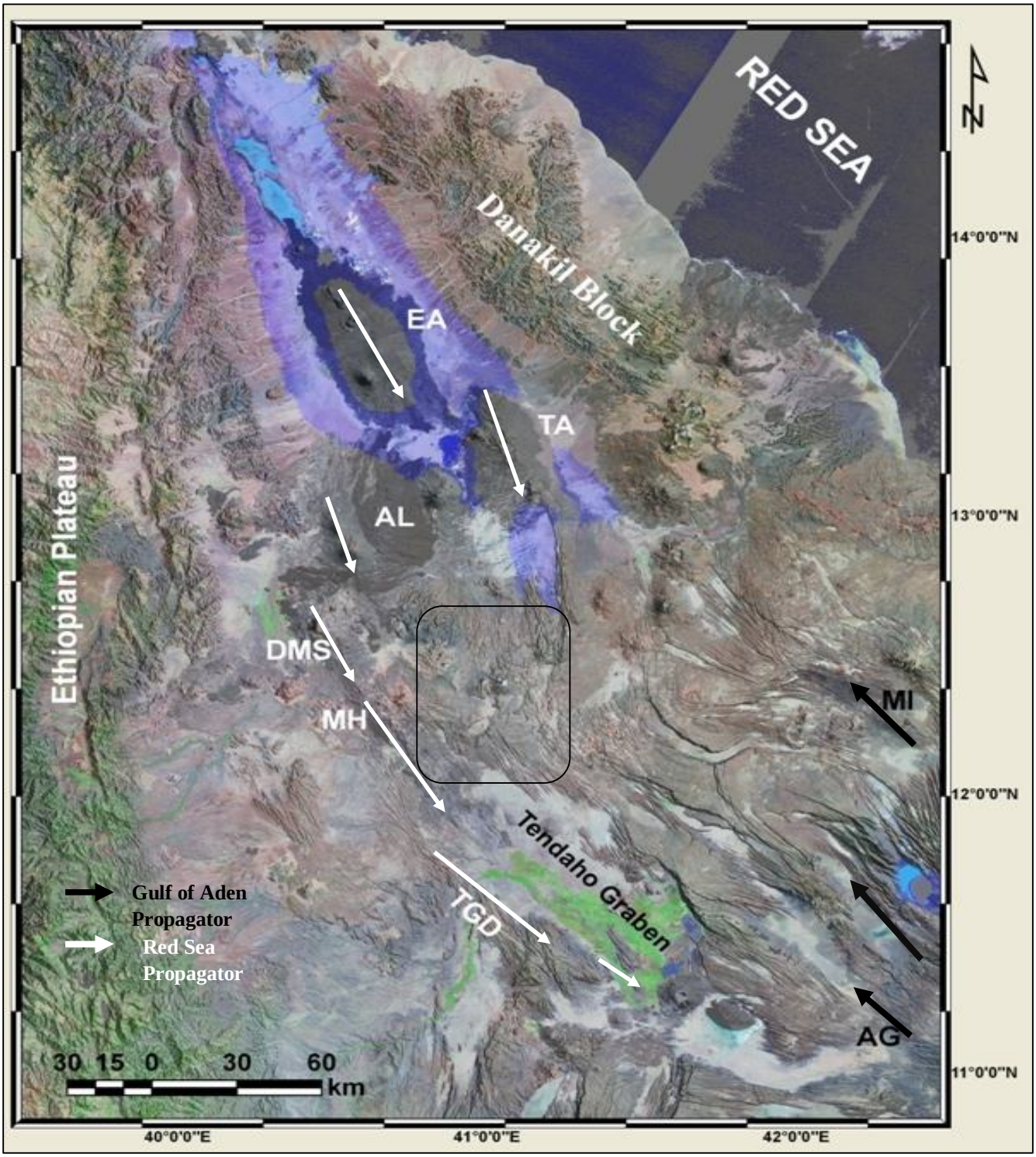

Fig. 1.2 Tectonic framework of rift propagation and overlap in Afar Depression (after Manighetti *et al.*, 2001). (EA=Erta'ale, TA=Tat'ale, AL=Alyata, DMS=Dabbahu Magmatic Segment, MH=Manda Hararo, TGD=Tendaho Gobbad Discontinuity, AG=Asal-Ghoubbet and MI=Manda Inakir.)

Chapter 2

Magmatism and Tectonic elements of the Afar Depression

2.1 Magmatism in Afar

The Ethiopian volcanic province represents an ideal environment to study the dynamics of mantle sources involved in continental volcanism and the manner in which sources interacted with continental lithosphere. This volcanic province is made up of a series of flood basalts overlain by large and conspicuous shield volcanoes.

The Miocene to recent basaltic activity associated with the development of Afar depression shows a much simpler compositional pattern than from the Kenya rift, reflecting both the greater homogeneity of the basement lithosphere and the developing tectonic regime (Vidal *et al*. 1991; Daniel *et al*. 1994). Basalts from Afar have lower Neodium and higher $^{87}Sr/^{86}Sr$ ratios than MORB (Mid Oceanic Ridge Basalts), and extend to values beyond that for the bulk earth. There is also a secular change in isotope character, between the older Miocene lavas and the most recent ones. This compositional variation in Afar depression have been interpreted to reflect the waning influence of the lithosphere and the increasing influence of the underlying Afar mantle plume following extension as Arabia drifted slowly away from Africa (Vidal *et al*. 1991; Daniel *et al*. 1994).

Previous studies of the Ethiopian-Yemen continental flood basalts and Plio-Quaternary lavas from the Afar region have indicated several distinct source domains that contribute to magma genesis. To first order, these components include Afar Plume, one or more additional mantle reservoir(s) and a subordinate contribution from the continental crust or mantle lithosphere (Hart *et al*. 1989; Chazot & Bertrand 1993; Baker *et al*. 1996; Pik *et al*. 1999; Kieffer *et al*. 2004). Geochemical evidence (Furman *et al*. 2006) indicated that the Afar plume is a long lived feature of the mantle and that its fundamental isotopic composition has effectively not changed during the transition from the Oligocene plume head to modern tail activity. Temporal changes thus appear to reflect the evolving tectonic environment rather than a significant change in sub-lithospheric source composition.

The involvement of mantle plumes in the evolution of the present topography and tectonics of the East Africa Rift has led to competing models as to the number of distinct plumes that may lie beneath. Ebinger and Sleep (1998) have suggested that magmatism throughout most of Africa could be related to a single deep mantle plume that initiated basalt volcanism in southern Ethiopia at 45Ma. In this model, upwelling plume material and associated basalt melts are channeled along the pre-existing 'thin' zones in the lower lithosphere until they reach regions of thin crust, such as that developed at Turkana, where eruptive activity takes place.

In contrast, George *et al.* 1998; Rogers *et al*. 2000 have suggested that two distinct plumes are required- one beneath modern Kenya and the other beneath modern Afar. In this model, the southward migration of basalt activity from southern Ethiopia towards Tanzania reflects the northeastward movement of Africa over the Kenya plume for about 50Ma, whereas magmatism in northern Ethiopia reflects 30Ma of sustained activity of the Afar plume.

The single plume model for Ethiopia (Ebinger and Sleep, 1998) and Afar (Schilling *et al*.1992) is not consistent with the recent geophysical studies (Debayle *et al*. 2001; Nyblade *et al*. 2000; Weeraratne *et al*. 2003). The consistent Pb isotope differences between contemporaneous sub-lithospheric magmas erupted in Ethiopia and Turkana (Furman *et al*. 2004) are compatible with the geophysical evidence for separate plume stems beneath these two areas.

In September 2005, the largest dyking episode occurred in the Dabbahu magmatic segment of the Afar depression. In this dyking episode, ~2.5km^3 of magma was injected as near vertical dykes in the upper ~10km of crust beneath the entire ~60km length of the Dabbahu magmatic segment and caused as much as ~8m of horizontal opening (Yirgu *et al,*. 2006). Preliminary petrographic study of Yirgu *et al*. (2006) from the lava dome indicates heating of the source magma chamber with an influx of hotter basaltic magma. According to Wright *et al*. (2006), the magnitude of opening that resulted from the volcano-tectonic crisis in Afar Depression can be compared to the 1975-1984 rifting Episode in Krafla, Iceland, (Sigmundsson, 2006), which is located in a well developed mid-Atlantic ridge.

According to Sigmundsson (2006), the magma during the crisis started flowing rapidly from magma chambers 5km under the neighboring Gabho and Dabbahu volcanoes. But rather than

flowing vertically towards the surface of the earth, this magma flowed horizontally tens of kilometers, forming a 60km long vertical "dyke" at a depth of 2-9km. The dyke might have been fed by a vertical flow of magma from greater depth. These magma flows split the crust laterally by up to 8 meters, relieving centuries of tensional stress caused by plate divergence.

2.2 Major Tectonic elements of the Afar Depression

The Nubian, Arabian and Somalian plate motions have induced major tectonic elements in the Afar depression. These include the Danakil, Ali Sabieh, Central afar, Manda Hararo-Goba'ad and Asal Manda Inakir.

2.2.1 Danakil Block

The elevated Danakil block region within the Afar depression, which consists of pre-rift geological units, has been referred to as a block, a horst, or a microplate reflecting the various views held as to its origin.

Souriot and Brun (1992) indicated that the Danakil Block has rotated 10^0 in the last ~7Ma and also indicated that the anti-clockwise rotation of the Danakil Block caused concentrated extension in the Northern Afar, clockwise rotation and diffused extension in the central Afar, oblique extension in the Tajura area and dextral strike-slip faulting in the southern Afar. Collet *et al.*, (2000) argued that the Crank arm model does not support the left lateral strike slip motion observed on the western Afar margin. Furthermore, Collet *et al.*, (2000) hinted that the stress field required for the anti-clockwise rotation of the Danakil block is incompatible with sinistral strike-slip motions observed on the northern Afar. Hence, Collet *et al.*, (2000) repositioned the Danakil Block to attain a best fit with the Nubian and Arabian plate margins and calculated a new pole of rotation at 13.31^0N, 34.39^0E.

The Danakil Block is interpreted as a micro-plate that extends into the Red Sea (Chu and Gordon, 1998). According to Eagles *et al.* (2002), the most recent, statistically significant, independent movement of the Danakil microplate can be related to the onset of ocean type accretion in Afar that promoted the ongoing propagation of the neighboring plate boundaries.

2.2.2 Ali-Sabieh Block

The region that extends from the Somalian plateau along the Aysha area towards the Afar depression is referred to as the Ali-Sabieh Block. This region has been characterized as strongly attenuated autochthonous continental block that remained attached to the Somalian plate during the Nubian and Somalian plate separation (Christiansen *et al*., 1975). The Ali-Sabieh Block was thought to have rotated 90^0 clockwise at a rate of 4.5^0 per Ma concurrent with the Danakil Block for the last 20Ma in a 'Saloon Door' fashion contributing to the opening of the Afar Depression (Manighetti *et al*., 2001). Furthermore, Manighetti *et al*.,(2001) observed that the western side of the Ali-Sabieh Block is marked by spatter cones that are aligned at ~90^0 to the E-W trending Somalian escarpment, along sinistral strike-slip faults that might have developed due to the clockwise rotation of the block. Evidences from Paleomagnetism on the Dahla basalts and Mabla rhyolites indicate clock wise rotation of about 15^0 (Audin *et al*., 2004).

2.2.3 Central Block

The SE-propagating Manda Hararo-Gobbad and the NW-propagating Asal-Manda-Inakir overlapping rifts in the southwest and northeast, respectively bound the Central Block. The overlapping and propagating rifts are believed to have induced dextral shearing that has caused clockwise rotation of the Central Block about a vertical axis due to differential spreading rates. The extension within the Central Block is localized in some major grabens such as the Dobi graben.

2.2.4 The Manda Hararo-Gobbad rift

The Red Sea spreading ridge south of $17^0$30'N branched into a SE and SSW trend (Chu and Gordon, 1998). The SE trend continues along the Red Sea axis and terminates in a seismically quite zone around the Hanish-Dubbi area (Barberi & Varet, 1975). The SSW trend runs along the Gulf of Zula, steps onto land within the Danakil Depression and continues south along the Erta'ale axial volcanic ranges to central Afar. The SSW-trend in turn splits south of Erta'ale into Tat'ale-Dadar trend in the east and the Alyata-Manda Hararo trends in the west. The propagation along the Erta'ale-Dadar trend probably stopped as the Tat'ale axial range reaches the 100ka

Dadar graben (Lahitte *et al.*, 2003). Propagation along the Alyata-Manda Hararo axial zone continues southward in to the Tendaho-Gobbad Discontinuity.

The southward advance of the SSW-trend along Erta'ale-Manda Hararo is broken into shorter rift and magmatic segments that are arranged into rift-in-rift structure as they approach the Tendaho and Gobbad axial ranges further south (Tazieff and Varet, 1972).

2.2.5 The Asal- Manda Inakir rift

The Aden ridge propagating westward into the Afar Depression via an overlap zone bounded by the Gulf of Tajura in the north and the Asal-Ghoubbet rifts in the south. The opening of the Gulf of Tajura changed courses from NE-SW and proceeded along the Ghoubbet-Asal-Manda Inakir rift in a NW direction (Dauteuil *et al.*, 2001). The Asal-Manda Inakir trend is characterized by rift propagation and spreading whereas the area to the southwest as far as the Tendaho-Gobbad Discontinuity is dominated by NE-SW extension and clockwise rotation.

Rift propagation and spreading along the Asal-Manda Inakir rifts are episodic and occur in intervals of 10^6 and 10^5 years, indicating alternative effusive and tectonic events (Courtillot *et al.*, 1984). Further, Courtillot *et al*. (1984) suggested that at~4Ma the Aden ridge reached the Gulf of Tajura, at~2Ma propagation reached up to Arta-Tajura, and at~1Ma began to open the Ghoubbet-Asal-Manda Inakir rift.

Chapter 3

Geology, Evolution and Rift model of Afar Depression

3.1 Geology of the Afar Depression

The geological units of the Afar depression and marginal areas can be divided into four broad groups (Varet,J & Gasse, F. 1978): 1) Neoproterozoic basement, Mesozoic sedimentary rocks, Eocene-Miocene basalts; 2) Miocene Igneous rocks; 3) Pliocene volcanic rocks; 4) Quaternary volcanic and sedimentary rocks (Fig. 3.1).

3.1.1 Neoproterozoic Basement, Mesozoic sedimentary rocks and Eocene-Miocene basalts

The neoproterozoic basement, which represents part of the Arabian-Nubian shield, is prevalent on the periphery of the Afar Depression. The Arabian-Nubian Shield covers vast terrain to the north and northwest of the Afar depression in eastern Eritrea and northern Ethiopia, respectively (Vail, 1985; Berhe, 1990; Stern, 1994). The neoproterozoic rocks of the Arabian-Nubian Shield also occupy the Danakil and Ali-Sabieh Blocks.

The neoproterozoic basement rocks are overlain by Mesozoic sedimentary rocks that get progressively younger towards the south and southwest on the Ethiopian and Somalian plateau, respectively. The pre-rift group (Neoproterozoic basement/Mesozoic sedimentary rocks) either does not exist in the Afar Depression or are covered beneath the Pliocene and Quaternary volcanics and sediments (Beyene and Abdulselam, 2005).

Many researchers (e.g. Almond, 1986; Crane & Bonatti, 1987; Sultan *et al*., 1992; Montenat *et al*., 1998) have concluded that the structural and stratigraphic evolution of the Main Ethiopian Rift, the Red Sea Rifts and the Gulf of Aden are influenced by the pre-existing neoproterozoic faults, penetrative structures and terrain boundaries. However, few researchers such as Mohr (1975) have argued that these rifts did not exploit pre-existing regional structural fabrics because the Main Ethiopian Rift runs oblique to the nearest neoproterozoic structural trends, the Red Sea obliquely cut the NNE-trending neoproterozoic schist belt, and although older neoproterozoic structures run parallel to the Sheba spreading axis other younger neoproterozoic structures are orthogonal to the spreading axis.

Within the Afar Depression, many structural features are found to suggest the influence of pre-existing fabric in its evolution. Black *et al*., (1974) identified the ~900km long pre-Miocene Marda Fault Zone, which continues from the Somalian escarpment towards the Indian Ocean, to be in a perfect alignment with the Red Sea western margin and the Erta'ale axial ranges.

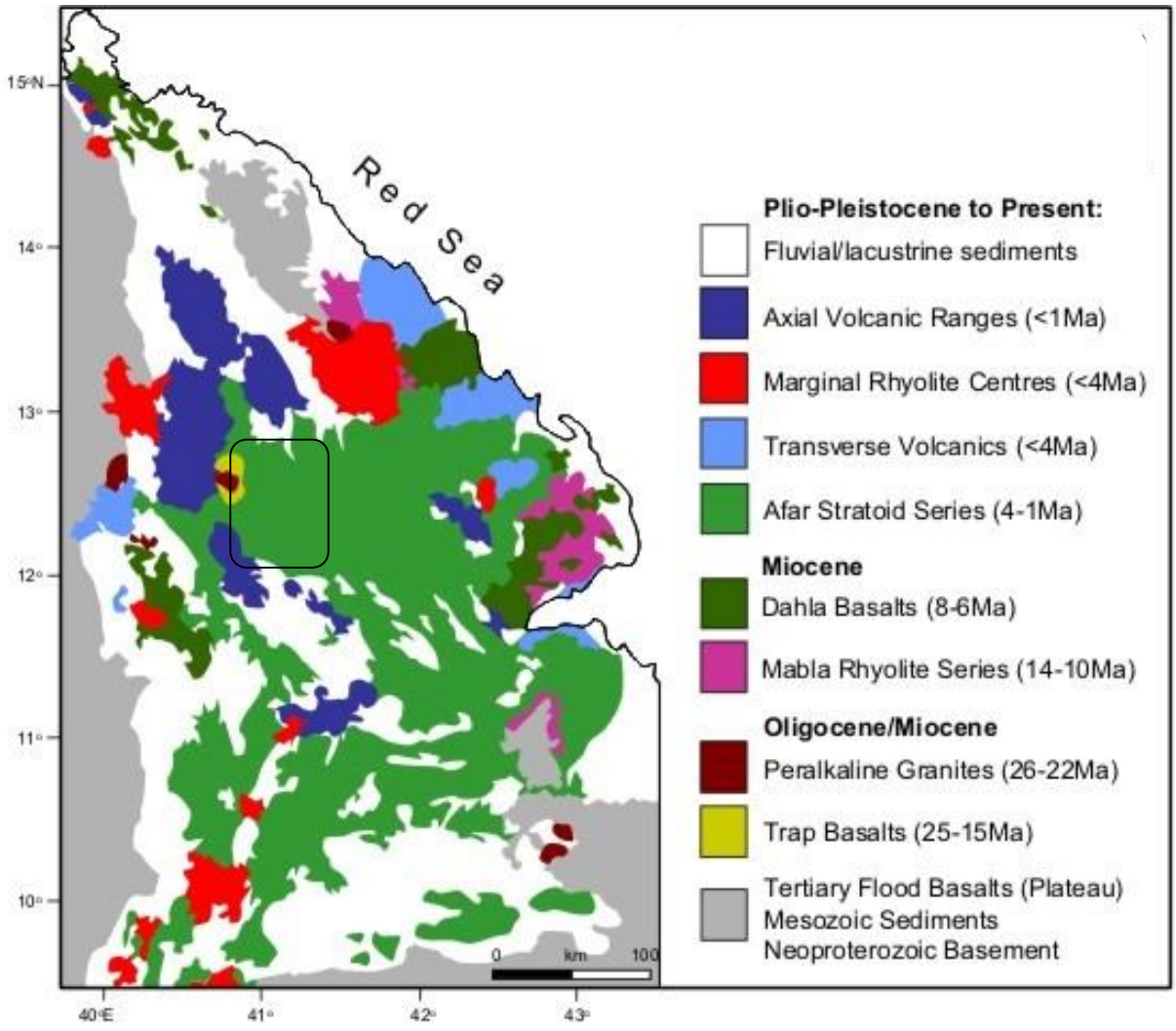

Fig. 3.1 Simplified geological map of the Afar depression (After Varet 1975; Beyene and Abdulselam, 2005).(see the detail geology map of the study area(black rectangle) attached at the end of the thesis)

The first known volcanism since the Neoproterozoic time appeared in northern Somalia and the first important volcanisum occurred at the southern and western margin of the proto-Afar during

the late Mesozoic (Mohr, 1975). The flood basalts of the trap series on the African plate covers ~500,000km^2 and these are ~2000m thick (Hofmann *et al*.,1997; Kazmin & Byakov, 2000).

Berhe *et al*. (1987) have identified three stages of volcanism in the trap series at ~50-40, 40-30 and 30-21Ma whereas Ebinger *et al*. (1993) proposed that the main phase of volcanism occurred between 45 and 30Ma. Hofmann *et al*. (1997) concluded from $^{40}Ar/^{39}Ar$ age dating in the Ethiopian plateau that the trap series volcanic rocks were erupted over a short period of time at ~30Ma.

3.1.2 Miocene igneous rocks

Barberi *et al*. (1975) defined four magmatic units. They consist either of eruptive basalt or of either eruptive or intrusive peralkaline silicics. These formations outcrop only along the margins of the depression.

3.1.2.1 Old Trap basalts

This unit was defined in the north-Tajura unit as the Adolei formation (Barberi *et al*., 1975) and was also found in eastern Afar (Civetta *et al*., 1974) and in Ali-Sabieh (Chessex *et al*., 1974). It consists of basalts commonly deeply altered with formation of Calcite, Chlorite, Zeolite and Silica. They are intensively affected by faulting (Varet, 1978).

3.1.2.2 Peralkaline Granite intrusions

Alkaline and peralkaline granitic intrusions have been mapped in central Afar along the western scarp limit (Black et al., 1972), in central Afar (Tazieff and Varet, J. 1972) and the southern extremity of the Danakil Alps. These three granitic bodies have fairly similar age, ranging between 26 to 22Ma (Varet, 1978). They are considered by Barberi *et al*. (1972), as the first magmatic event clearly related to the initiation of the Danakil rift. In fact, peralkaline granites are known to occur at the initial stage of continental break up.

3.1.2.3 Mabla rhyolites

This unit consists of thick flows, domes and ignimbrites of slightly peralkaline rhyolites, with some intercalated basaltic flows and pumice deposits. The rhyolites were emplaced via faults of N-S and $N20^0$ to 40^0 directions as shown by alignments of domes and dykes (Varet, 1978).

The formation was affected by a phase of erosion before being covered by the basalts of the Dahla formation.

3.1.2.4 Dahla basalts

This unit consists of a series of basaltic flows with rare intercalations of ignimbrites and detritic deposits, and reaches the thickness of 800m. It becomes intensively faulted when approaching the Gulf of Tajura and Afar.

The Dahla unit is deeply eroded, particularly along the Red Sea coast, and is covered often in unconformity by the Afar Stratoid series. This unit has an age of 4-3Ma (Kidane *et al*., 2003).

3.1.3 Pliocene-Pleistocene volcanic rocks

The most important volcanic unit in Afar is the Stratoid series that covers approximately the 2/3 of the Afar floor. This unit preserves igneous features and tectonic activities in Afar. The Afar Stratoid series is affected by numerous faults and fissures over all Afar except its eastern margin. Faulting and block tilting have been continuous during the emplacement of the stratoid series, as indicated in several fault scarps by the increase of the dip towards the basis.

The thickness of the stratoid series reaches up to 1500m with individual flows varying from one to six meters (Varet and Gasse, 1978; Tefera *et al*., 1996).

The Afar stratoid series was originally dated to be between 0.4 and 4.4Ma in age (Varet & Gasse, 1978). Using both updated K-Ar and ^{40}Ar-^{39}Ar, Courtillot *et al*. (1984) reduced this range to 1.3-2.2Ma.

3.1.4 Quaternary volcanic and sedimentary formations

Quaternary volcanic rocks in the Afar depression are composed of basaltic flows, scoria cones and silicic rocks (Tefera *et al*., 1996). In most places basaltic fissure eruptions were followed by central eruptions that produced differentiates of basalt comprising alkaline and per-alkaline

silicic rocks (Varet and Gasse, F. 1978; Tefera *et al*., 1996). However, the rift-parallel axial ranges in the northern and east central Afar are dominated by basalts which are ~1Ma old. Rhyolites occur here and there in some of the axial units. They are well developed at Boina (also known as Dabbahu) (Barberi *et al*, 1975), but small patches also occur at Dama'ale and Manda Hararo (Gablaytu).

Quaternary sedimentary rocks in the Afar depression are dominated by lacustrine deposits. Significant lacustrine sedimentary rocks were deposited in the central Afar along the Manda Hararo-Gobbad rift zones between ~12 and 1Ka (Rognon, 1975). The Hadar formation in the west side of central Afar has a thickness of 180m to 240m which outcrops via deep furrows cut by the Awash and its tributaries (Varet, J & Gasse, F. 1978).

The very recent tectonic and magmatic activity has happened in Dabbahu Magmatic Segment of North Afar. In September 2005 a seismo-volcanic event of unprecedented scale and intensity took place along this magmatic segment. Between September 4 and October 4, 163 earthquakes with Mb between 3.9 and 5.6 occurred. This event produced volcanic products of thin layers of fine to coarse pumice clasts, dense glass and lithcs of rhyolitic lava.

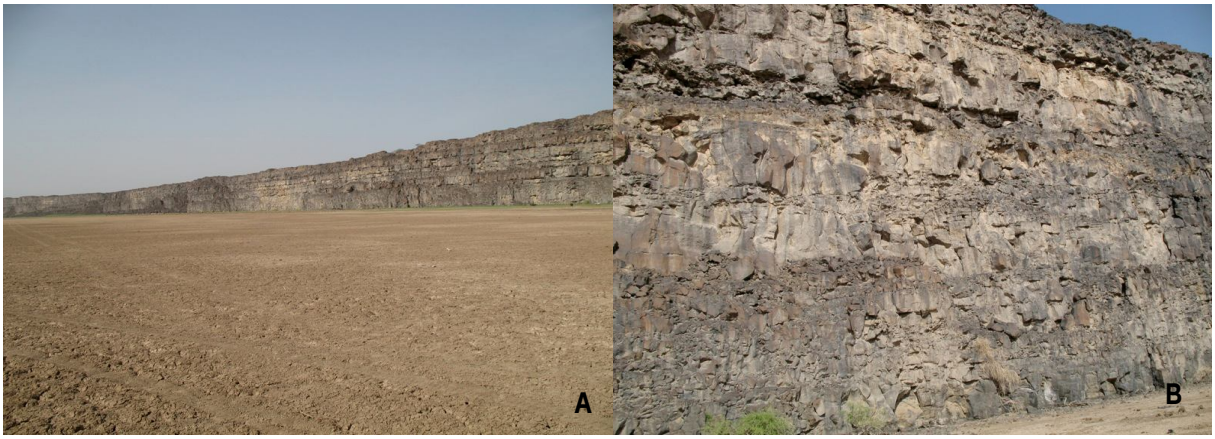

Fig. 3.2 Sedimentary deposits (**A**) and high angle NW-SE oriented normal faults (**B**) in saha area.

3.2 Evolution of the Afar Depression

The timing of initiation of rifting in Afar is not well established. Barberi *et al*. (1975) and CNR-CNRS (Afar team) (1973) pointed out that crustal extension in southern Afar and northern part of the Main Ethiopian Rifts (MER) began at 25Ma (Oligocene, Miocene).

Kazmin *et al*. (1980) argued that rifting in the boundary zone between the Afar and MER started at 14Ma (Middle Miocene). Despite the disagreement regarding the age of rifting in the southern Afar and northern Main Ethiopian Rift, it appears that they developed roughly simultaneously (Kazmin *et al*., 1980; Berhe 1986; Tesfaye *et al*., 2003).

Many researchers believe that (e.g. Hofmann *et al*., 1997) eruption of the Ethiopian trap series about 30Ma ago facilitated the breakup of Arabia and Africa and, after an initial phase of incipient breakup along the East African Rift and the Red Sea, the Gulf of Aden rift propagated from the Indian ocean toward the area weakened by the hot spot; it arrived on the Shukra-el-sheik discontinuity (~45^0E) about 20Ma ago. The propagation was an episodic process with stages of rapid propagation, mostly at rates >10cm/yr, interrupted by million year pauses on transverse discontinuities coinciding with rheological boundaries between different crustal provinces of the Arabian-Somalian plate. The longest pause was at Shukra-el-sheik where the ridge tip stalled for ~13Ma, between 17 and 4Ma. West of that discontinuity, rifting and spreading took place at an azimuth (N$25^0\pm10^0$E) and rate (1.2±0.3cm/yr) different from those of the global Arabian-Somalian motion vector (N39^0E, 1.73cm/yr), implying an additional component of movement (N$65^0\pm10^0$E, 0.7±0.2cm/yr) due to the rotation of the Danakil micro-plate (Manighetti *et al*., 1997).

The Gulf of Aden bypasses Bab el Mandeb, which is now seismically inactive and probably represents an extinct segment of the Red Sea rift (Acton and Stern, 1991), to penetrate directly into Afar, through the Gulf of Tajura and Ghoubbet strait. It then veers into another narrow, NW trending belt of active volcanisum and faulting that hugs the west side of the Danakil Block, to the Manda Inakir rift (Tapponnier *et al*., 1990; Acton *et al*., 1990; Manighetti, 1998).

In the period (~30-20Ma), the Red Sea rift had propagated toward the hot spot area after branching SE and SSW. The SE trend continues along Red Sea axis and terminates at Hanish-Dubbi area. The SSW trend jumps to the Afar Depression and continues along the Erta'ale axial volcanic range to central Afar, which again splits into Tat'ale-Dadar trend in the east and Alyata-Manda Hararo in the west. At the hot spot area, the lithosphere was so softened that both the Gulf of Aden and the Red Sea rifts were unable to break; the Afar depression started to stretch via both localized (disconnected rift segments) and diffuses faulting, associated with magmatisum. Two 'micro-plates', the Danakil and Ali-Sabieh blocks were isolated and the depression started opening. Since about 1Ma, the Aden rift has localized along the western edge of the Danakil block, where it has been propagating northward in a series of discontinuous jumps.

While the Manda Hararo rift remained active in the same general configuration, the Gulf of Aden once again propagated westward between 2 and 1Ma, creating the Asal-Ghoubbet rift about 0.9Ma ago. There was therefore an overlap between the Asal-Ghoubbet and Manda Hararo rifts, bounded to the west by what is approximately now the Gamarri-Alol zone and to the east by the Hol Hol fault zone. This initial overlap zone functioned between about 0.9 and 0.2Ma, with its fault bounded elongate blocks rotating following a book shelf mechanism (Tapponnier *et al.*, 1990; Manighetti *et al.*, 2001a). About 200,000 years ago, the Gulf of Aden rift once again propagated as a right step to the NW, generating the Mak'arrasou transfer zone, and the Manda Inakir rift. This more than doubled the size of the overlap between the two main rift branches and initiated faulting and bookshelf rotation of the north Immino, Siyarrou, Isso-Dobi and Unda-Gamarri blocks.

3.3 Rifting models for the evolution of Afar Depression

The evolution of the Afar Depression has been characterized as passive and/or active rifting or the combination of two based on the sequence and timing of the rifting process related to the Main Ethiopian Rift, the Red Sea and the Gulf of Aden, the uplift of the Afar dome and the flood basalt volcanisms. The basic difference between the passive and active rifting models is whether the asthenosphere (induced by mantle convection or mantle plume) is passively raising as the

lithosphere moves away due to a pull of subducting slab or whether a raising asthenosphere forces the lithosphere (through thermal erosion due to mantle convection or mantle plume) to open along the rift zones (Sengor and Burke, 1978; Sengor, 2001). The progression of events in passive rifting would be Rifting-Uplift-Volcanism, for active rifting the sequence becomes Uplift-Volcanism-Rifting (Sengor and Burke, 1978; Bohannon *et al*., 1989). There is a consensus that the vast volcanism in the Afro-Arabian region is related to upwelling mantle plume. The question remains, however, whether or not the lithosphere is stretching and thinning primarily passively responding to the tensile far field stress (Makris and Ginzburg, 1987) or it is a manifestation of an active local stress due to an upwelling mantle plume (Gass, 1970; Schilling, 1973; Schilling *et al*., 1992). Contrary to both models, Menzies *et al*. (1992) argued that the sequence of events in the Afar Depression could be best described by volcanism-rifting-uplift, which fits neither passive nor active rifting models.

Hempton (1987) and Bohannon *et al*. (1989) suggested that forces external to the African and Arabian plates triggered early stretching and thinning of the Gulf of Aden and the Red Sea. This was followed by the suggestion that the Arabian plate has passively moved away from the African plate due to far-field stress exerted as a result of the Eurasian and the Arabian plates convergence along the Zagros Orogenic Front following the closure of the Tethys Sea (Courtillot *et al*., 1987; Joffe and Garfunkel, 1987; Schilling *et al*., 1992).

At an early stage of lithospheric rupture by passive rifting, plate margins would be diffused and deformation would involve broad zones instead of sharp, narrow boundaries (Courtillot, 1982). Lithospheric rupture, taking the W-propagating Gulf of Aden spreading system as an example, might have started as a result of far-field stress possibly along pre-existing zones of weakness and propagated towards a locked zone (Courtillot. 1982). The lithosphere was subsequently deformed by normal faulting at the brittle surface layer and plastic necking at deeper levels (Manighetti *et al*., 2001b). Courtillot (1982) suggested that the Afar Depression might have acted as a locked zone when the Red Sea and Gulf of Aden rifts were propagating towards its center.

Far-field stress inducing intra-plate rifting is followed by volcanism due to decompression or melting. The initiation of the trap series volcanism in the region as early as ~50-40Ma (Berhe *et*

al., 1987, Ebinger *et al*., 1993) with the main phase occurring at ~30Ma (Hofmann *et al*., 1997) suggests that the mantle plume reached the base of the lithosphere at this time (White and Mckenzie, 1989). White and Mckenzie (1989) suggested a model of melt generation in which a passively upwelling mantle plume beneath rifted continental lithosphere is responsible for the majority of rift related igneous provinces including the Afar Depression.

The Active rifting (Upwelling mantle plume) model involves thinning of the continental lithosphere via thermal and mechanical erosion resulting from an impinging mantle plume (Schilling *et al*., 1992). Up welling mantle plume as a means of transporting temperature, melting of mantle material and lithospheric accretion in the Afar Depression was first proposed by Morgan *et al*. (1970) and Gass (1970). Consequently, Barberi *et al*. (1974) proposed that a tendem extrusion of mantle material occurred along the NW-trending axial ranges of the Danakil Depression and on the pre-existing rift transverse structures on the western and eastern Afar Depression.

The African plate (Nubia and Somalia), which is geometrically symmetrical, with ridges both east and west, is believed to be nearly stationary with respect to the underlying mantle. This allows us to neglect any viscous drag of the astenosphere, the effect of subduction zones. The ridges are assumed to be spreading symmetrically, so that they are retreating from continent and leaving fresh oceanic lithosphere essentially stationary with respect to the underlying mantle. The African continent is compressed by ridge push stresses. The extension along the east African rift zone indicates that, part of the continent is in tension. This suggests that far field stress exerted on the African plate due to slab pull in the north might have not been enough to rupture the lithosphere and drive the Somalian plate away from the Nubian plate. In addition, the Somalian plate moved away from the Nubian plate in a direction not related to the subduction of the Arabian plate (Bilham *et al*., 1999). Moreover, the Somalian plate motion is counter-balanced by spreading across the Gulf of Aden ridge, the East Sheba ridge and the central Indian ridge (Bilham *et al*., 1999). Hence, it is most likely that the separation of the Nubian and the Somalian plates might have been reinforced by the upwelling mantle plume. The slow rate of opening across the Main Ethiopian Rift (~4mm/year, Bilham, 1999) is most likely due to the effect of ridge push surrounding the Somalian plate to the east resulting in a counter-balance of

the extensional force exerted by the upwelling mantle plume (Beyene, A and M.G. Abdelselam, 2005).

Chapter 4

Structure of Red Sea Rift

The Red Sea and the Aden rifts seem to be propagating in SE and NW trending directions, respectively: but the two rifts have actually bifurcated and stepped on to the Afar via a series of active rifts and volcanic systems known as propagators.

The Red Sea penetrates the Afar Depression from the Gulf of Zula and turns and continues along the SE-propagating Manda Hararo-Tendaho-Gobaad rifts. In the northern afar depression, the red Sea structures are N-trending but assume NW-WNW-trend in central Afar. The part of the Manda Hararo-Tendaho-Gobaad rift is referred to as Tendaho- Gobaad Discontinuity as it approaches to the Afar triple Junction. South of the Gulf of Zula, the Red Sea structure splits into a western and an eastern branch following the Erta'ale-Alyata and Erta'ale-Tat-ale trends. The western branch is recognized as the south-west continuation of a set of right laterally displaced rifts (Manighetti et al., 2001a,b). These segments jump southeast ward from Alyata, Manda Hararo to Manda Hararo- Gobaad. Distinct NW-trending regularly spaced parallel faults are observed within the Tendaho-Gobaad Discontinuity in its northwestern and southeastern parts. These faults deform the recent basalt of the rift segments that are associated with the development of Manda Hararo-Gobaad extension.

Tectonic and magmatic activity along the southern Red Sea propagator in central afar occurred (in the last 1.8Ma) in the Tendaho Graben and subsequently, Manda Hararo rift (Fig.4.1 & 4.2). V. Acocella *et al*. 2008, suggest that the activity of southern Red Sea propagator was characterized, between ~1.8Ma and ~0.2Ma, by moderate extension and significant magmatisum. However, both decreased in the last 0.2Ma, along the Manda Hararo rift. Such an evolution of the southern red sea propagator in central Afar, in the last ~2Ma, may be related to that of the Aden propagator, in eastern Afar.

The evolutionary model of V. Acocella *et al*. 2008, suggests that spreading in central Afar mainly took place along one active propagator at any one time, first with the southern Red Sea

(approx. 2-0.6Ma) and subsequently with the Aden propagator (approx. 0.6Ma to present) (Fig.4.1).

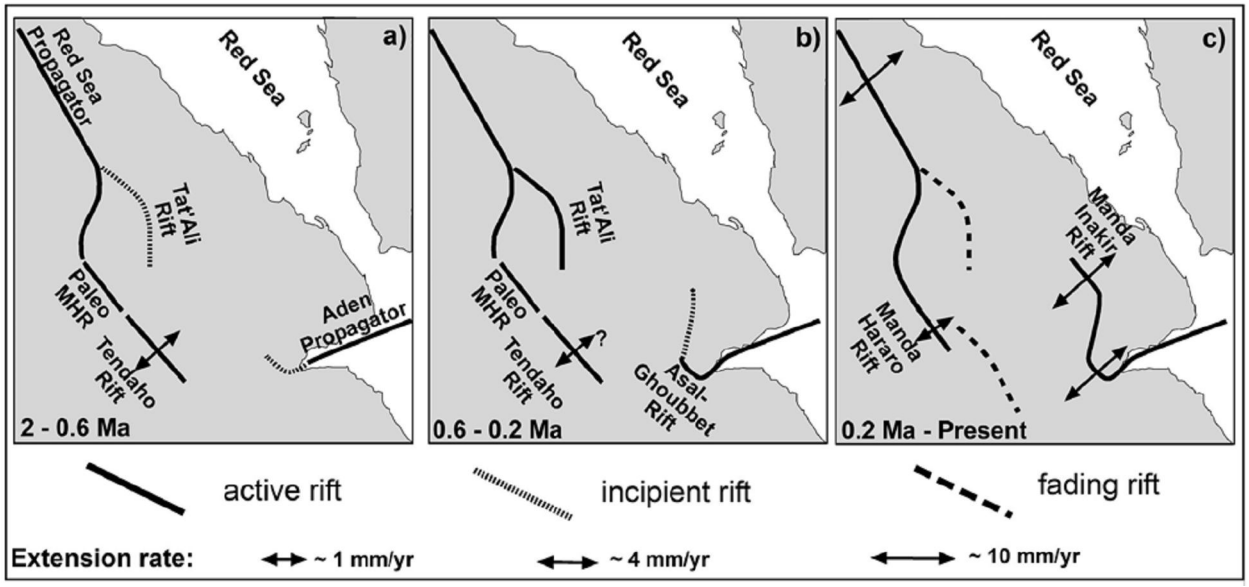

Fig. 4.1. The evolution model of Manda Hararo Rift (after V. Accocella *et al*., 2008).

The Manda Hararo has a prevalently fissural nature. Its products cover an area extended for more than 100km in NNW-SSE direction. Its width varies between 20 and 30km (Aquater, 1976). This is a rather complex volcanic unit which includes fissural activity zones, small embryonic shield type volcanoes and local folding, due to uprising magma.

A shield volcano (Unda Hararo), located in this area, is characterized by a top crater with a diameter of 800m. This crater is then surrounded by several parasitic vents placed in a semi-circle; according to Varet (1978), these craters could be the surface expression of a cone sheet. A uniform lava field (Gumatmali) is found SSW of the unda Hararo, which was formed by several fissural eruptions along NW-SE fractures. The small Gablaytu volcano is located in the south-eastern part of the Manda Hararo complex. It is characterized by intense tensional tectonics, which determines the formation of a perfect top graben, this in turn, characterizes the volcano Profile. This tectonic activity follows the deposition of rather viscous lava products, which were the last to erupt from the Gablaytu.

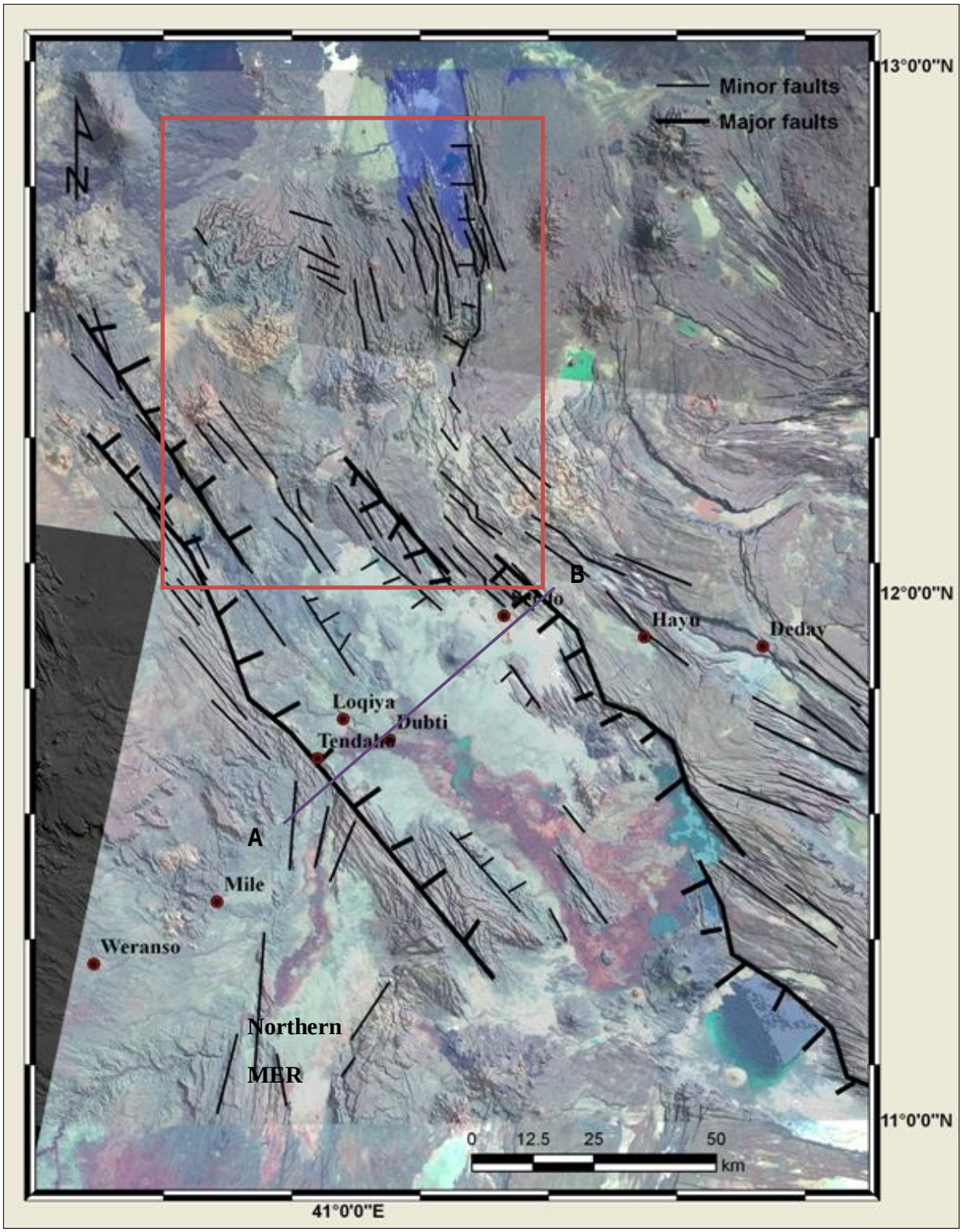

Fig. 4.2. Landsat ETM+ mosaic (bands 5, 3, 1 in R, G, B) of the Manda Hararo and Tendaho rifts. The red rectangle shows the study area. Note the orientation of faults in the area studied.

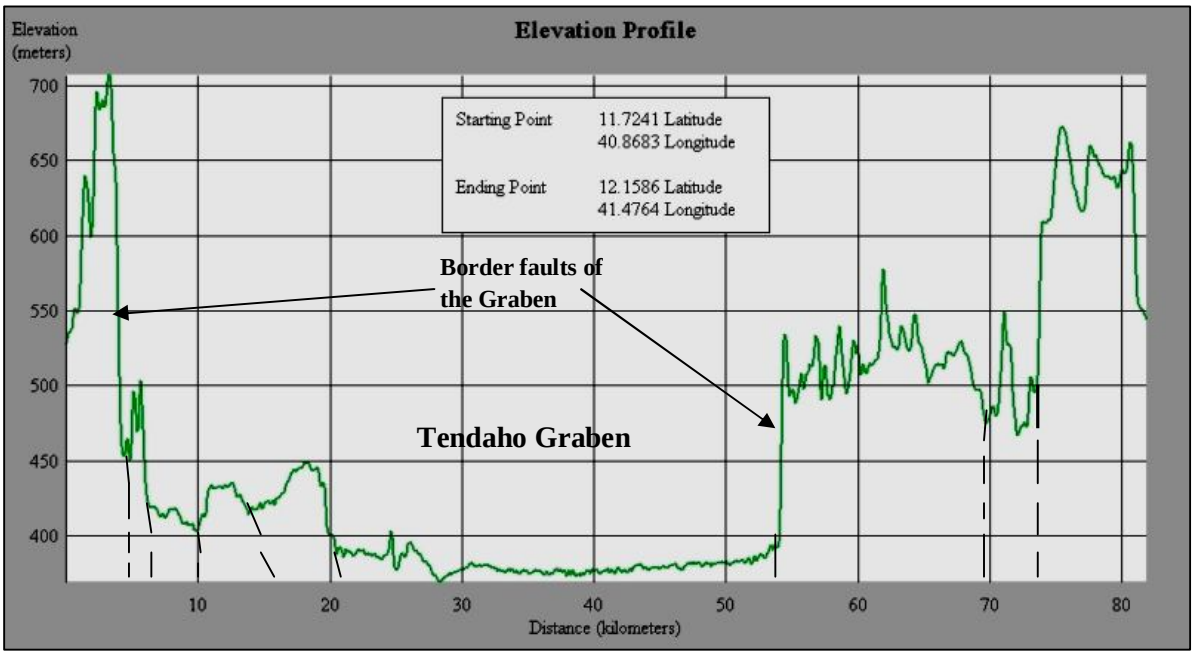

Fig. 4.3. Topographic profile (A-B from fig. 4.2) across the Tendaho graben, generated from DEM of 90m resolution.

The Manda Hararo rift is affected by pure extension, even though these faults exhibit a moderate left lateral component. Neglecting any strike slip component, V. Acocella *et al*. 2008, estimated a total extension of 76.7m in the northernmost to 9.5m in the southernmost part of the rift.

Another tectonic feature worth mentioning is the Dabbahu magmatic segment which is situated in the Northern end of the Manda Hararo rift. This volcano comes back to life in 2005 with a rhyolitic eruption from the Da'Ure vent (Wright, *et al*., 2006).

The Dabbahu magmatic segment (DMS) is ~60km in length and ~15km in width. The orientation of the segment changes near Ado'Ale. In the vicinity and to the south of Ado'Ale edifice the segment trends NW-SE. To the north of Ado'Ale, the segment swings to a more northerly trend such that the rift axis is oriented to 60^0 oblique to the direction of relative plate motion. Numerous active volcanoes occur at the northern tip of the segment, including the major silicic strato-volcano, Dabbahu, and the somewhat smaller Gab'ho volcano.

Dabbahu volcano, standing 1350m a.s.l. and with a diameter of ~10km, is the largest topographic load in the segment. Gab'ho volcano reaches 850m a.s.l. and is elliptical in plan view; major axes trend N-S and E-W, with lengths of 4.5 and 3km, respectively. Smaller volcanoes and cinder cones define a linear vent zone to the northwest of Dabbahu volcano. Between Dabbahu volcano and Ado'Ale, the segment is elevated up to 150m a.s.l. above the regional level of ~400m a.s.l.

A well developed axial graben extends from the southern flank of Dabbahu volcano to the south, but its topographic expression diminishes towards Ado'Ale. Although heavily dissected, the Ado' ale volcanic complex reaches elevations of >750m a.s.l. and extends over a broad region of the central DMS. Ado' ale constitutes a significant topographic load on the present tectono-magmatic system, and may have an important influence on the current configuration of faulting (e.g. Lahitte *et al.*, 2003). South of Ado'Ale, the elevation of the rift zone is less than the regional level.

Hayward (1997) recognized over 1200 distinct faults by analyzing ≤30m resolution Landsat TM and <15m resolution Large Format Camera space shuttle photography. Faults have a mean strike of 333^0, oblique to the NE-trending extension direction (Vigny *et al.*, 2006a,b), but there is a considerable variation. The greatest range in strike occurs just north of Ado'Ale, where the overall trend of the segment changes direction. South of Ado'Ale, where rifting is orthogonal, the mean strike of faults is perpendicular to the extension direction. However, north of Ado'Ale where rifting is oblique, the mean strike of faults is 352^0, parallel to the rift axis and oblique to the extension direction.

Faults have a mean length of 1.9km, however, linkage between north-and north-west trending fault segments has generated en-echelon fault zones up to 20km in length. As a percentage of the cumulative length of all measured faults, almost 60% are down thrown towards the segment axis, which is defined for the most part by the axial graben. Faults and their associated fissures are very closely spaced (<<500m) within ~7km of the rift axis, coextensive with the youngest basaltic lava flows (Fig. 4.2).

At the surface the faults are vertical, or near vertical, have throw and opening displacements (commonly <20m and 1-3m, respectively) and show no evidence of frictional contact between the fault surfaces. In each case, the surface outcrops of the vertical faults have formed initially by the opening of pre-existing cooling joints (Rowland *et al.*, 2007). Deep fissures are common between footwall and hanging wall blocks. In some cases, fissures have operated as conduits for the transport of mafic magma: small basaltic constructions are localized on fissures, and flows are observed to originate from fissures.

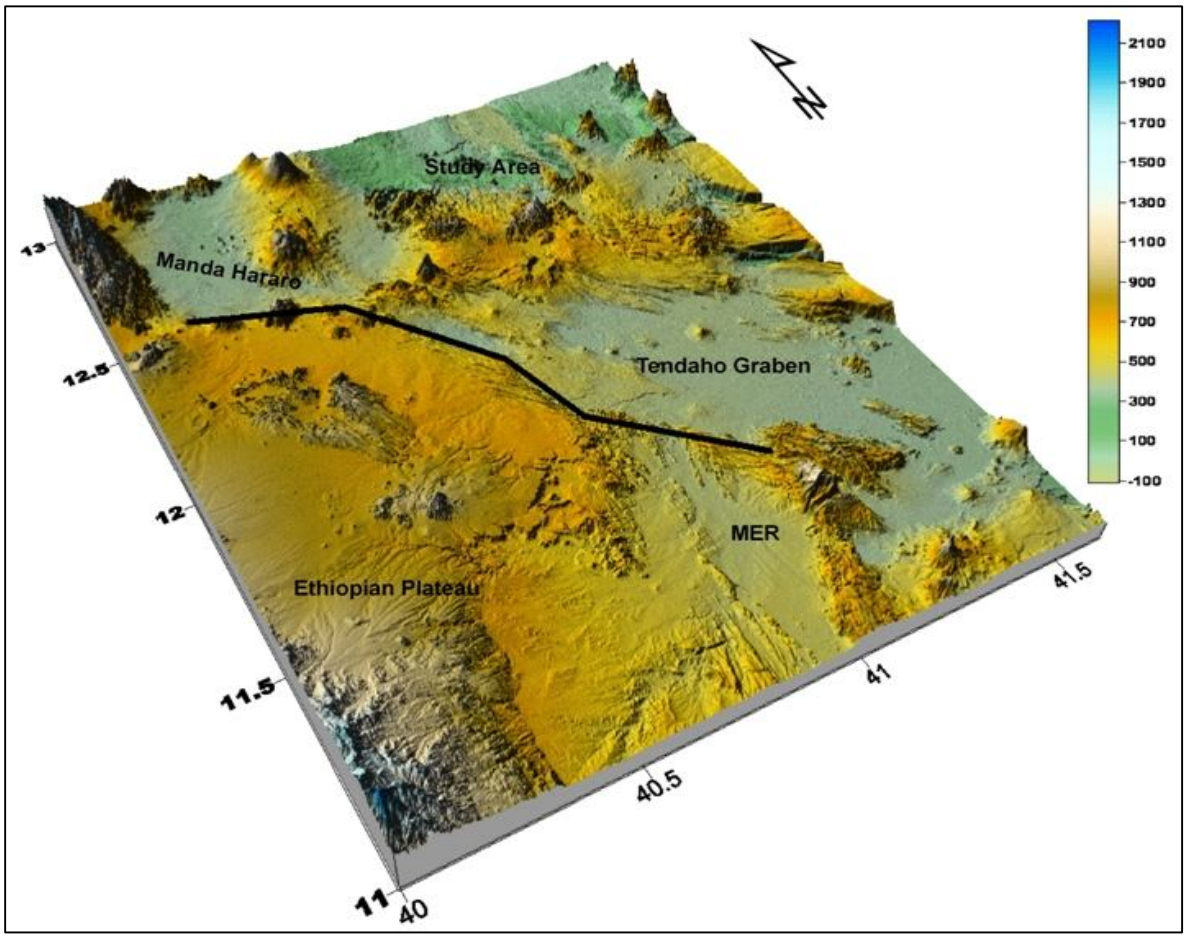

Fig. 4.4. Physiographic setting of the Manda Hararo rift and Tendaho graben (The Black thick line is marginal fault of the Red Sea rift).

Chapter 5

Paleomagnetism-application to tectonics

5.1 Overview

Paleomagnetism is the study of the direction and intensity of earth's magnetic field via geologic time. It is useful for determining the movement of rocks both on a large and small scale. On a large scale, Paleomagnetism helps show how the continental and oceanic plates have drifted relative to the earth's spin axis and to one another. On a small scale, it helps to determine the movement of crustal blocks in continents, particularly vertical axis rotation.

5.1.1 The earth's magnetic field

The primary component (>90%) of the magnetic field observed at the earth's surface is generated internal to the planet by electric currents flowing in its liquid outer core. This field varies slowly with time and space, and can be described by mathematical model such as International Geomagnetic Reference Field (IGRF) and the world magnetic model.

At any point on the surface, the earth's magnetic field can be represented by a vector with a specific length and direction. When averaged over a long period of time (greater than 10^5 years), this field can be represented by a dipole magnet at earth's centre with its north-south axis being the same as the spin axis of the earth.

Therefore, according to Geocentric Axial Dipole (GAD) model, a rock that acquired its magnetization at the equator would have a time averaged vector inclined to 0^0 to horizontal. Similarly, a rock that acquired its magnetization at the North Pole would have a vector inclined 90^0 to the horizontal. Those in between have a vector described by the equation $\boldsymbol{\tan I = 2 \tan \lambda}$, where, **I** is Inclination and λ is Latitude.

5.1.2 Magnetism in Rocks

Magnetization in rocks is due to the magnetic moments of neighboring atoms in minerals in the rock being coupled parallel or anti-parallel. These magnetic minerals usually make up a few percent or less of the rock. One of the most common ones is Magnetite (Fe_3O_4). There are two

sites; A- and B- sites. A site: Fe ion is surrounded by four oxygen; B sites: Fe ion is surrounded by six oxygen ions. The magnetism is due to the spin on the electrons in A-sites being anti-parallel to the spin on the electrons in B-sites. Another common magnetic mineral is hematite (Fe_2O_3). In the presence of no magnetic field, these minerals have a spontaneous magnetization. This magnetization consists of different regions of the crystal having their magnetic vector going in a different random direction. These regions are called domains. The presence of a large magnetic field can enlarge or reorient these domains in such a way that when the field is removed, the original domain sizes and orientations are not recovered. The rock now has permanent magnetization, known as remnant magnetization.

The magnetic field of the earth is not strong enough to produce remnant magnetization except in special circumstances, which vary according to rock type. Igneous rocks become susceptible to magnetization by the earth's field once they are heated to a temperature known as *Curie temperature*. This temperature is different for different minerals (for example magnetite=580^0C and hematite=680^0C).

As the rocks cool to a slightly lower temperature, known as *Blocking temperature*, the magnetization becomes permanently locked within them, and will remain unless they are reheated to near the blocking temperature. Blocking temperatures for magnetite bearing rocks range from 500-580^0C. Magnetization acquired by this kind of heating and cooling is known as thermoremnant magnetization (TRM). It is often acquired in several steps throughout the slow cooling history of the rock.

Sedimentary rocks acquire their magnetization as magnetic grains fall through the water and accumulate with other sediments. These grains can become aligned with the ambient magnetic field as they are deposited, resulting in depositional remnant magnetization (DRM). In addition, chemical changes in the rock during the process of lithification can cause new magnetic minerals to grow. Once these minerals reach a critical grain size (about 0.2 μm for hematite) they will acquire a chemical remnant magnetization (CRM).

These original magnetizations can be partially overprinted by subsequent geologic events, such as metamorphisum, hydrothermal alteration, and small influences of the earth's more recent

magnetic field acquired over long period of time (Viscous remnant magnetization), and electrical currents caused by lightning strikes (isothermal remnant magnetization). Although partial demagnetization in the laboratory can often erase lightning induced IRM, the best policy is to avoid lightning-prone areas. When possible, topographic highs should be avoided, especially in tropical regions (Butler, 1992).

5.1.3 Paleomagnetic sampling and Analysis

The hierarchy of a generalized paleomagnetic sampling scheme is shown in Fig.5.1. A rock unit is a sequence of cooling units in an igneous complex, usually a member of a geological formation, an entire formation or even a sequence of formations.

A site is an exposure of a particular cooling unit in an igneous complex (a lava flow or dike). If it is assumed that a primary NRM direction can be determined from the rock unit, results from an individual site provide a record of the geomagnetic field direction at the sampling locality during the (ideally short) time interval when the primary NRM was formed.

Samples are separately oriented pieces of rocks. Comparison of NRM directions from sample to sample within a site allows site homogeneity of the NRM to be evaluated.

Specimens are pieces of samples prepared to appropriate dimensions for measurements of NRM.

There are several goals in sampling rock units. One is to average the errors involved in sampling process itself. Another is to access the reliability of the geological recording medium. In addition, we often wish to average the scatter caused by secular variation of the geomagnetic field in order to estimate the time averaged paleomagnetic field direction representative of the time that the rock unit acquired its magnetization.

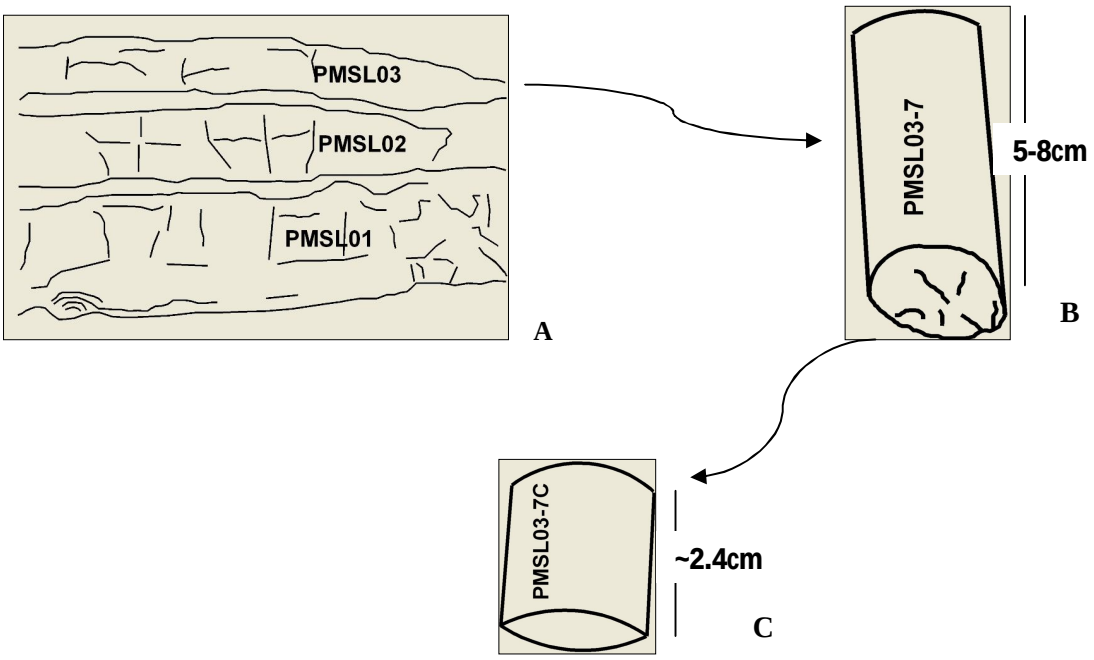

Fig 5.1 Generalized Paleomagnetic sampling schemes. A- Multiple sampling sites (lava flows) are collected within a rock unit; B-sample collected from a site; C-Specimen for laboratory measurements is prepared from samples.

The objective of averaging geological and sampling "noise" is achieved by taking a number N of individually oriented paleomagnetic samples from a single rock unit (called a paleomagnetic site). The most careful sample orientation procedure has an uncertainty of some 3^0. Precision is gained proportional to $\sqrt{N}$, so to improve the precision from 3^0 to 1^0, nine individually oriented samples are required. The number of samples taken should be tailored to the particular project at hand. If one wishes to know polarity, perhaps three samples would be sufficient (those would be taken primarily to assess "geological noise"). If, on the other hand, one wished to make inference about secular variation of the geomagnetic field, more samples would be necessary to suppress sampling noise.

Samples can be taken in the field using a gasoline powered drill or as "hand samples". The samples must be oriented before they are taken from the rock units. If a magnetic compass is used to orient samples in the field, the measured azimuth must be adjusted by the local magnetic declination. A dial with a vertical needle (a "gnomon") is placed on the horizontal platform. The angle (α) that the sun's shadow makes with the drilling direction is noted as well as the exact

time of sampling and the location of the sampling site. With this information and the aid of the Astronomical Almanac or a simple algorithm, it is possible to calculate the desired direction to the reasonable accuracy.

There are several levels of paleomagnetic data analysis at which mean directions must be calculated:

I) If more than one specimen was prepared from a sample, then ChRM directions for the multiple specimens must be averaged.

II) Site mean ChRM direction is then calculated from the sample ChRM directions.

III) Generally, a paleomagnetic investigation involves numerous sites within a particular rock unit. These site-mean directions must be averaged to yield either the average ChRM direction or a paleomagnetic pole position from the rock unit.

Where linear vector components were identified the ChRM is determined using the Principal Components Analysis (abbreviated as P.C.A). From a set of observation, P.C.A. determines the best fitting line through a sequence of data points. In addition, a Maximum Angular Deviation (MAD) is calculated to provide a quantitative measure of the precision with which the best fit line is determined. Although no strict convection exists, line fits from p.c.a. that yield MAD$\geq 15^0$ are often considered ill defined and of questionable significance (Butler, 1992).

Once a mean direction is calculated, the precision parameter (k) and a confidence limit (α_{95}) are determined. Precision parameter (k) measures the dispersion of the population of directions from which the sample data set was drawn whereas the confidence limit (α_{95}) is a measure of the precision with which the true mean direction has been estimated.

The above mentioned basics and principles of Paleomagnetism were applied in this study in order to explain the tectonics of the northern Afar.

5.2. Methodology and approach of the study

The study was done in three phases, which were (I) pre-field, (ii) field work and (iii) laboratory work

5.2.1 Pre-field work

The pre-field work mainly includes literature reviews, collection of existing data, analysis and study of the Digital Elevation Model (DEM), satellite imageries and aerial photos of the study area. The two days preliminary field work from 28/11/08 to 29/11/08 around Metehara area of the Main Ethiopian Rift was made to be familiar with the sampling and drilling techniques of oriented core samples and gasoline powered portable drilling apparatus. A total of 12 oriented core samples were drilled from Ignimbrite exposure and sun angle correction (Table 1) is made with the aid of Paleomac software package. Global Mapper, Erdas Imagine, Arc GIS, Mapinfo, 3DEM and Surfer are the GIS and Remote sensing software packages that were used throughout the study. Three Landsat ETM+ scenes were analyzed and processed in order to show the lithologcal and structural features of the study area; in particular and Manda Hararo rift; in general. Paleomac and Remasoft were used for the paleomagnetic data analysis and interpretation.

Table 1- corrected data for sun angle using paleomac software

Site: METEHRA
Lat= 8°54'24.00" (8.9067°)
Lon= 39°54'40.00" (39.9111°)
Date (dd/mm/AZyear): 28/11/2008

Sample	Time	AzMag	AzSun	AzGeo	Decl
MT01-1	13:55	165.0	105.0	170.3	5.3
MT01-2	14: 2	189.0	132.0	197.7	8.7
MT01-3	14: 6	190.0	132.0	198.0	8.0
MT01-5	14:13	315.0	249.0	315.4	.4
MT01-6	14:17	351.0	306.0	12.6	21.6

5.2.2 Field work

In general, 34 sites were sampled for paleomagnetic study during the field work which was held from Feb. 18, 2009 to Feb. 30, 2009. In most cases sampling was restrained to middle and lower parts of the flows in order to detect reheating effects and partial alteration of magnetic oxides. Sampling locations were selected as a function of lithology and degree of weathering. Weathered and jointed rocks are very susceptible for oxidations and hence could have been affected by remagnetization. The primary purpose of sampling different flows is to average out secular magnetic variation.

Samples, 5-8cm long and 2.5cm in diameter, were cored from exposures using a portable gasoline powered drilling apparatus with water cooled diamond bit. After drilling an orientation stages was slipped over the sample while it was still attached to the outcrop at its base. Orientation stages have an inclinometer for determining inclination (dip) of the core axis and both magnetic and sun compass for determining azimuth of the core axis. The main advantages of the coring techniques are the ability to obtain samples from a wide variety of natural and artificial exposures.

At least 6 and up to 12 cores were drilled at a site. We sampled as many individual flows as could be safely reached from thick sequences of volcanic flows that are exposed along the scarps of horst blocks and few sites were from valley cut of intermittent streams.

5.2.3 Laboratory analysis

When a sample is measured in the laboratory, all the magnetization the rock has acquired since it was first formed is still present. This is called Natural Remnant Magnetization (NRM) and frequently the original (primary) magnetization, is overprinted by a younger, but weaker, secondary magnetization picked up by the earth's current magnetic field. Recognition and erasure of the secondary component of NRM is the major goal of this laboratory analysis (Butler, 1992).

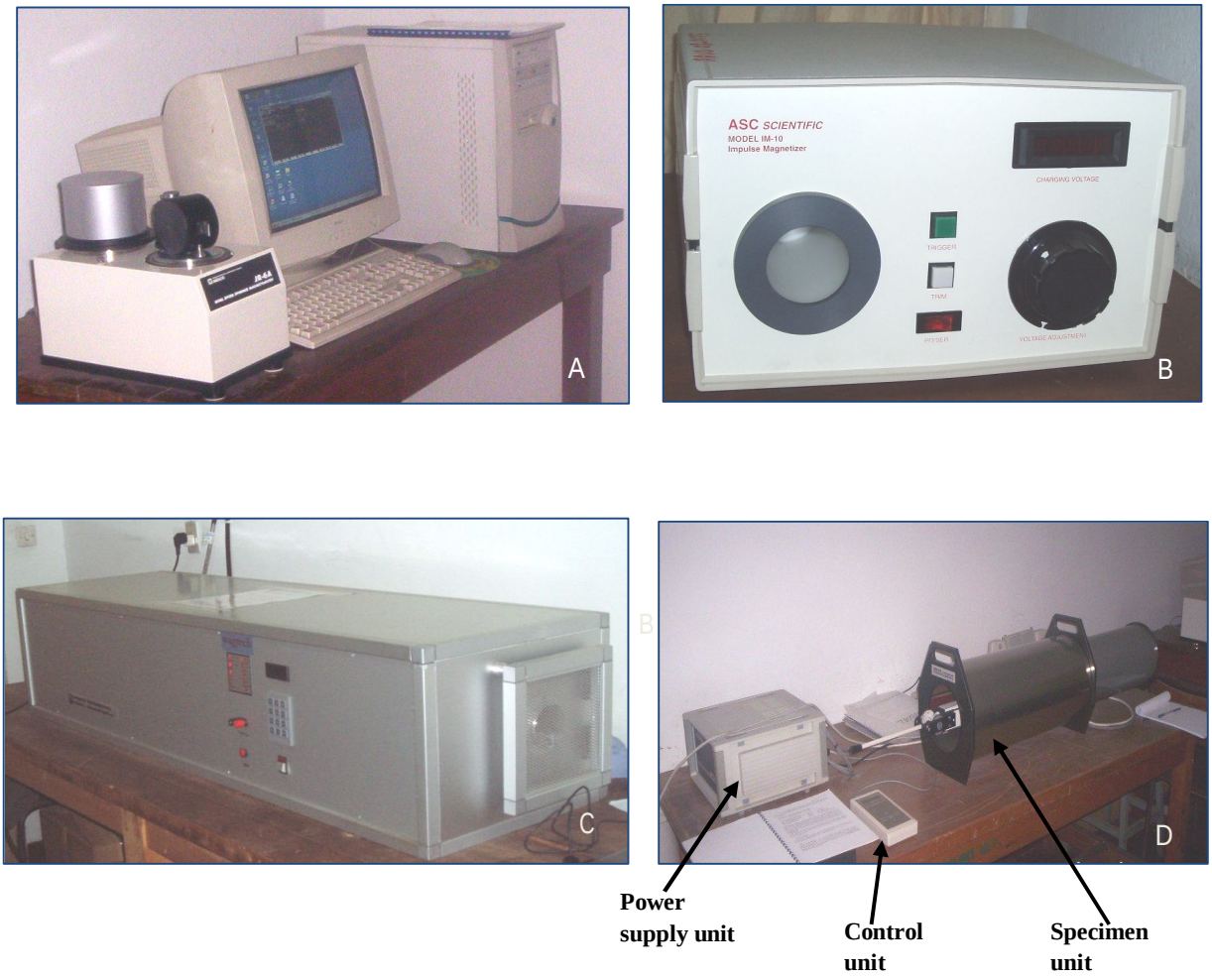

Fig.5.2. Laboratory facilities for Paleomagnetic study in Earth Sciences dept. of AAU .A) JR-6A spinner magnetometer attached to Dell machine; B) ASC Impulse Magnetizer; C) MMTD Thermal demagnetizer; D) LDA-3A Alternating filed demagnetizer; E) Dual blade core slicing saw.

The Laboratory analysis was conducted in paleomagnetic laboratory of Earth Sciences department of Addis Ababa University (Fig. 5.2). The laboratory is equipped with one JR6-A spinner magnetometer (nominal sensitivity ~2.4μA/m) attached to windows 2000 Dell machine and automated and micro-processor controlled LDA-3A triple mu-metal shielded Alternating field demagnetizer. This instrument consists of *three* units: the *specimen unit* consists of large mu-metal shielding that protects the specimen from the earth's magnetic field, the *power supply unit* generates electrical current that induces alternating magnetic field inside the demagnetizing coil and the *control unit* controls the whole process of demagnetization. The ASC IM impulse magnetizer is designed to produce a short duration high field pulse for the purpose of magnetization of samples. It is ideally suited for the study of acquisition of isothermal remnant magnetization (IRM) and anisotropy of IRM. Samples were sliced in to two or three cylindrical specimens with a typical volume of ~11cm^3 using Dual blade core slicing saw. Partial demagnetization experiment, alternating field was performed in the laboratory to isolate the Characteristic Remnant Magnetization (ChRM).

5.3 Sampling

Paleomagnetic samples were collected as part of the field excursion of Dabbahu rift which was organized by scientists from UK, New Zealand and Ethiopia. The aim of the expedition was to study the Dabbahu magmatic segment in the Manda Hararo rift of north afar.

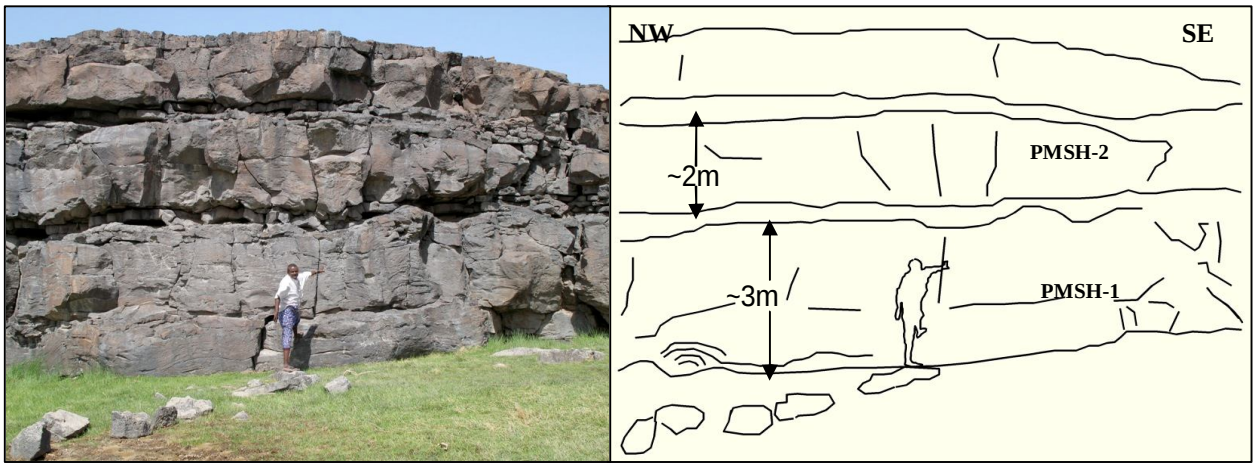

Fig 5.3 - NW-SE oriented normal fault in Saha area. Three lava flows with variable flow thickness can be identified.

271 oriented core samples were collected for paleomagnetic study from 34 sites. Sampling sites were chosen to be representative of a single lava flow and the location of each site is established using GPS. Cores were oriented in the field with both solar and magnetic compass except for site PMKR 03 which was oriented in the shadow. The orientation procedure was done in order to obtain accurate geographic orientation of each sample (Butler, 1992). The sun angle and local time are recorded as a check because of possible magnetic disturbances that might affect the magnetic compass reading. The overall mean difference between sun and magnetic azimuths is 2.8^0, with a standard deviation of 12.8^0 and standard error of 0.73^0.When 22 samples with differences larger than 15 are removed; the averages become 2.1^0, with standard deviation of 12.4^0 and standard error of 0.72^0. The rhyolites and vesiculated basalts were relatively difficult to drill and shorter and fewer number of samples were collected. Structural measurement (strike= 255^0 and dip= 009^0) was also made in the field for one site, PMKR 13, from rhyolite dome near Gago village; mid-way between Silsa and Kori. Sampling was mainly from 4 different localities; from Saha area (PMSH 1-3), Kori area (PMKR 1-18), Silsa area (PMSL1-7) and on the way to

Afdera (PMAF1-6) (see fig.5.5). Due to logistic difficulties, which include hot temperature, rugged terrain and very few access roads, most sample locations are within the Highway from Serdo to Afdera and a dry weather road from Silsa to Kori village.

The geological map of the study area was modified after the geological map of Danakil Depression (CNRS-CNR (Afar Team), 1973) by combining field and remote sensing studies and collected samples for paleomagnetic analysis. Three landsat Enhanced Thematic Mapper (ETM+) scenes, p168r051, p167r051 and p167r052, were mosicked and processed to delineate the different lithologic units which letter be named by results from petrographic analysis. The extents of mappable units are defined on the basis of field sampling and interpretation of processed landsat ETM+ data. The images clearly show volcanic features as well as fractures and faults (fig. 5.5).

Major faults in the northern part of the study area are oriented in NNW-SSE to N-S directions, whereas the southern part is affected by faults of NW-SE direction, orientation similar to Manda Hararo rift segment. The NNW-SSE normal faults could probably be the southern termination of the Tat'ale-Dader magmatic segment (see fig. 1.2 and 5.16).

The paleomagnetic sampling concentrated mainly on Basalts of recent volcanic products (Gulf Basalt of Kidane *et al*., 2003), which are known to be good recorders of magnetization. This unit mainly outcrops at the northeastern margin of Manda Hararo rift system. According to Kidane *et al*., 2003; the ages for this formation range between 0.59±0.16 and 1.11±0.09Ma. A total of 16 K-Ar age results are available for the studied area from P.Lahitte *et al*. (2003). Dating of rocks around Saha area revealed an age of 0.102±0.035 to 0.97±0.15Ma. Relatively older formations found south and west of Silsa, on the way to Kori village, having an age of 0.95±0.025 to 1.09±0.07Ma. Further north of Silsa, on the way to Afdera, the age ranges between 0.09±0.012 to 0.654±0.012Ma. Thus, the paleomagnetic results are indicative only of recent tectonics.

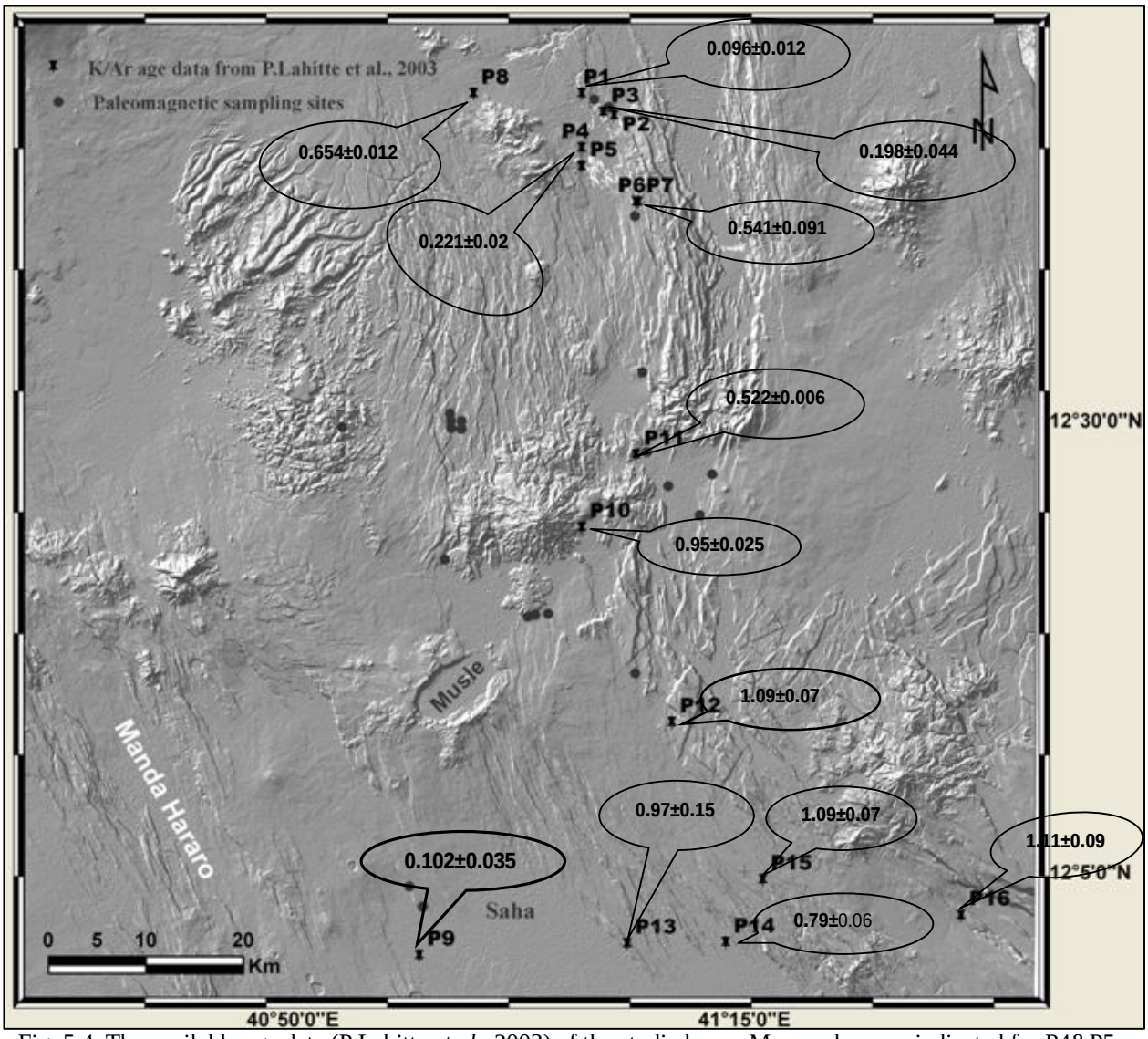

Fig. 5.4. The available age data (P.Lahitte *et al.*, 2003) of the studied area. Mean values are indicated for P4&P5 and P2&P3.

5.4 Laboratory treatment

The laboratory treatment was started by selecting six core samples from individual sites for specimen preparation. The rest of the samples are kept in the laboratory for further analysis. The cores were cut in the laboratory into 2.4cm long specimens.

For most of the cores, twin specimens were produced; one of the twins was demagnetized with AF while the other will be demagnetized thermally. In some cases, where the cores didn't

produce two specimens, some of them were treated with AF while the rest will be treated with thermal technique. Labeling was done in a systematic fashion for each core from top to base (away from the exposed surface in the field). A total of 347 specimens (from 204 samples) were obtained; and 175 were analyzed using Alternating field demagnetizer and led to the results presented here. All the measurements were performed in Paleomagnetic laboratory of the Addis Ababa University, Earth Sciences department.

The demagnetization process was done using alternating field demagnetizer. The alternating field instrument allows AF demagnetization to a maximum of 100mT and uses tumbler apparatus that rotates the specimen within several nested gears. The tumbler is designed to present in sequence all axes of the specimen to the axis of the demagnetizing coil. The tumbler thus allows demagnetization of all axes of the specimen during the course of a single demagnetization treatment. There were ten demagnetization steps used; 5, 10, 15, 20, 25, 30, 40, 60, 80 and 100mT with time of demagnetization of 30 seconds. These demagnetization steps were used based on the previous work of Kidane *et al*. (1999, 2003) of recent volcanic in Afar.

The remaining NRM was measured following each demagnetization step using a JR-6A spinner magnetometer. The program driving the magnetometer (REMA6) executes spin sequences and calculates the intensity in [A/m] corrected for the volume of the specimen. This program generates the text file with extension [.TXT] which later were transferred into Paleomac format and analyzed using PALEOMAC software package (Cogne, 2003) and the data file [.JR6], which is used as an input file for the Data Interpretation by software REMASOFT (Chadima & Hrouda, 2009) .

Standard measurement of the remnant magnetization vector consists of successive measurements in four positions of specimen. The complete measurement yields four values for Z component of RM vector and two values of X and Y components from which the average values are calculated (see Annex I). This process eliminates any residual non-compensated value of the holder RM and reduces measuring errors caused by an inaccurate shape of the specimen and by instrument noise.

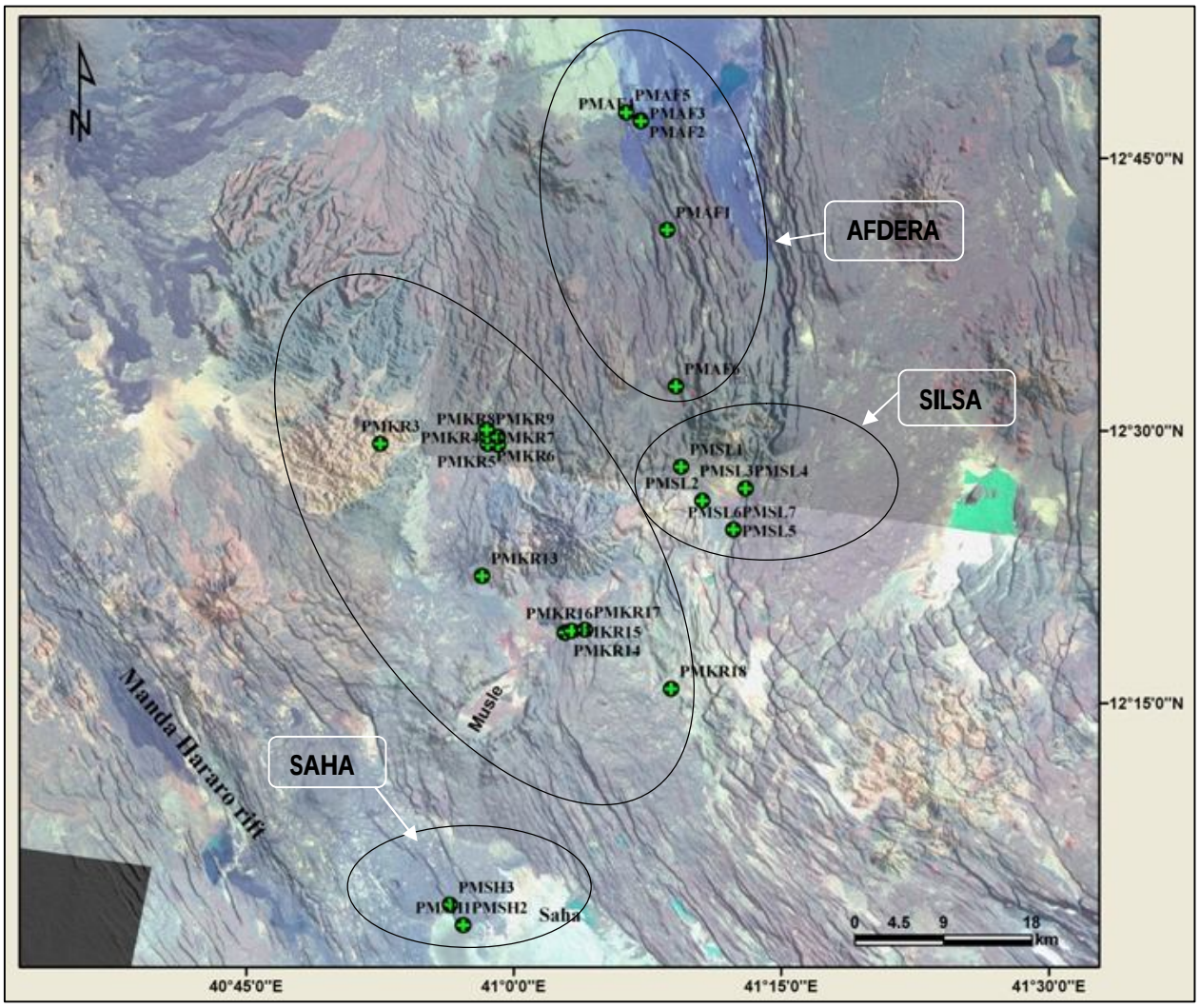

Fig.5.5 Landsat ETM+ imagery (bands 5, 3, 2 in R, G, B) showing sampling site overlaid by Digital elevation model of 90m resolution. All sites cannot be shown in areas with dense sampling.

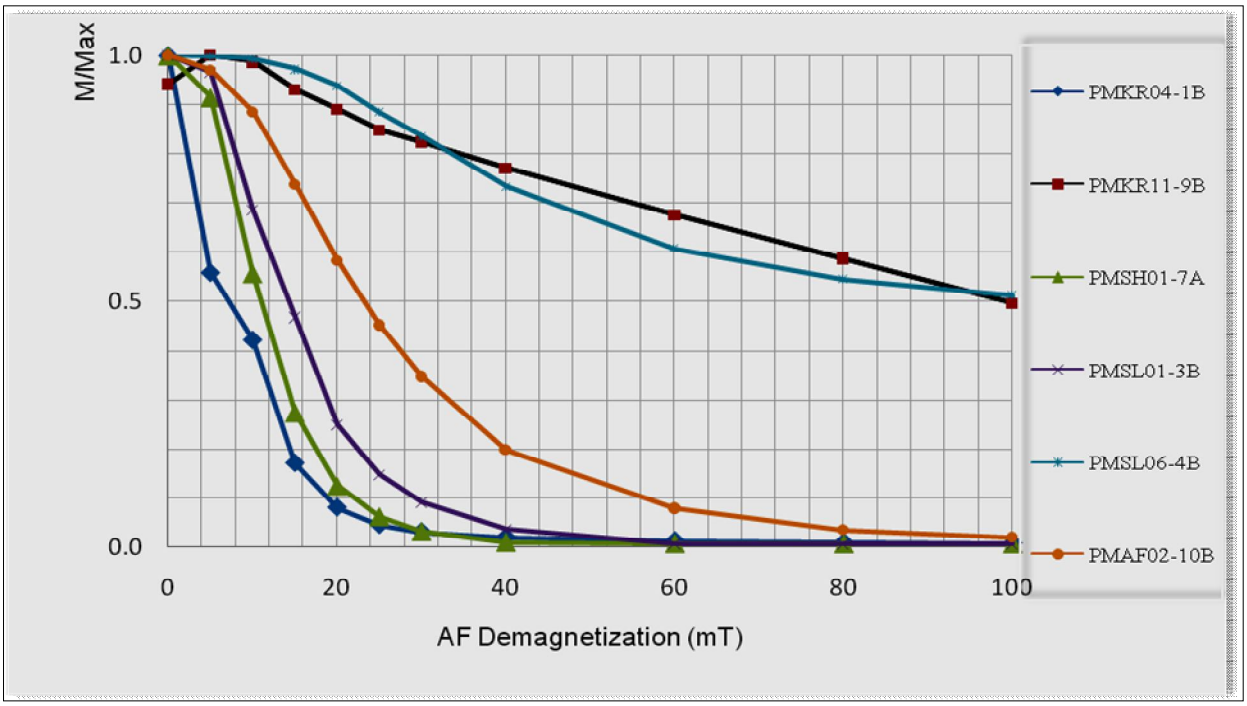

Fig. 5.6. Representative normalized intensity decay curve showing the result of alternating field.

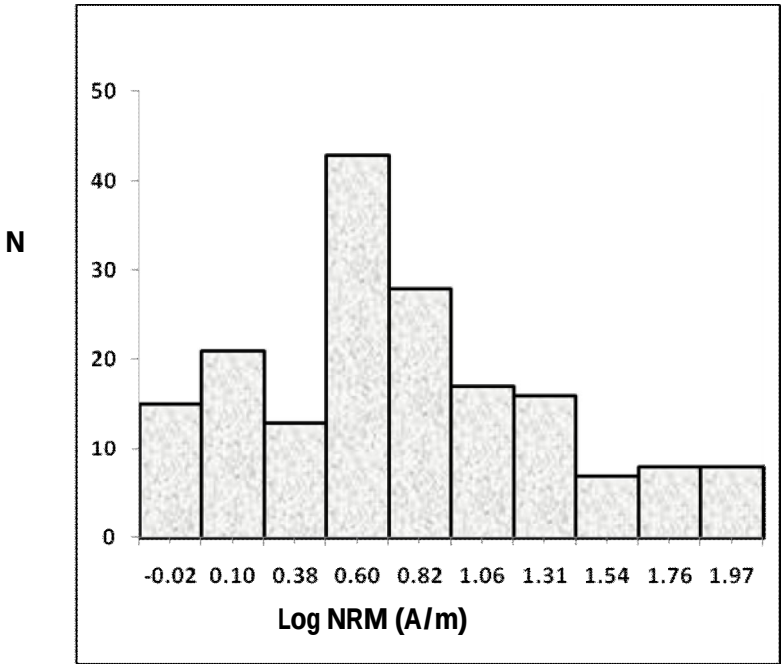

Fig.5.7 Histogram of NRM of the analyzed samples.

5.5 Data Analysis

On the orthogonal vector diagram, where linear vector components are identified, the ChRM is determined by least square technique (Kirchvink, 1980). Remagnetization circles (Halls, 1976, 1978) are used to deal with samples for which ChRM cannot be isolated directly because of overlapping blocking temperature spectra (coercivity spectra) or lightning strikes. This curvilinear array vector end point in the demagnetization diagram is shown in fig. 5.8.d. These remagnetization circles may intersect at the direction of one of the NRM components.

The Alternating field treatment identified one or two components of remnant magnetization. In general, AF between 0 and 30mT isolates the first component. The ChRM is interpreted as a straight line segment directed towards the origin which is isolated above 30mT. The natural remnant magnetizations (NRM) are shown in the histogram form in fig. 5.7. The NRM of cores ranges from 0.948A/m to 229A/m. the lowest value is observed from sample PMKR03, which the petrographic analysis showed, a lithic tuff unit. The intensity of NRM shows unimodal distribution with an overall mean of 9.77A/m. Strongly magnetized samples which correspond to lighting show intensity over several 10^2A/m (e.g. PMAF01-4B=229A/m).

Site mean directions were obtained from at least three cores. The confidence interval ($\alpha 95$) for most of the site means ChRM is less than 7^0. Only 3 samples show intervals greater than 10^0. Maximum Angular Deviation (MAD) of most of samples are $<1^0$ and no sample has MAD $>5^0$. Median Destructive Field (MDF) ranges from 4mT to above 90mT with most samples having MDF between 20mT and 35mT, suggesting that Pseudo Single Domain (PSD) grains as remnant magnetization carriers (Dunlop and Ozdemir, 1997). Demagnetization behavior for most of cores shows that 90% of NRM decay occurs between 15 and 70mT. This AF decay range is typical of Magnetite and Maghaemite (Dunlop and Ozdemir, 1997).

For almost all samples, the magnetization decay curve (Fig. 5.6) depicts a behavior in that the maximum intensity is attained at the NRM values, which would suggest that they are remagnetized in a direction similar to the ChRM.

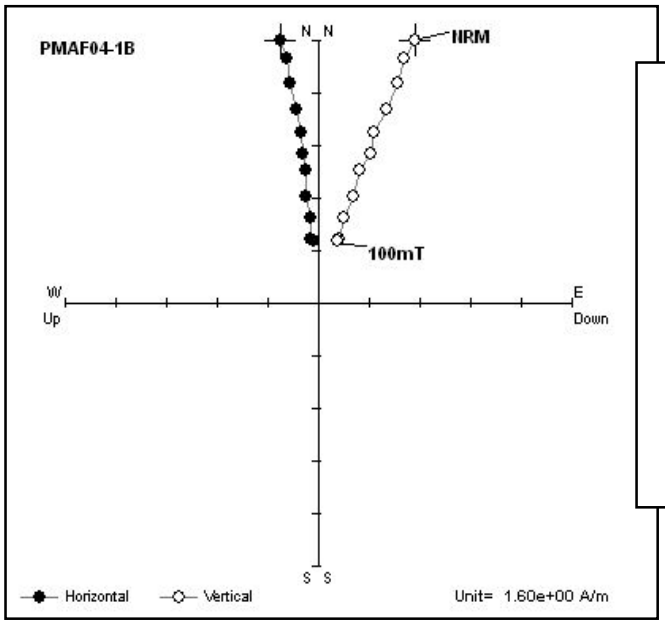
PMAF04-1B
N
N
NRM
100mT
W
E
Up
Down
S
S
Horizontal
Vertical
Unit= 1.60e+00 A/m

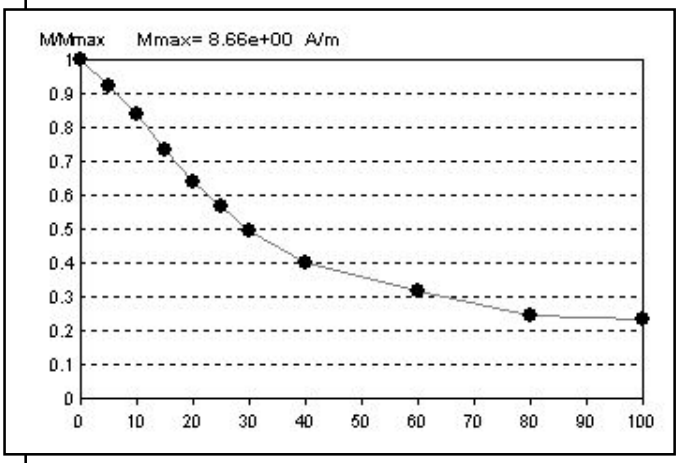
M/Mmax
Mmax= 8.66e+00 A/m
1
0.9
0.8
0.7
0.6
0.5
0.4
0.3
0.2
0.1
0
0
10
20
30
40
50
60
70
80
90
100

A

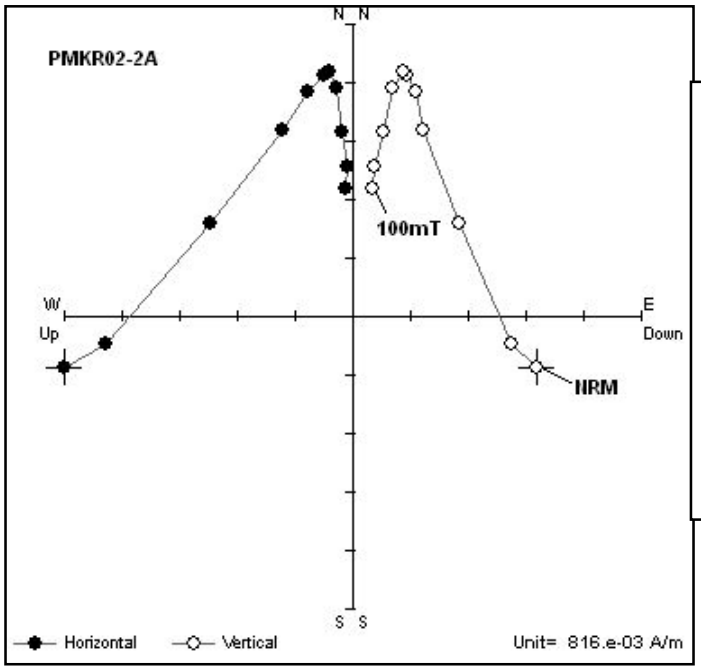
PMKR02-2A
N
N
100mT
W
E
Up
Down
NRM
S
S
Horizontal
Vertical
Unit= 816.e-03 A/m

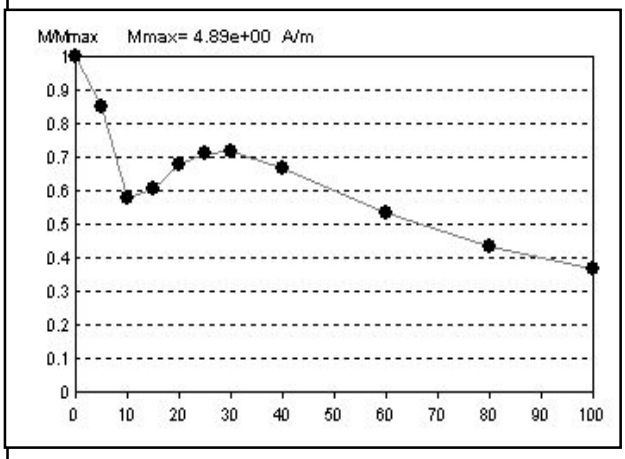
M/Mmax
Mmax= 4.89e+00 A/m
1
0.9
0.8
0.7
0.6
0.5
0.4
0.3
0.2
0.1
0
0
10
20
30
40
50
60
70
80
90
100

B

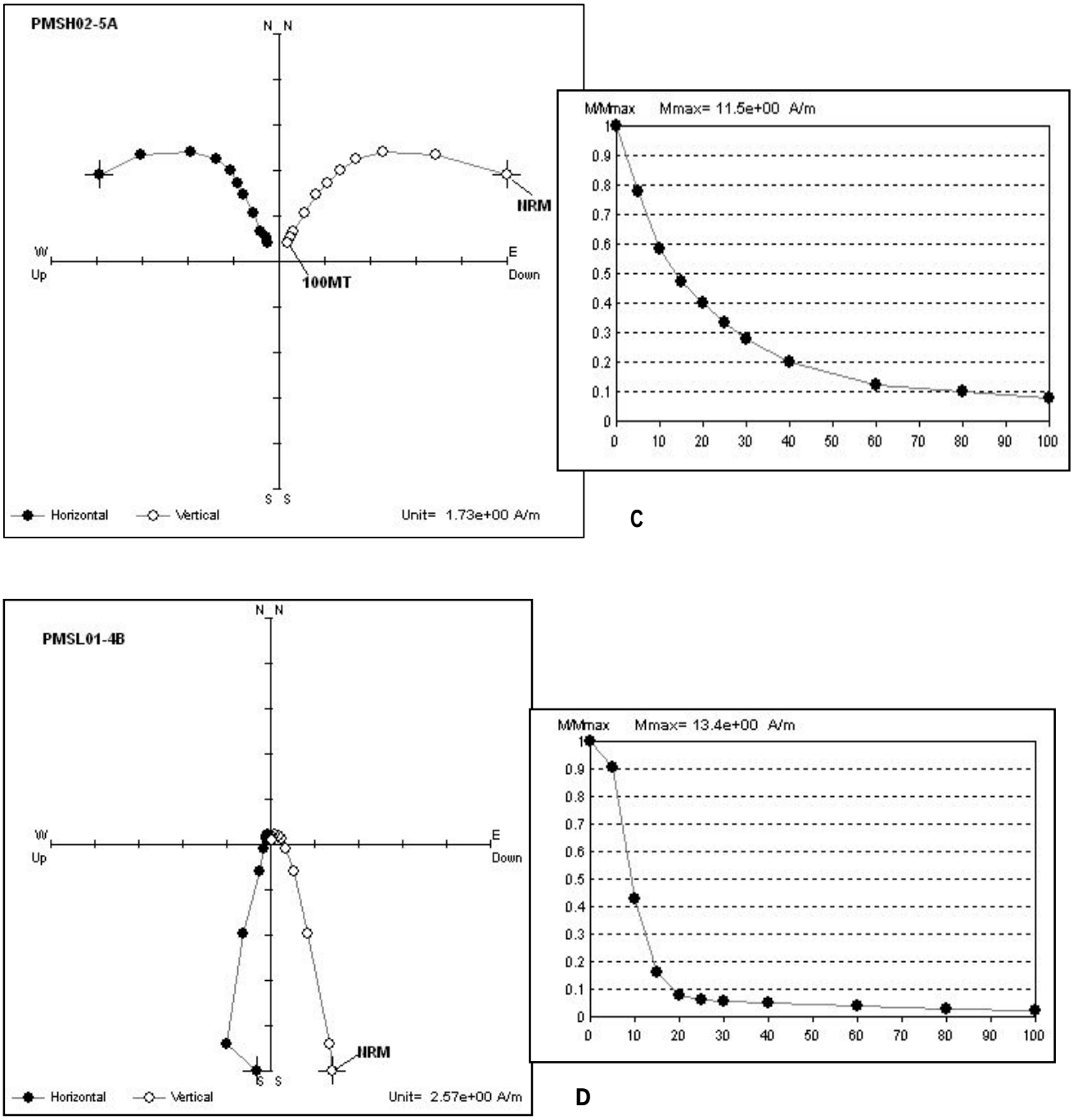

Fig. 5.8. Vector component diagram with normalized intensity decay plot of AF demagnetization behavior for four representative samples (A, B, C, and D).

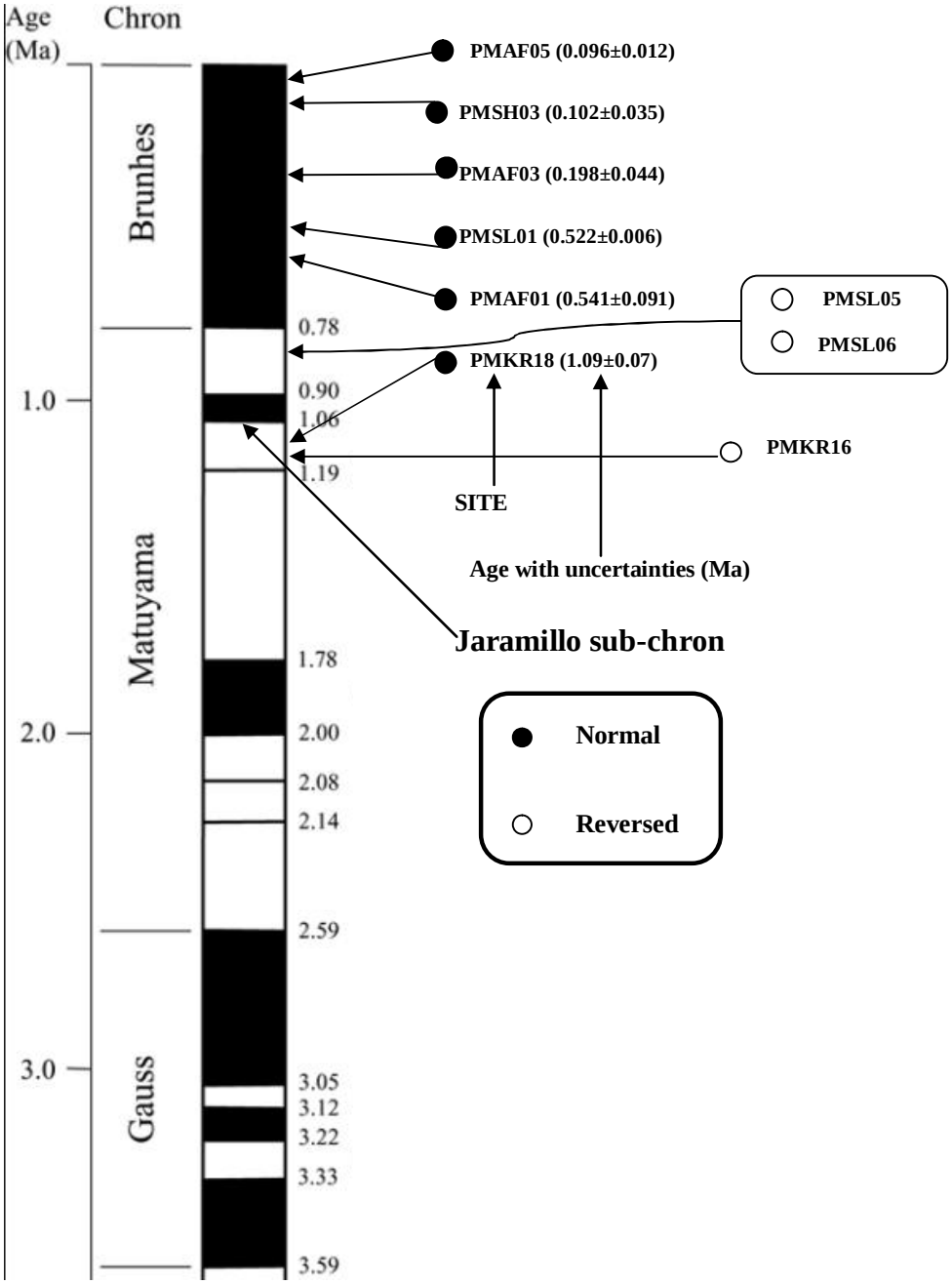

Cande and Kent (1995)

Fig. 5.9 Paleomagnetic polarity of some of the sampling sites plotted with the Geomagnetic Polarity Time Scale (GPTS) of (Cande and Kent, 1995).

5.6. Paleomagnetic Direction

The ChRM values determined at the specimen level then were used to calculate the core and site (flow) averages using Fischer (1953) statistices for combined analysis of remagnetization circles and stable linear segments. The mean directions with normal and reversed polarity seem to follow a fisherian distribution, although the direction from PMKR04 deviates from the overall distibution.

The mean direction is described for the three different localities. 18 oriented core samples were obtained from Kori locality, the mean direction is Ds=357.4^0, Is=15.1^0, N=17, K=32.1 and α_{95}=6.4**,** after excluding PMKR04 from the mean calculation due to anomalous direction(shown in italics in Table 2). The mean direction of Afdera from six samples is D=2.3^0, I=3.3^0, K=23.9 and α_{95}= 14.0. This high value of α_{95} (14.0) arises due to small number of sampling sites. The mean direction from Silsa is D=356.6^0, I=11.5^0, K=131.5, N=7 and α_{95}=5.3. Due to small number of observation from Saha area (three sites), the mean direction is described in the overall mean of the studied area.

The site averages calculated for all 34 sites are reported in Table 2. Out of the 34 sites, 30 sites show normal polarity and four sites reversed polarity. Becouse both normal and reversed polarities of the ChRM were observed, the time intreval of intrusion must have covered at least parts of two polarity intervals. Figure 5.11. illustrates all the mean paleomagnetic direction. The normal and reversed polarities are ~180^0 apart, indicating that the ChRM directions are free of secondary NRM components and that the time sampling afforded by the set of paleomagnetic data has adequately averaged geomagnetic secular variation. When an overall mean direction is calculated for 33 sites, the following values are obtained: Ds=357.1^0, Is=10.6^0, N=33, K=32.6 and α_{95}=4.4. Becouse there was no tilting of the young flows (except PMKR13) investigated in the study area, there is no difference in the site mean direction in geographic and stratigraphic coordinates. The tectonic correction for PMKR13 was negligible (ΔD=0.5). The paleomagnetic polarity and ages of samples of PMAF05, PMSH03, PMAF03, PMSL01, PMSL05, PMSL06, PMKR16 and PMAF01 show consistency with the Geomagnetic Polarity Time Scale (GPTS) reported

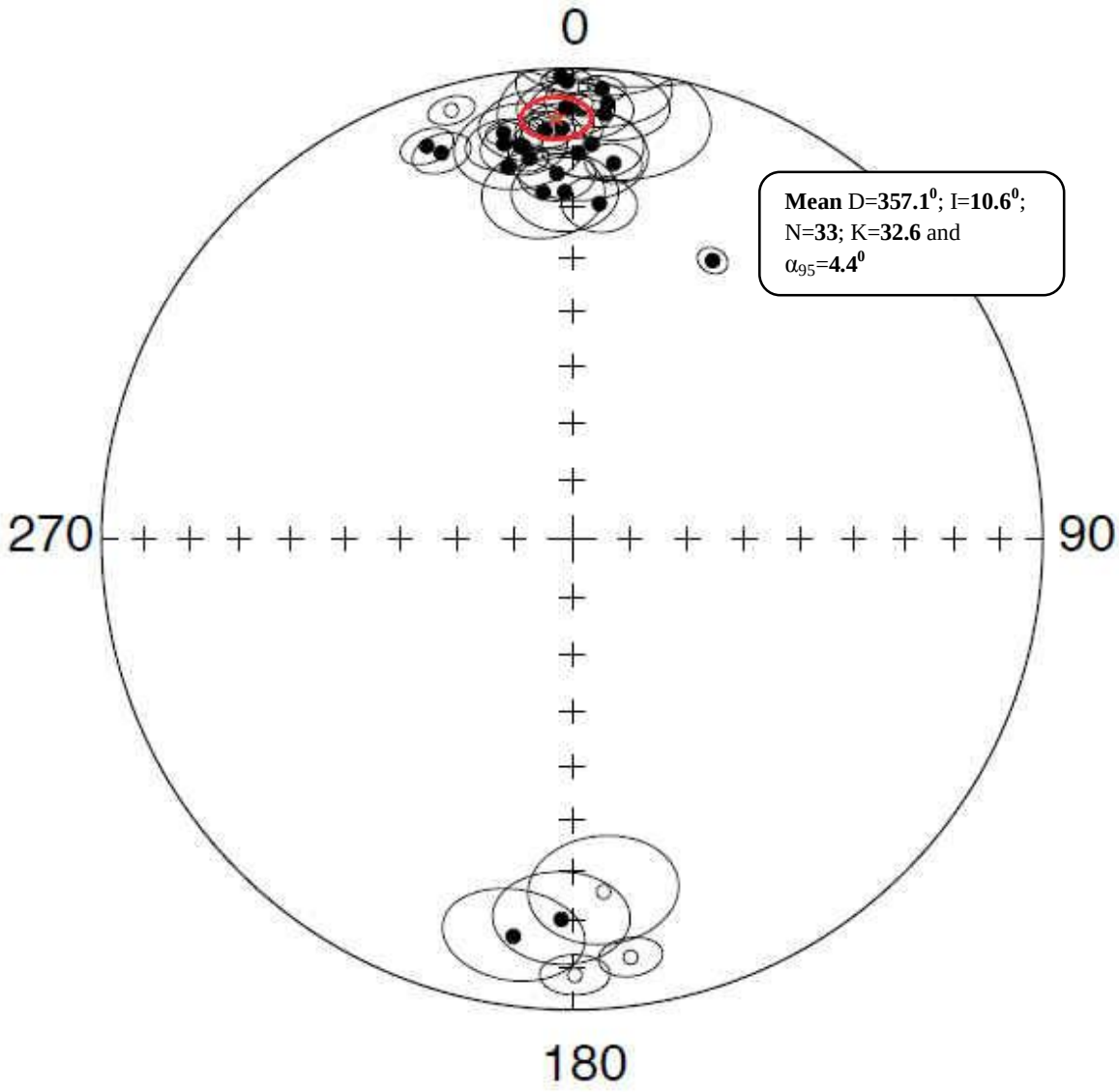

Fig. 5.10. Stereographic projections of all 34 sites. The red circle shows the overall mean of 33 sites (excluding PMKR04) having anomalous direction.

by Cande and Kent (1995)(Fig.5.9). The age of PMKR18 suggests that it is formed during the reversed Matuyama chron. However, taken the age determination error in to consideration, it is plausible that the lava flow was formed during Brunhes normal chron. This suggests that PMKR18 reflects a behaviour of geomagnetic field at the polarity transition.

Table 2. Summery of sampling sites and paleomagnetic results. The site in italics is not used in the mean calculation.

SITE	Coordinate		N	Ds	Is	Ks	α_{95}
	North(^{0})	East(^{0})					
PMAF01	12.6880	41.1490	10	355.0	-12.6	41.9	7.8
PMAF02	12.7890	41.1250	6	2.9	17.1	108.3	7.2
PMAF03	12.7880	41.1250	6	6.3	20.8	268.0	4.1
PMAF04	12.7880	41.1252	7	181.6	20.3	44.8	9.7
PMAF05	12.7960	41.1110	5	358.6	13.7	191.2	5.5
PMAF06	12.5440	41.1560	6	2.8	-3.5	47.4	9.8
PMKR01	12.4920	40.9890	4	359.1	9.2	203.8	6.5
PMKR02	12.4920	40.9890	4	3.8	4.6	944.0	3.0
PMKR03	12.4940	40.8790	3	357.6	23.3	494.4	5.6
[*PMKR04*]	*12.4930*	*40.9790*	*10*	*26.8*	*34.1*	*430.3*	*2.4*
PMKR05	12.4930	40.9800	3	4.6	7.9	230.2	8.1
PMKR06	12.4930	40.9810	3	1.3	9.3	330.5	6.8
PMKR07	12.4930	40.9795	3	339.7	12.0	1102.6	3.7
PMKR08	12.5000	40.9790	6	341.3	14.5	261.6	4.2
PMKR09	12.4990	40.9790	5	0.9	19.1	61.6	9.8
PMKR10	12.4991	40.9890	10	350.3	20.8	1730.8	1.2
PMKR11	12.4989	40.9891	6	350.2	15.9	157.5	5.4
PMKR12	12.5059	40.9785	6	352.4	16.7	352.4	9.1
PMKR13	12.3715	40.9734	3	353.0	17.0	416.8	6.0
PMKR14	12.3186	41.9503	5	1.8	-8.3	696.8	2.9
PMKR15	12.3189	41.0506	6	358.6	1.9	1285.0	1.9
PMKR16	12.3202	41.0568	4	174.9	-25.7	257.1	11.0
PMKR17	12.3213	41.0689	2	324.2	18.0	2.5	0.0
PMKR18	12.2664	41.1492	5	4.6	29.3	184.6	5.6
PMSH01	12.0508	40.9531	6	358.8	27.1	73.1	7.9
PMSH02	12.0508	40.9533	6	355.2	27.0	55.5	9.1
PMSH03	12.0070	40.9409	6	344.3	-6.0	465.5	3.1
PMSL01	12.4704	41.1602	6	4.4	10.3	23.3	14.2
PMSL02	12.4390	41.1799	5	350.4	13.6	966.9	2.5
PMSL03	12.4501	41.2203	6	353.6	19.7	583.9	2.8

PMSL04	12.4500	41.2210	6	356.2	14.0	271.8	4.1
PMSL05	12.4120	41.2087	6	172.0	-11.2	243.2	4.3
PMSL06	12.4120	41.2875	8	179.6	-8.1	146.3	4.6
PMSL07	12.4124	41.2089	6	359.4	3.1	427.2	3.2
MEAN (K)			17	357.4	15.1	32.1	6.4
MEAN(AF)			6	2.3	3.3	23.9	14.0
MEAN(SL)			7	356.6	11.5	131.5	5.3
MEAN	**12.4534**	**41.0902**	**33**	**357.1**	**10.6**	**32.6**	**4.4**

Site; geographic coordinate (North and East); N=number of samples; Ds and Is= Declination and Inclination in statigraphic coordinates; K= Fisher precision parameter and α_{95} is the confidance limit, MEAN(K)= Mean(Kori), MEAN(AF)= Mean(Afdera); MEAN(SL)= Mean(Silsa).

Reversed polarity (excursion) of PMKR04 is observed in the normal Brunhes chron (fig. 5.12).Several of such reversed excursions were evidenced in the normal Brunhes chron (e.g. Nowaczyk *et al*., 1994; Cande and Kent, 1995) in different parts of the world. These excursions are linked to pronounced lows in geomagnetic field intensities (e.g. Lund *et al*., 1998).

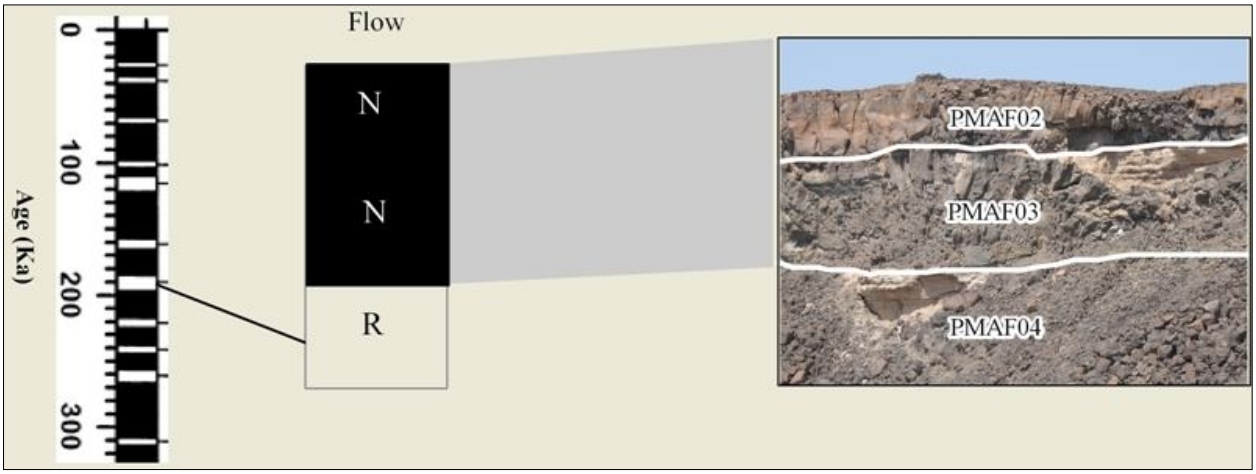

Fig. 5.11. Paleomagnetic polarity result from a series of 3 successive flows from Afdera site plotted against geomagnetic polarity time scale of Langeries *et al.* (1997), Lund *et al.* (1998), Nowaczyk & Frederichs (1999). Black represents normal and white represents reversed polarity.

Normal polarity site PMKR03 (Fig.5.4) is dated to be 0.198±0.044Ma. Considering the uncertainities, the age ranges between 0.242 and 0.154Ma. Fig. 5.11. indicates that the reversed

polarity PMKR04 is dated to be between 0.185Ma and 0.195Ma. Thus, K/Ar age determination and better defination of paleomagnetic polarity transition levels provided the chance of a better estimate for the age of lava flows from Afdera site.

5.7. Tectonic rotation

Fig. 5.14. indicates site mean directions from Kori and Saha areas. The paleomagnetic direction from the two areas is $D=353.8^0$, $I=13.7^0$ $\alpha_{95}=6.0^0$. Comparison of these direction with the predicted direction for stable Africa for ~2Ma (Kidane *et al.*, 2003), shows statistically significant rotation has occurred in the two sites. The rotation about a vertical axis is shown by difference in declination, **$R=-5.9^0\pm(8.6^0)$.** This value proves statistically significant counter clock wise rotation has occurred. Further comparison of the mean direction from the two sites with the Apparent Polar Wander Path curve of Besse and Courtillot, (1991), shows a rotation of **$-7.1^0\pm(6.7^0)$**.

As observed in other studies of Afar (e.g. Courtillot *et al.*,1984; Manighetti *et al.*, 1993; Kidane *et al.*, 1999, 2003; Acton *et al.*, 2000), the inclination is shallow when compared to the expected direction. The inclination flattening is $5.8^0\pm7.2^0$, which is in an agreement with the previous studies.

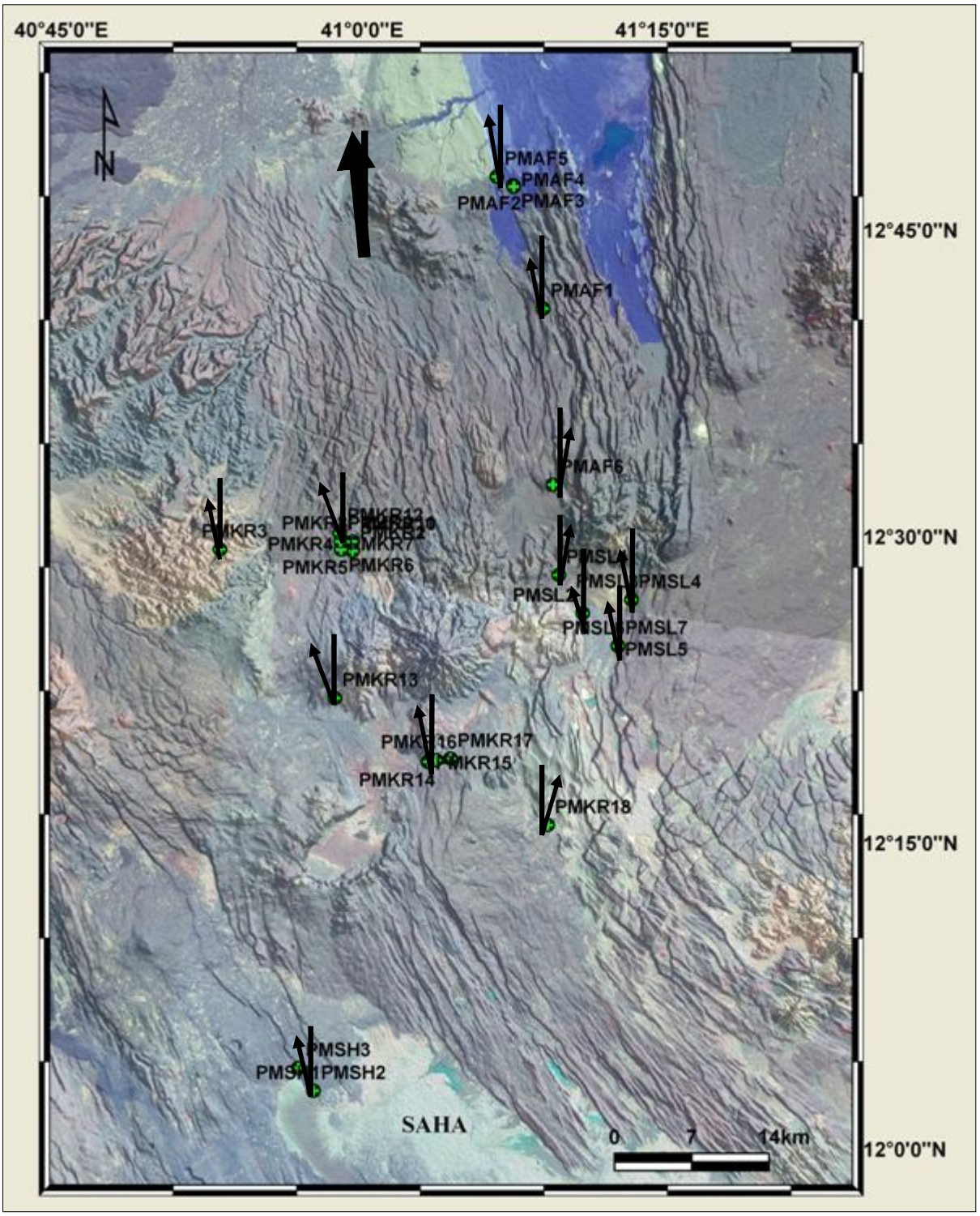

Fig. 5.12. Same as fig. 2.5. the site mean paleomagnetic directions are shown in black arrows. At each site, north direction is indicated by a longer dark line. The bold arrow indicates the overall mean paleomagnetic direction. The sites with stable reversed polarities are changed to their stable normal counterparts.

5.8. Paleosecular variation (PSV) and Virtual Geomagnetic Polarity (VGP)

Table 3 presents the VGPs of individual sites together with the mean paleomagnetic pole. A mean pole of, $\lambda=83.1^0$, $\phi=238.8^0$ K=56.2 and $\alpha_{95}=4.4^0$ is calculated for the 33 sites considered. This value is statistically similar to the value $\lambda=87.2^0$,$\phi=217.1^0$, and $\alpha_{95}=4.0^0$ of Kidane *et al*. 2003, for 'stable' part of Africa for the peirod ~2Ma.

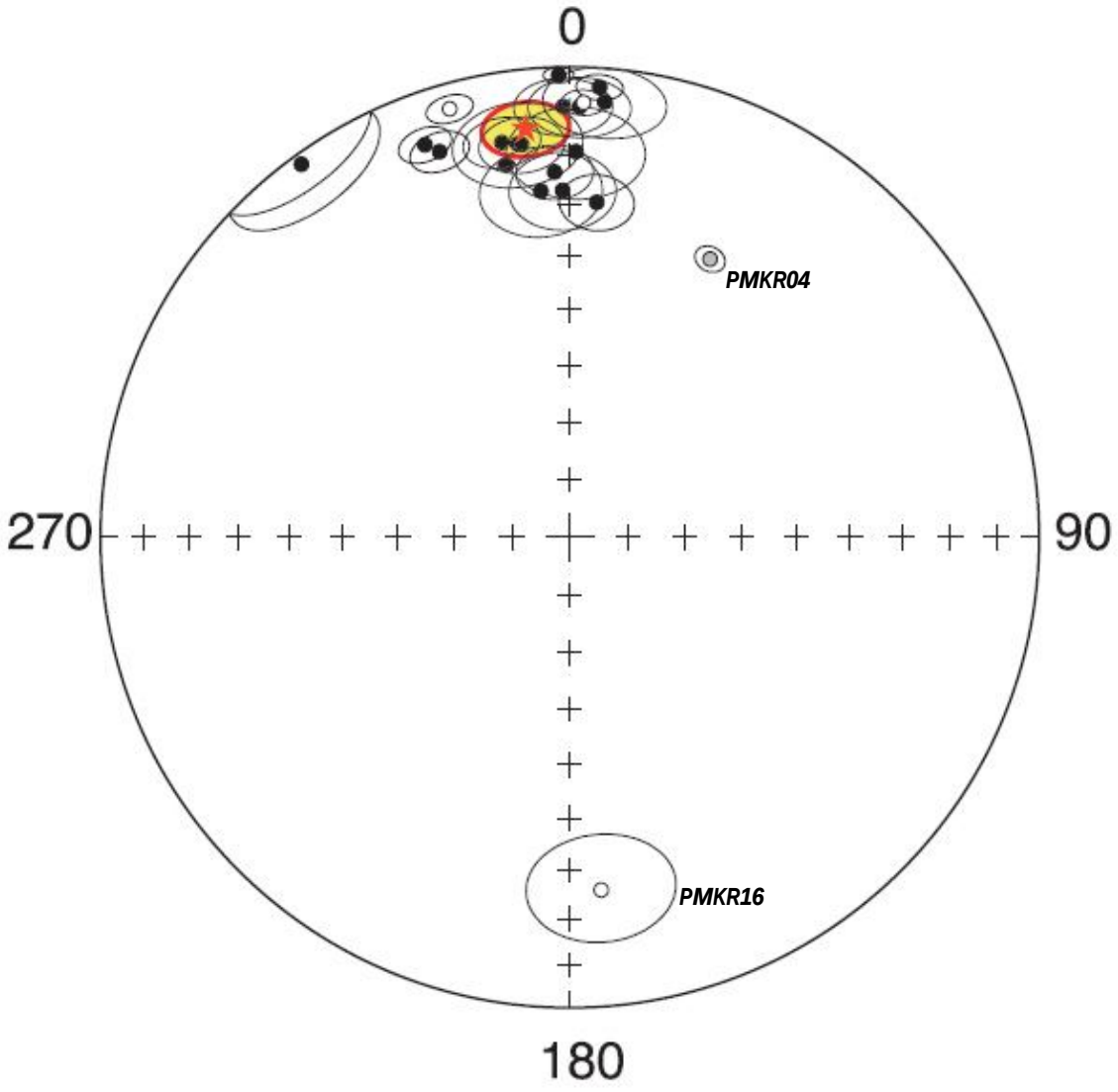

Fig. 5.13. Stereographic projections of sites from Saha and Kori. The red star indicates the mean for the two sites.

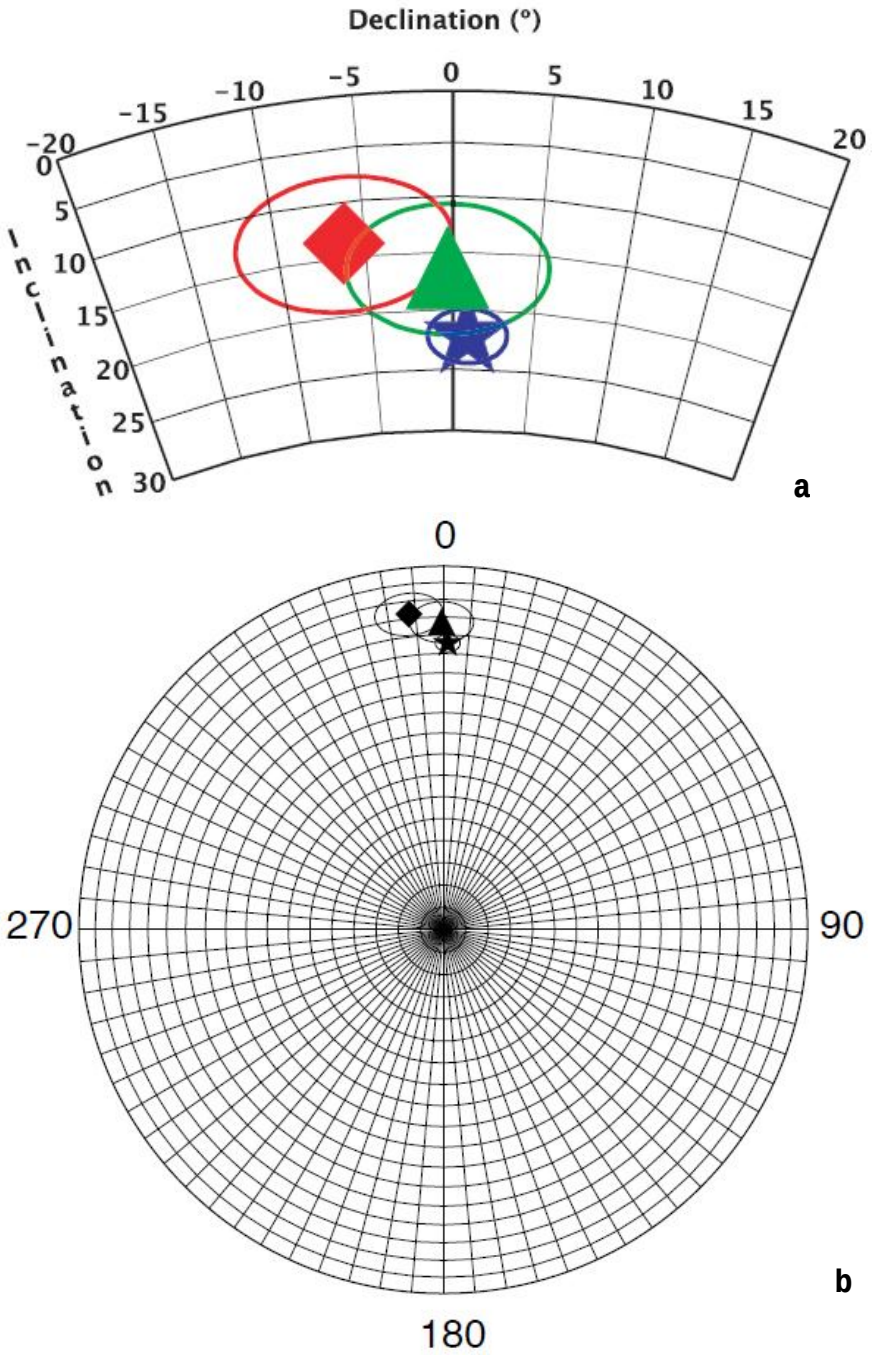

Fig. 5.14. Stereogram of mean ChRM from Kori and Saha after inverting the reversed polarity (PMKR16) to its normal counterpart and excluding anomalous direction of PMKR04. In both cases (a and b), the triangle and the star indicate expected direction for stable Africa for ~2Ma (Kidane et al.,2003) and mean expected referance dipole geomagnetic field (Besse and Courtillot, 1991), respectively. The diamond shape indicates the observed mean ChRM from Kori and Saha.

Table 3. site mean Virtual paleomagnetic poles (VGPs) for all analyzed sites and a mean paleomagnetic pole for 33 sites considered.

SITE	N	ϕ_s	λ_s	K	α_{95}
PMAF01	10	235.8	70.2	4	7.9
PMAF02	6	186.1	85.1	3.9	7.5
PMAF03	6	148.9	83.5	2.3	4.3
PMAF04	7	37	-66.7	5.3	10.2
PMAF05	5	234.8	84	2.9	5.7
PMAF06	6	210.1	75.5	4.9	9.9
PMKR01	4	227.4	82.1	3.3	6.5
PMKR02	4	200.8	79.1	1.5	3
PMKR03	3	303	87.7	3.1	5.9
(PMKR04)	*10*	*113.9*	*63.5*	*1.6*	*2.8*
PMKR05	3	192.4	80.3	4.1	8.2
PMKR06	3	211.6	82.1	3.5	6.9
PMKR07	3	295	69	1.9	3.8
PMKR08	6	297.2	70.9	2.2	4.3
PMKR09	5	202.3	87.2	5.3	10.2
PMKR10	10	301.8	80.3	0.7	1.3
PMKR11	6	287.5	79.4	2.8	5.5
PMKR12	6	283.6	81.5	4.9	9.4
PMKR13	3	283.6	82.1	3.2	6.3
PMKR14	5	214.6	73.4	1.5	2.9
PMKR15	6	228.2	78.5	0.9	1.9
PMKR16	4	145.8	-84.9	6.4	11.9
PMKR18	5	94	84.4	3.4	6.2
PMSH01	6	13.4	87.5	4.7	8.6
PMSH02	6	336.7	84.8	5.4	9.9
PMSH03	6	267.9	68.3	1.6	3.1
PMSL01	6	188.5	81.9	7.3	14.3
PMSL02	5	281.8	79.1	1.3	2.5
PMSL03	6	292.2	83.3	1.5	2.9
PMSL04	6	256.9	83.5	2.1	4.2
PMSL05	6	91.3	-79.7	2.2	4.4
PMSL06	8	43.7	-81.7	2.3	4.6
PMSL07	6	224.6	79.2	1.6	3.2
All Mean	**33**	**238.8**	**83.1**	**56.2**	**3.3**

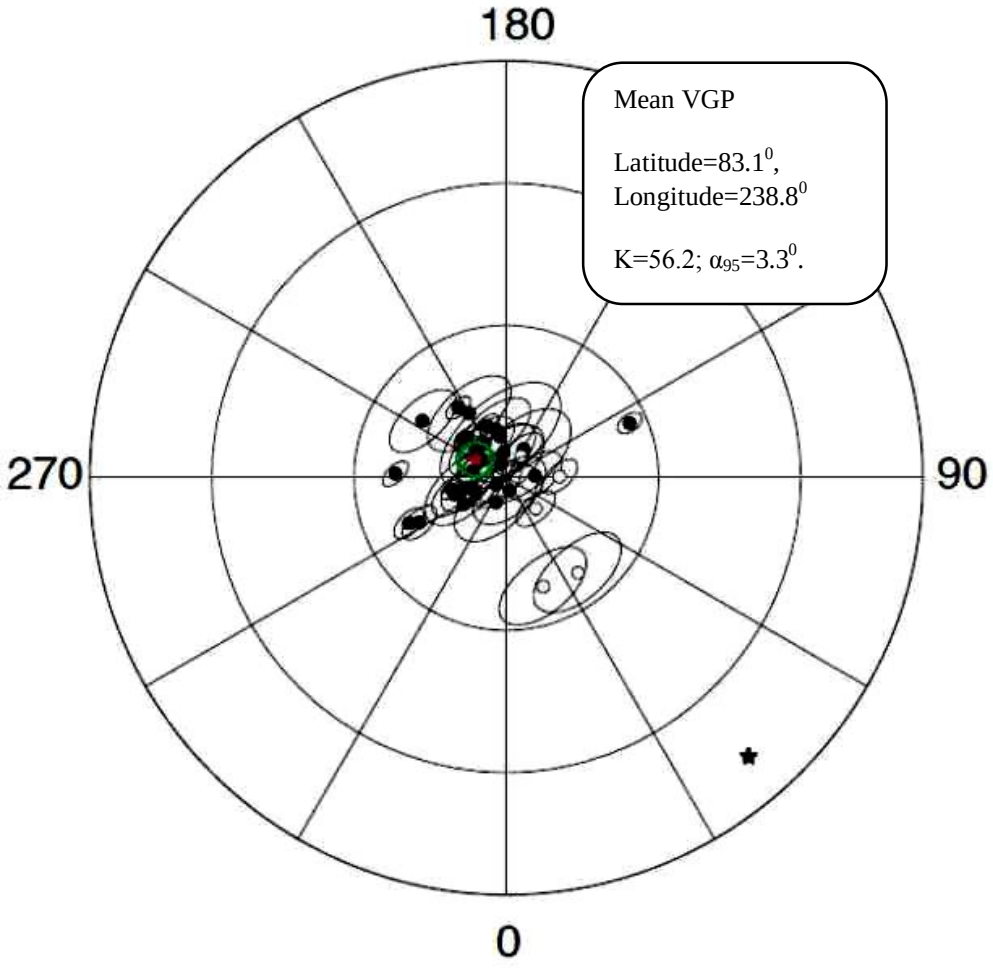

Fig. 5.15. Stereographic projection showing the VGP sactter of all the sites.

5.9 Discussion

The overlap and propagation of Red Sea and Gulf of Aden rifts in Afar depression is best described by the "Bookshelf" model of Tapponier *et al*. (1990) and Maneghetti *et al*.,(2001). This model requires rotation of small rigid blocks and is belived to induce dextral shearing that have caused the clock wise rotation about a vertical axis that is compensated by strike slip displacment along faults that are parallel to the rift. The initial overlap zone between Asal-Ghoubbet and Manda Hararo functioned between about 0.9Ma and 0.2Ma. About 0.2Ma, the Gulf of Aden propagated as a right step to NW of Afar. This more than double the size of the

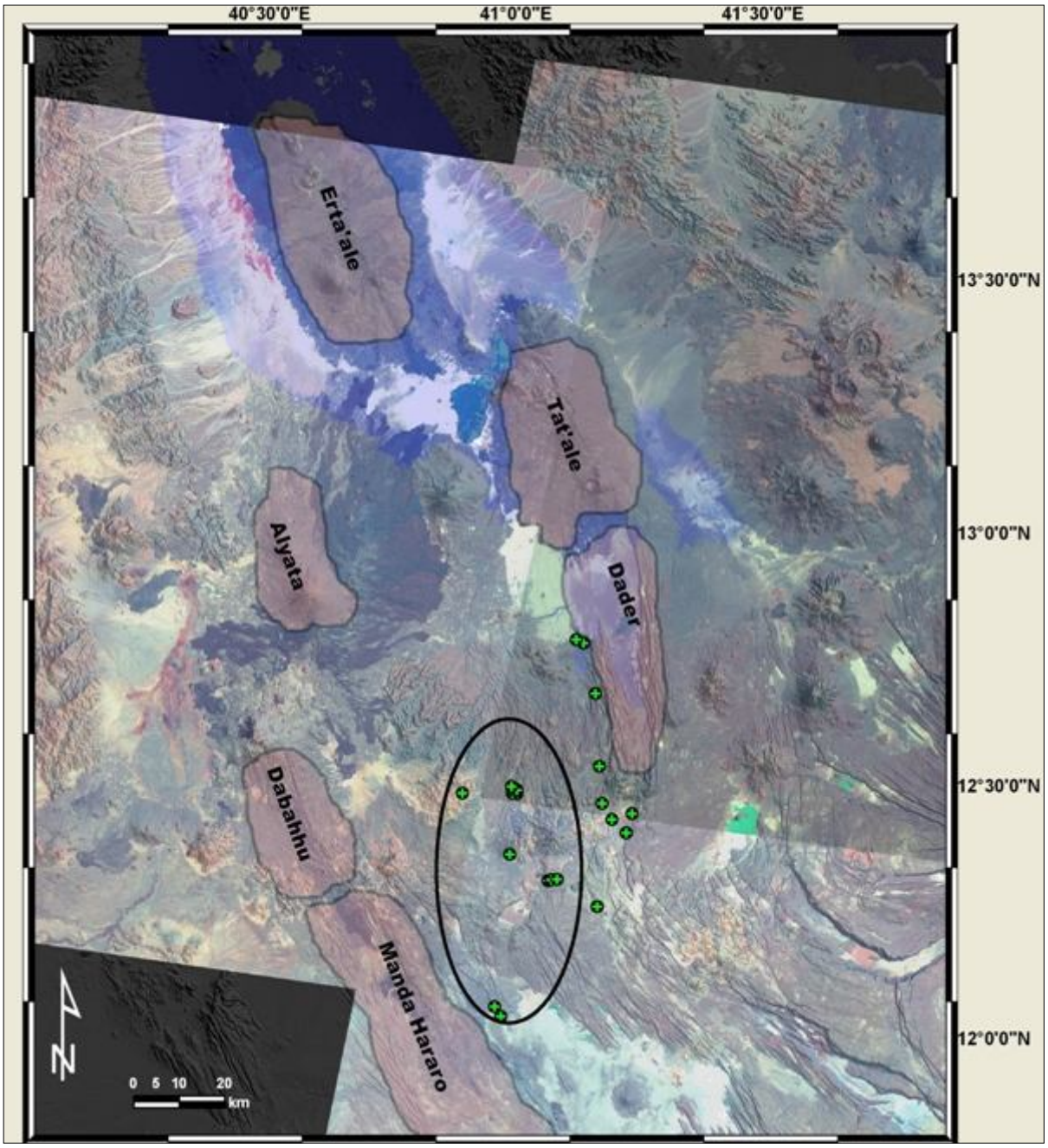

Fig. 5.16. Rift propagation and overlap of Erta'ale-Manda Hararo and Erta'ale-Dader trends (modified after Manighetti et al.,2001). The circle indicates sites where statistically significant counter clock wise rotation is recorded.

overlap betweeen the two main rift branches and initiated faulting and bookshelf rotation in different parts of the overlap zone. Manighetti *et al*.,(2001a) predicted a rotation of 13 ± 1.5^0 for all blocks belonging to the first, older and only 2 ± 0.2^0 for blocks in the younger overlap. Courtillot *et al.,* (1984) revealed a clockwise rotation (14.5 ± 7.5^0) in the Afar Stratoid series of a wide region between Lake Abhe and the Asal-Ghoubbet region, Acton *et al*., (1991, 2000) estimated ~11^0clock wise rotation for blocks in eastern Afar and ~3 to 4^0 for blocks in central Afar (i.e. NW of Gamarri-Alol tear zone) in the last ~2Ma. Courtillot *et al*. (1984) and Tappoinner *et al*. (1990) consider some basalt younger than the Afar Stratoid Series south of Lake Asal to be unrotated. Vellutini (1990) dated these basalts to be 0.9Ma and regards this age as an upper limit of rotation. Different micro-blocks in the Central Block have rotated clockwise at different rates ranging between 0^0 and 13^0 with respect to the Ali-Sabieh block in the last 2Ma (Kidane *et al*., 2003).

Statistaically, significant counter clock wise rotation occurred from sites of kori and Saha areas. This rotation is attributed to the overlap of Erta'ale-Manda Hararo in the west and Erta'ale-Dader in the east (fig. 5.17). Propagation along the Erta'ale-Dader trend probably stopped as the Tat'ale axial range reaches the 0.1Ma Dader graben (Lahitte, *et al*.,2003). Propagation along Erta'ale-Manda Hararo axial zone continous southward in the Tendaho-Gobbad discontinuity.

Thus, the current paleomagnetic observation is consistant with the idea that the North west of the overlap zone is not subjected to significant recent rotation, and only sizable rotations are predicted in areas where significant overlap occurred.

5.10. Conclusion

The paleomagnetic observation mainly concentrated on recent volcanic rocks of age 0.09 to 1.11Ma (Lahitte *et al*.,2003). Alternating filed demagnetization was used to isolate the ChRM. Least square technique (Kirchvink, 1980) was used where linear vectors are identified, where as the remagnetization circle (Halls, 1976,1978) was used to deal with samples for the ChRM can not be isolated directly.

Magnetic polarities of samples show consistency with the Geomagnetic Polarity Time Scale (GPTS) of Cande and Kent (1995). Geomagnetic Polarity Time Scale of Langeries *et al*. (1997), Lund *et al*. (1998), Nowaczyk & Frederichs (1999) is used to plot the reversed polarity excursion of PMKR04 in the normal brunhes chron. The normal and reversed polarities are 180^0 apart, showing that ChRM directions are free of the secondary component. Thus the AF treatment was efficient to determine the ChRM (e.g. Kidane *et al*.,2003).

Comparison of the overall mean direction with those predicted by Kidane *et al*.,(2003) for stable Africa~2Ma, shows statistically negligible rotation for the Manda Hararo rift but significant amount of local counter clock wise rotation is observed from Saha and Kori areas.

5.11. Recommendation

Based on the experience gained from this study and review of different journal articles, I recommend the following points.

- The paleomagnetic results should be accompanied with good radiometric age data to enhance the possiblity of using the results in future studies.
- Thermal demagnetization should also be used to identify the magnetization carrier minerals and for more precise determination of the ChRM.
- Afar wide paleomagnetic study is required to explain regional deformation in Afar depression prior to Modeling.

DECLARATION

I, the undersigned, declare that this is my work and that all sources of materials used in the thesis are dully acknowledged.

Ameha Atnafu Muluneh

Signature……

This Thesis has been submitted for examination with my approval as research advisor.

Dr. Tesfaye Kidane

Signature……

Addis Ababa, January 2010

SITE	STEPS	X	Y	Z	M
PMSL06-10B	NRM	7.35	11.69	14.62	2.011
	M5	8.34	12.24	14.43	2.069
	M10	8.37	12.41	14.38	2.076
	M15	8.26	12.02	14.11	2.029
	M20	8.34	11.23	13.48	1.943
	M25	7.57	10.85	12.57	1.825
	M30	6.82	10.27	11.71	1.7
	M40	6.03	8.84	9.68	1.442
	M60	4.53	7.5	6.45	1.088
	M80	3.13	6.8	3.86	0.8417
	M100	2.76	7.07	2.11	0.7879
	M100	2.76	7.07	2.11	0.7879
PMSL06-6B	NRM	3.7	9.05	7.85	1.3
	M5	3.63	9.16	7.83	1.259
	M10	3.77	9.01	7.81	1.25
	M15	3.74	8.84	7.72	1.232
	M20	3.29	8.34	7.45	1.165
	M25	3.43	7.85	7.07	1.11
	M30	2.97	7.44	6.61	1.039
	M40	2.61	6.3	5.75	0.8921
	M60	1.87	4.6	4.1	0.6434
	M80	1.47	3.24	2.84	0.4551
	M100	1.01	1.56	3.68	0.4124
	M100	1.01	1.56	3.68	0.4124
PMSL06-2C	NRM	0.3	10.78	-3.54	1.135
	M5	0.45	10.78	-3.54	1.136
	M10	0.34	10.75	-3.56	1.133
	M15	0.61	10.57	-3.46	1.114
	M20	0.46	10.15	-3.41	1.072
	M25	0.39	9.63	-3.32	1.019
	M30	0.32	9.06	-3.24	0.962
	M40	0.21	8.02	-2.94	0.8545
	M60	0.12	6.56	-2.65	0.7077
	M80	0.18	5.92	-2.39	0.6388
	M100	0.12	5.75	-2.16	0.6141
	M100	0.12	5.75	-2.16	0.6141
PMSL06-4B	NRM	1.1	11.76	-2.19	1.202
	M5	1.14	11.74	-2.23	1.2
	M10	0.7	11.69	-2.27	1.193
	M15	1.11	11.39	-2.33	1.168
	M20	1.04	11	-2.27	1.128
	M25	0.98	10.32	-2.32	1.063
	M30	1.03	9.74	-2.24	1.005
	M40	0.65	8.51	-2.2	0.8812
	M60	0.78	6.99	-1.96	0.7302
	M80	0.61	6.25	-1.81	0.6539
	M100	0.35	5.83	-1.95	0.6163
	M100	0.35	5.83	-1.95	0.6163
PMSH02-2C	NRM	-1.5	4.01	6.15	7.497
	M5	-1.39	3.44	5.73	6.825
	M10	-1.27	2.92	5.02	5.943
	M15	-1.06	2.57	4.19	5.023
	M20	-0.8	2.07	3.42	4.075
	M25	-0.67	1.69	2.83	3.363
	M30	-0.61	1.47	2.41	2.888
	M40	-0.509	1.148	1.838	2.226
	M60	-0.309	0.82	1.4	1.652
	M80	-0.266	0.62	1.048	1.246
	M100	-0.221	0.505	0.852	1.014
	M100	-0.221	0.505	0.852	1.014
PMSH02-1B	NRM	1.53	3.9	5.98	7.304
	M5	1.18	3.4	5.22	6.344
	M10	0.96	3.05	4.68	5.665
	M15	0.98	2.71	4.08	4.995
	M20	0.71	2.32	3.47	4.232
	M25	0.67	1.91	2.84	3.486
	M30	0.43	1.52	2.3	2.79
	M40	0.365	1.137	1.649	2.036
	M60	0.256	0.667	1.095	1.308
	M80	0.182	0.45	0.818	0.9509
	M100	0.168	0.343	0.735	0.8279
	M100	0.168	0.343	0.735	0.8279
PMSH02-10B	NRM	-5.06	-8.23	-0.56	9.674
	M5	-4.37	-7.83	-0.25	8.972
	M10	-4.02	-6.9	-0.01	7.985
	M15	-3.38	-5.97	0.2	6.865
	M20	-2.86	-5.17	0.24	5.913
	M25	-2.35	-4.49	0.28	5.074
	M30	-1.99	-3.89	0.26	4.378
	M40	-1.26	-3.18	0.24	3.579
	M60	-1.16	-2.33	0.27	2.621
	M80	-0.912	-1.861	0.232	2.085
	M100	-0.792	-1.602	0.177	1.795

	M100	-0.792	-1.602	0.177	1.795
PMSH02-7B	NRM	-5.28	-10.29	0.97	11.61
	M5	-5.1	-9.57	0.72	10.86
	M10	-4.61	-8.59	0.74	9.777
	M15	-3.93	-7.59	0.82	8.589
	M20	-3.48	-6.69	0.83	7.581
	M25	-2.95	-6.05	0.79	6.775
	M30	-2.42	-5.4	0.73	5.967
	M40	-2.22	-4.43	0.59	4.993
	M60	-1.8	-3.5	0.41	3.961
	M80	-1.39	-2.75	0.39	3.103
	M100	-1.11	-2.19	0.35	2.483
	M100	-1.11	-2.19	0.35	2.483
PMAF01-3B	NRM	30.79	57.6	-84.5	109
	M5	35.9	57	-88.6	111.2
	M10	25.2	55.4	-85.9	105.3
	M15	14	49.4	-65.7	83.39
	M20	8.9	40.6	-45.8	61.79
	M25	5.2	31.2	-31.5	44.63
	M30	2.5	24.1	-20.7	31.84
	M40	0.68	14.37	-9.75	17.38
	M60	-0.29	6.8	-3.22	7.527
	M80	-0.19	4.36	-1.61	4.653
	M100	-0.36	3.2	-1.12	3.404
	M100	-0.36	3.2	-1.12	3.404
PMAF01-4B	NRM	8.8	122.4	-192.9	228.6
	M5	4.1	121.4	-196.8	231.3
	M10	-10.2	123	-186.8	223.9
	M15	-12.2	112.1	-151.2	188.7
	M20	-10.9	94.8	-115.6	149.8
	M25	-10.9	76.2	-87.4	116.4
	M30	-7.2	60.7	-62.7	87.57
	M40	-4.4	36.6	-30.9	48.12
	M60	-1.83	14.51	-8.81	17.07
	M80	-1.04	7.72	-3.89	8.705
	M100	-0.67	4.94	-2.1	5.404
	M100	-0.67	4.94	-2.1	5.404
PMAF01-2B	NRM	34.8	54.6	-121.3	137.5
	M5	32.4	53.9	-127.5	142.1
	M10	24.9	49.5	-127.7	139.2
	M15	13.6	47.7	-101.5	113
	M20	7.9	40.1	-72	82.78
	M25	4.9	31.7	-47.6	57.43
	M30	2.4	24.9	-32.6	41.09
	M40	-0.32	15.13	-14.89	21.23
	M60	-0.73	7.15	-4.82	8.657
	M80	-0.71	4.67	-2.79	5.489
	M100	-0.59	3.53	-1.98	4.087
	M100	-0.59	3.53	-1.98	4.087
PMAF01-6B	NRM	0.6	37.5	-91.5	98.91
	M5	-1.5	35.6	-9.43	100.8
	M10	-3.4	32	-81.6	87.77
	M15	-1.9	26.8	-51.1	57.74
	M20	-2.2	19.6	-29.7	35.66
	M25	-2.03	13.96	-18.26	23.07
	M30	-1.41	9.71	-11.07	14.79
	M40	-1.55	6.12	-6.35	8.958
	M60	-1.01	3.38	-3.21	4.773
	M80	-0.91	2.41	-2.14	3.344
	M100	-0.774	1.959	-1.71	2.713
	M100	-0.774	1.959	-1.71	2.713
PMAF03-1B	NRM	-0.236	-0.732	0.847	1.144
	M5	-0.23	-0.72	0.834	1.126
	M10	-0.214	-0.71	0.817	1.103
	M15	-0.227	-0.689	0.79	1.073
	M20	-0.197	-0.676	-0.197	1.033
	M25	-0.202	-0.655	0.725	0.998
	M30	-0.204	-0.626	0.693	0.9563
	M40	-0.187	-0.589	0.63	0.882
	M60	-0.16	-0.502	0.53	0.7474
	M80	-0.124	-0.437	0.437	0.63
	M100	-0.083	-0.374	0.368	0.531
	M100	-0.083	-0.374	0.368	0.531
PMAF03-5B	NRM	-0.443	-1.583	0.308	1.672
	M5	-0.408	-1.576	0.309	1.657
	M10	-0.407	-1.545	0.308	1.627
	M15	-0.39	-1.523	0.309	1.602
	M20	-0.385	-1.492	0.305	1.571
	M25	-0.394	-1.451	0.299	1.533
	M30	-0.355	-1.409	0.301	1.484
	M40	-0.311	-1.316	0.294	1.384
	M60	-0.268	-1.122	0.271	1.185
	M80	-0.214	-0.987	0.249	1.04
	M100	-0.187	-0.884	0.222	0.9302

	M100	-0.187	-0.884	0.222	0.9302
PMAF03-3B	NRM	-0.308	-0.943	0.846	1.304
	M5	-0.279	-0.932	0.838	1.284
	M10	-0.286	-0.922	0.821	1.267
	M15	-0.259	-0.905	0.799	1.235
	M20	-0.237	-0.874	0.771	1.196
	M25	-0.236	-0.852	0.738	1.151
	M30	-0.219	-0.817	0.709	1.103
	M40	-0.195	-0.755	0.649	1.014
	M60	-0.147	-0.652	0.538	0.8583
	M80	-0.128	-0.553	0.452	0.7255
	M100	-0.102	-0.482	0.38	0.6221
	M100	-0.102	-0.482	0.38	0.6221
PMAF03-9B	NRM	-0.19	0.07	2.67	2.681
	M5	-0.18	0.06	2.66	2.665
	M10	-0.2	0.06	2.63	2.633
	M15	-0.17	0.05	2.56	2.571
	M20	-0.18	0.04	2.48	2.492
	M25	-0.16	0.01	2.39	2.4
	M30	-0.16	0	2.31	2.314
	M40	-0.14	-0.01	2.14	2.147
	M60	-0.111	-0.024	1.88	1.883
	M80	-0.077	-0.045	1.618	1.621
	M100	-0.085	-0.064	1.467	1.47
	M100	-0.085	-0.064	1.467	1.47
PMKR04-1B	NRM	-100.14	-20	-36.4	109.5
	M5	-54.4	-21.2	-18.3	61.2
	M10	-44.3	-13.1	-2.8	46.24
	M15	-18.03	-5.39	-0.03	18.82
	M20	-8.56	-1.82	0.19	8.751
	M25	-4.83	-0.13	-0.14	4.834
	M30	-3.29	0.46	-0.2	3.33
	M40	-2.05	0.66	-0.25	2.172
	M60	-1.154	0.688	-0.176	1.355
	M80	-0.821	0.547	-0.125	0.9945
	M100	-0.64	0.464	-0.099	0.7969
	M100	-0.64	0.464	-0.099	0.7969
PMKR04-3B	NRM	0.45	-9.19	16.39	18.8
	M5	-1.31	-3.01	8.36	8.981
	M10	-1.86	0.67	3.78	4.265
	M15	-1.72	1.24	2.66	3.401
	M20	-1.59	1.45	2.1	3.006
	M25	-1.39	1.406	1.788	2.665
	M30	-1.254	1.342	1.561	2.411
	M40	-0.984	1.144	1.194	1.924
	M60	-0.683	0.823	0.772	1.319
	M80	-0.445	0.633	0.514	0.9294
	M100	-0.33	0.571	0.374	0.7585
	M100	-0.33	0.571	0.374	0.7585
PMKR04-5B	NRM	-0.93	-3.53	9.66	10.33
	M5	-1.77	0.62	4.64	5
	M10	-1.77	1.99	2.64	3.754
	M15	-1.61	2.1	2.05	3.346
	M20	-1.48	1.911	1.739	2.978
	M25	-1.276	1.777	1.514	2.661
	M30	-1.155	1.603	1.303	2.367
	M40	-0.948	1.354	1.015	1.94
	M60	-0.557	0.899	0.679	1.256
	M80	-0.454	0.75	0.457	0.9891
	M100	-0.359	0.67	0.338	0.8317
	M100	-0.359	0.67	0.338	0.8317
PMKR04-2B	NRM	-2.91	0.21	10.77	11.16
	M5	-2.84	1.33	2.96	4.315
	M10	-2.55	2.23	1.01	3.542
	M15	-2.26	2.34	0.62	3.311
	M20	-1.97	2.22	0.46	3.007
	M25	-1.87	2.02	0.37	2.784
	M30	-1.55	1.835	0.265	2.416
	M40	-1.332	1.529	0.167	2.035
	M60	-0.908	1.103	0.065	1.43
	M80	-0.617	0.876	0.009	1.071
	M100	-0.46	0.74	-0.021	0.8716
	M100	-0.46	0.74	-0.021	0.8716
PMKR09-6B	NRM	7	-0.7	27.8	28.62
	M5	6.9	-1.4	26.6	27.49
	M10	4.07	-3.35	17.91	18.67
	M15	1.43	-4.56	9.06	10.24
	M20	0.31	-4	4.85	6.294
	M25	0	-3.47	3.21	4.729
	M30	-0.06	-2.99	2.22	3.726
	M40	-0.21	-2.33	1.47	2.766
	M60	-0.16	-1.621	0.893	1.858
	M80	-0.162	-1.212	0.638	1.379
	M100	-0.092	-0.971	0.506	1.099

	M100	-0.092	-0.971	0.506	1.099
PMKR09-1B	NRM	3.7	-54.2	92.4	107.2
	M5	6.9	-52.7	90.8	105.2
	M10	5	-49.7	75.8	90.77
	M15	4.8	-43.2	54.8	69.92
	M20	3.3	-35.2	37.8	51.79
	M25	3.1	-27.2	26.1	37.79
	M30	2.2	-20.7	18.9	28.14
	M40	0.3	-12.45	10.1	16.03
	M60	0.37	-5.54	4.12	6.912
	M80	0.08	-3.12	2.05	3.737
	M100	0.18	-2.01	1.32	2.412
	M100	0.18	-2.01	1.32	2.412
PMKR09-2B	NRM	12.7	-17.1	58.9	62.67
	M5	13	-17.6	57.1	61.17
	M10	9.7	-18.8	44.8	49.55
	M15	7	-16.1	29.3	34.16
	M20	4.64	-13.78	18.42	23.47
	M25	2.44	-10.59	11.7	15.97
	M30	1.55	-7.94	7.61	11.1
	M40	0.72	-4.8	3.95	6.253
	M60	0.24	-2.53	1.72	3.068
	M80	0.161	-1.614	0.978	1.894
	M100	0.11	-1.179	0.683	1.367
	M100	0.11	-1.179	0.683	1.367
PMKR09-3B	NRM	27.5	-26	84.1	92.19
	M5	27.2	-27.4	81.7	90.36
	M10	21.3	-27.9	63.9	72.87
	M15	14.9	-24.3	41.8	50.53
	M20	7.9	-19.1	26.4	33.59
	M25	5.35	-14.83	18.49	24.3
	M30	3.13	-10.81	11.96	16.43
	M40	1.62	-6.68	5.98	9.109
	M60	0.52	-3.19	2.47	4.066
	M80	0.186	-1.937	1.427	2.413
	M100	0.093	-1.374	0.994	1.699
	M100	0.093	-1.374	0.994	1.699
PMKR01-7B	NRM	-0.82	-5.03	-5.19	7.272
	M5	-1.89	-4.23	-5	6.816
	M10	-2.18	-2.92	-3.76	5.239
	M15	-1.45	-1.92	-2.7	3.613
	M20	-1.221	-1.302	-1.919	2.62
	M25	-0.868	-1.031	-1.495	2.013
	M30	-0.837	-0.708	-1.092	1.547
	M40	-0.488	-0.511	-0.759	1.037
	M60	-0.215	-0.321	-0.428	0.5768
	M80	-0.0829	-0.1798	-0.1815	0.2686
	M100	-0.298	-0.197	-0.222	0.4201
	M100	-0.298	-0.197	-0.222	0.4201
PMKR01-6B	NRM	-0.44	-9.38	-4.68	10.49
	M5	-1.41	-7.18	-4.46	8.571
	M10	-1.51	-4.67	-3.42	5.983
	M15	-1.31	-3.11	-2.46	4.175
	M20	-1.1	-2.12	-1.79	2.984
	M25	-0.702	-1.574	-1.354	2.192
	M30	-0.675	-1.26	-1.071	1.786
	M40	-0.408	-0.846	-0.682	1.161
	M60	-0.123	-0.592	-0.374	0.711
	M80	-0.188	-0.399	-0.316	0.5424
	M100	-0.128	-0.317	-0.25	0.4234
	M100	-0.128	-0.317	-0.25	0.4234
PMKR01-11B	NRM	-2.18	-8.11	3.11	8.951
	M5	-1.62	-5.63	-0.86	5.925
	M10	-1.64	-2.67	-1.3	3.386
	M15	-1.55	-1.93	-1.289	2.791
	M20	-1.488	-1.543	-1.236	2.475
	M25	-1.441	-1.335	-1.177	2.29
	M30	-1.39	-1.395	-1.171	2.291
	M40	-1.263	-1.21	-1.039	2.034
	M60	-1.24	-1.061	-0.955	1.891
	M80	-1.148	-0.992	-0.856	1.742
	M100	-1.028	-0.844	-0.771	1.538
	M100	-1.028	-0.844	-0.771	1.538
PMKR16-3B	NRM	-9.23	9.57	-14.46	19.64
	M5	-6.75	8.15	-9.26	14.06
	M10	-4.34	4.22	-6.04	8.553
	M15	-3.34	2.48	-4.47	6.11
	M20	-2.68	1.54	-3.54	4.705
	M25	-2.42	0.98	-3.01	3.986
	M30	-2.08	0.65	-2.57	3.368
	M40	-1.78	0.26	-2.06	2.732
	M60	-1.306	-0.189	-1.393	1.919
	M80	-1.091	-0.281	-1.121	1.589
	M100	-0.876	-0.287	-0.868	1.266

	M100	-0.876	-0.287	-0.868	1.266
PMKR16-5B	NRM	-12.12	12.33	-12.65	21.42
	M5	-7.84	8.99	-8.32	14.54
	M10	-5.48	4.81	-5.44	9.094
	M15	-4.25	2.92	-4.03	6.543
	M20	-3.59	1.93	-3.29	5.234
	M25	-3.18	1.33	-2.81	4.446
	M30	-2.8	1.09	-2.36	3.823
	M40	-2.26	0.58	-1.86	2.979
	M60	-1.596	0.081	-1.268	2.04
	M80	-1.279	-0.085	-0.905	1.569
	M100	-1.082	-0.181	-0.69	1.296
	M100	-1.082	-0.181	-0.69	1.296
PMKR16-7B	NRM	-17.17	4.12	-14.91	23.11
	M5	-12.94	2.3	-8.61	15.71
	M10	-9.31	0.12	-4.96	10.55
	M15	-6.69	-0.61	-3.22	7.447
	M20	-5.3	-0.73	-2.35	5.845
	M25	-4.34	-0.64	-1.89	4.773
	M30	-3.7	-0.72	-1.51	4.063
	M40	-2.84	-0.66	-1.12	3.121
	M60	-2.03	-0.54	-0.75	2.227
	M80	-1.61	-0.439	-0.648	1.79
	M100	-1.426	-0.428	-0.509	1.573
	M100	-1.426	-0.428	-0.509	1.573
PMKR08-4B	NRM	-3.89	-7.27	-6.75	10.65
	M5	-3.57	-6.36	-6.29	9.632
	M10	-2.2	-4.4	-3.42	5.989
	M15	-1.38	-2.98	-1.88	3.787
	M20	-1.08	-2.37	-1.34	2.929
	M25	-0.93	-2.02	-0.99	2.432
	M30	-0.774	-1.754	-0.826	2.087
	M40	-0.637	-1.365	-0.607	1.624
	M60	-0.464	-0.951	-0.363	1.119
	M80	-0.328	-0.729	-0.262	0.841
	M100	-0.257	-0.56	-0.19	0.645
	M100	-0.257	-0.56	-0.19	0.645
PMKR08-1B	NRM	-4.04	-5.1	-4.11	7.697
	M5	-3.49	-4.56	-4.24	7.139
	M10	-2.13	-2.93	-2.47	4.383
	M15	-1.38	-2.09	-1.43	2.886
	M20	-1.036	-1.833	-1.032	2.346
	M25	-0.913	-1.542	-0.809	1.966
	M30	-0.765	-1.358	-0.668	1.696
	M40	-0.582	-1.105	-0.478	1.338
	M60	-0.402	-0.782	-0.289	0.9259
	M80	-0.305	-0.633	-0.217	0.7359
	M100	-0.338	-0.514	-0.196	0.6461
	M100	-0.338	-0.514	-0.196	0.6461
PMKR08-2B	NRM	-5.76	-4.08	-6.31	9.467
	M5	-4.91	-3.58	-5.88	8.452
	M10	-2.92	-2.4	-3.32	5.033
	M15	-1.879	-1.709	-1.873	3.156
	M20	-1.437	-1.467	-1.3	2.43
	M25	-1.245	-1.31	-0.999	2.065
	M30	-1.079	-1.209	-0.787	1.802
	M40	-0.818	-0.95	-0.569	1.376
	M60	-0.52	-0.639	-0.335	0.889
	M80	-0.408	-0.495	-0.263	0.6934
	M100	-0.315	-0.402	-0.189	0.5446
	M100	-0.315	-0.402	-0.189	0.5446
PMKR08-3B	NRM	-4.09	-5.13	-6.77	9.429
	M5	-3.57	-4.59	-6.37	8.627
	M10	-2.27	-2.83	-3.59	5.104
	M15	-1.4	-2.03	-2.08	3.229
	M20	-1.196	-1.705	-1.491	2.561
	M25	-0.934	-1.458	-1.143	2.074
	M30	-0.843	-1.322	-0.91	1.813
	M40	-0.609	-1.014	-0.648	1.348
	M60	-0.466	-0.734	-0.413	0.9631
	M80	-0.338	-0.549	-0.278	0.7021
	M100	-0.237	-0.441	-0.217	0.5454
	M100	-0.237	-0.441	-0.217	0.5454
PMSL07-3B	NRM	-0.87	-5.73	-1.64	6.025
	M5	-0.68	-5.52	-1.58	5.781
	M10	-0.64	-5.22	-1.43	5.452
	M15	-0.54	-4.82	-1.24	5.006
	M20	-0.78	-4.39	-1.07	4.588
	M25	-0.38	-3.99	-0.88	4.101
	M30	-0.56	-3.63	-0.79	3.757
	M40	-0.36	-3.03	-0.6	3.106
	M60	-0.3	-2.28	-0.41	2.331
	M80	-0.294	-1.809	-0.283	1.855
	M100	-0.169	-1.464	-0.193	1.486

	M100	-0.169	-1.464	-0.193	1.486
PMSL07-1B	NRM	0.03	-5.95	-1.53	6.141
	M5	-0.38	-5.75	-1.55	5.972
	M10	-0.41	-5.5	-1.35	5.676
	M15	-0.47	-5.07	-1.16	5.222
	M20	-0.57	-4.55	-1.02	4.702
	M25	-0.37	-4.16	-0.87	4.27
	M30	-0.4	-3.81	-0.8	3.913
	M40	-0.23	-3.27	-0.61	3.33
	M60	-0.22	-2.45	-0.46	2.503
	M80	-0.14	-2	-0.35	2.04
	M100	-0.037	-1.67	-0.262	1.69
	M100	-0.037	-1.67	-0.262	1.69
PMSL07-7B	NRM	-1.58	-5.35	-1.71	5.832
	M5	-1.36	-5.2	-1.72	5.641
	M10	-1.2	-4.89	-1.57	5.27
	M15	-1.07	-4.58	-1.36	4.893
	M20	-0.96	-4.18	-1.2	4.456
	M25	-0.85	-3.79	-1.05	4.022
	M30	-0.88	-3.51	-0.92	3.731
	M40	-0.69	-2.96	-0.75	3.136
	M60	-0.53	-2.28	-0.55	2.405
	M80	-0.406	-1.844	-0.418	1.934
	M100	-0.221	-1.511	-0.343	1.565
	M100	-0.221	-1.511	-0.343	1.565
PMSL07-8B	NRM	-1.24	-4.51	-1.95	5.069
	M5	-1.27	-4.39	-1.93	4.962
	M10	-0.99	-4.2	-1.77	4.663
	M15	-0.92	-3.86	-1.55	4.254
	M20	-0.77	-3.52	-1.38	3.856
	M25	-0.85	-3.23	-1.22	3.556
	M30	-0.75	-2.95	-1.11	3.244
	M40	-0.61	-2.5	-0.92	2.733
	M60	-0.45	-1.99	-0.67	2.145
	M80	-0.354	-1.584	-0.496	1.697
	M100	-0.333	-1.341	-0.43	1.447
	M100	-0.333	-1.341	-0.43	1.447
PMSL03-1B	NRM	-1.44	-2.44	-0.49	2.876
	M5	-1.37	-2.43	-0.51	2.839
	M10	-1.33	-2.42	-0.49	2.803
	M15	-1.26	-2.3	-0.45	2.665
	M20	-1.16	-2.18	-0.39	2.497
	M25	-1.02	-1.99	-0.31	2.257
	M30	-0.965	-1.858	-0.257	2.109
	M40	-0.666	-1.507	-0.16	1.656
	M60	-0.47	-1.025	-0.118	1.134
	M80	-0.385	-0.748	-0.137	0.8522
	M100	-0.359	-0.534	-0.145	0.6598
	M100	-0.359	-0.534	-0.145	0.6598
PMSL03-2B	NRM	-1.66	-2.06	-0.71	2.746
	M5	-1.59	-2.13	-0.7	2.743
	M10	-1.62	-2.03	-0.67	2.678
	M15	-1.453	-1.94	-0.631	2.504
	M20	-1.457	-1.804	-0.564	2.386
	M25	-1.289	-1.717	-0.469	2.197
	M30	-1.137	-1.567	-0.404	1.978
	M40	-0.973	-1.289	-0.32	1.643
	M60	-0.624	-0.899	-0.218	1.115
	M80	-0.47	-0.626	-0.2	0.808
	M100	-0.415	-0.488	-0.198	0.6711
	M100	-0.415	-0.488	-0.198	0.6711
PMSL03-5B	NRM	-1.485	-1.66	-1.137	2.501
	M5	-1.431	-1.705	-1.141	2.501
	M10	-1.417	-1.61	-1.093	2.408
	M15	-1.302	-1.53	-1.003	2.246
	M20	-1.225	-1.394	-0.886	2.057
	M25	-1.06	-1.276	-0.756	1.823
	M30	-0.93	-1.144	-0.651	1.612
	M40	-0.723	-0.88	-0.481	1.236
	M60	-0.494	-0.6	-0.351	0.8522
	M80	-0.376	-0.45	-0.313	0.6648
	M100	-0.348	-0.337	-0.292	0.5652
	M100	-0.348	-0.337	-0.292	0.5652
PMSL03-7B	NRM	-1.491	-1.733	-0.944	2.473
	M5	-1.528	-1.718	-0.937	2.483
	M10	-1.338	-1.674	-0.892	2.322
	M15	-1.337	-1.588	-0.797	2.223
	M20	-1.157	-1.413	-0.694	1.954
	M25	-1.001	-1.318	-0.581	1.754
	M30	-0.801	-1.11	-0.484	1.452
	M40	-0.648	-0.916	-0.346	1.174
	M60	-0.47	-0.598	-0.264	0.8055
	M80	-0.393	-0.448	-0.24	0.6425
	M100	-0.322	-0.33	-0.214	0.5083

	M100	-0.322	-0.33	-0.214	0.5083
PMKR14-6B	NRM	1.69	-7.87	-5.98	10.02
	M5	1.21	-7.31	-5.14	9.017
	M10	0.48	-5.88	-3.73	6.976
	M15	-0.04	-5.1	-2.99	5.917
	M20	0.03	-4.43	-2.44	5.06
	M25	0.03	-3.91	-2.02	4.396
	M30	-0.18	-3.46	-1.7	3.858
	M40	-0.04	-2.73	-1.25	3.003
	M60	-0.047	-1.873	-0.836	2.052
	M80	-0.028	-1.391	-0.616	1.522
	M100	-0.056	-1.123	-0.515	1.237
	M100	-0.056	-1.123	-0.515	1.237
PMKR14-2B	NRM	0.89	-7.68	-7.27	10.61
	M5	0.71	-6.88	-5.77	9.012
	M10	-0.23	-5.62	-3.92	6.851
	M15	-0.09	-4.93	-3.11	5.826
	M20	-0.33	-4.29	-2.5	4.982
	M25	-0.23	-3.75	-1.98	4.245
	M30	-0.29	-3.24	-1.66	3.653
	M40	-0.17	-2.52	-1.23	2.811
	M60	-0.085	-1.68	-0.78	1.854
	M80	-0.16	-1.225	-0.576	1.363
	M100	-0.11	-0.935	-0.444	1.041
	M100	-0.11	-0.935	-0.444	1.041
PMKR14-3B	NRM	0.67	-7.33	-6.19	9.621
	M5	0.32	-6.78	-5.31	8.617
	M10	-0.44	-5.7	-3.83	6.884
	M15	-0.25	-5.08	-3.06	5.941
	M20	-0.25	-4.44	-2.5	5.098
	M25	-0.26	-3.85	-2.02	4.356
	M30	-0.17	-3.34	-1.66	3.737
	M40	-0.09	-2.66	-1.27	2.947
	M60	-0.131	-1.775	-0.797	1.95
	M80	-0.205	-1.286	-0.595	1.432
	M100	-0.119	-1.03	-0.515	1.158
	M100	-0.119	-1.03	-0.515	1.158
PMAF02-2B	NRM	6.8	-45.9	-7.7	47.02
	M5	7.9	-46.1	-6.2	47.17
	M10	8.6	-43.3	-0.6	44.2
	M15	6.7	-34.8	3.6	35.63
	M20	2.6	-25.7	5.2	26.34
	M25	2.62	-18.12	5.29	19.06
	M30	1.35	-12.81	4.54	13.66
	M40	0.79	-7.14	3.19	7.856
	M60	0.04	-3.14	1.72	3.585
	M80	0.087	-1.765	1.138	2.102
	M100	0.053	-1.242	0.852	1.507
	M100	0.053	-1.242	0.852	1.507
PMAF02-6B	NRM	-33.4	-60.2	-9.8	69.55
	M5	-30	-58.8	-6.7	66.38
	M10	-25.6	-54.4	1.1	60.1
	M15	-15.6	-41	6.2	44.36
	M20	-9.8	-28.8	6.9	31.2
	M25	-6	-20.7	6.1	22.4
	M30	-3.35	-14.77	4.94	15.93
	M40	-1.59	-8.21	3.17	8.94
	M60	-0.38	-3.35	1.49	3.683
	M80	-0.271	-1.828	0.864	2.04
	M100	-0.088	-1.163	0.555	1.292
	M100	-0.088	-1.163	0.555	1.292
PMAF02-8B	NRM	-10.34	-85.5	-42	140.6
	M5	-99.5	-83.9	-37.4	135.4
	M10	-82.4	-75.2	-24.2	114.1
	M15	-61.7	-61.7	-11.2	87.98
	M20	-40.8	-47.4	-3.7	62.64
	M25	-27.3	-35	0	44.42
	M30	-17.8	-26.2	2	31.72
	M40	-7.24	-13.91	1.99	15.81
	M60	-2.3	-5.72	1.48	6.342
	M80	-0.66	-2.66	0.75	2.842
	M100	-0.353	-1.532	0.49	1.647
	M100	-0.353	-1.532	0.49	1.647
PMAF02-10B	NRM	-118.2	-102.9	9.2	157
	M5	-113.6	-100.3	15	152.3
	M10	-95.4	-97.5	26.2	139
	M15	-69.6	-87.5	30.9	116
	M20	-47.9	-72.4	29.5	91.67
	M25	-31.9	-58.5	24.5	70.99
	M30	-22.3	-45.8	19.4	54.54
	M40	-9.9	-27.3	11.7	31.29
	M60	-2.55	-11	4.81	12.28
	M80	-0.89	-4.92	2.14	5.441
	M100	-0.62	-2.75	1.21	3.071

	M100	-0.62	-2.75	1.21	3.071
PMSL05-2B	NRM	-1.41	8.51	-5.74	10.36
	M5	-1.33	8.43	-5.79	10.31
	M10	-1.22	8.1	-5.65	9.953
	M15	-1.44	7.51	-5.36	9.337
	M20	-1.22	7.07	-5.02	8.758
	M25	-1.29	6.66	-4.75	8.285
	M30	-1.08	6.33	-4.54	7.859
	M40	-1.03	5.75	-4.18	7.182
	M60	-0.89	5	-3.63	6.241
	M80	-0.72	4.43	-3.17	5.501
	M100	-0.66	3.98	-2.85	4.941
	M100	-0.66	3.98	-2.85	4.941
PMSL05-4B	NRM	1.86	13.36	-2.65	13.74
	M5	1.61	13.31	-2.74	13.68
	M10	1.25	12.7	-2.82	13.07
	M15	1.46	12.08	-2.8	12.48
	M20	1.18	11.39	-2.71	11.76
	M25	1.29	10.91	-2.64	11.3
	M30	1.09	10.44	-2.53	10.79
	M40	1.16	9.72	-2.38	10.08
	M60	0.56	8.45	-2.21	8.75
	M80	0.67	7.46	-1.95	7.743
	M100	0.4	6.61	-1.76	6.854
	M100	0.4	6.61	-1.76	6.854
PMSL05-6B	NRM	5.08	6.18	8.35	11.56
	M5	4.9	6.2	8.31	11.47
	M10	4.21	5.82	7.62	10.47
	M15	4.11	5.45	6.99	9.773
	M20	3.78	5.16	6.38	9.037
	M25	3.74	4.83	6	8.564
	M30	3.32	4.57	5.62	7.969
	M40	3.21	4.18	5.06	7.312
	M60	2.5	3.49	4.22	6.018
	M80	2.15	2.93	3.61	5.123
	M100	1.81	2.53	3.1	4.396
	M100	1.81	2.53	3.1	4.396
PMSL05-5B	NRM	4.44	6.77	7.36	10.94
	M5	4.26	6.51	7.29	10.66
	M10	3.93	6.24	6.69	9.96
	M15	3.79	6.02	6.05	9.336
	M20	3.41	5.38	5.57	8.461
	M25	3.39	5.2	5.21	8.103
	M30	3.13	4.98	4.9	7.655
	M40	2.66	4.57	4.38	6.871
	M60	2.29	3.82	3.67	5.77
	M80	1.89	3.31	3.11	4.92
	M100	1.67	2.83	2.66	4.224
	M100	1.67	2.83	2.66	4.224
PMKR10-3B	NRM	-3.1	-4.85	3.62	6.805
	M5	-2.24	-3.86	1.94	4.87
	M10	-1.49	-2.04	-0.04	2.53
	M15	-1.302	-1.163	-0.723	1.89
	M20	-1.118	-0.748	-0.88	1.608
	M25	-1.014	-0.467	-0.883	1.424
	M30	-0.88	-0.355	-0.822	1.255
	M40	-0.665	-0.156	-0.722	0.9936
	M60	-0.449	-0.054	-0.517	0.6866
	M80	-0.376	-0.05	-0.411	0.559
	M100	-0.285	-0.03	-0.378	0.4739
	M100	-0.285	-0.03	-0.378	0.4739
PMKR10-4B	NRM	-2.59	-3.13	4.87	6.34
	M5	-1.84	-2.87	2.15	4.028
	M10	-1.485	-1.808	-0.202	2.348
	M15	-1.311	-1.291	-0.748	1.986
	M20	-1.089	-0.965	-0.859	1.69
	M25	-1.012	-0.8	-0.847	1.543
	M30	-0.837	-0.674	-0.782	1.329
	M40	-0.669	-0.477	-0.634	1.038
	M60	-0.495	-0.326	-0.474	0.7591
	M80	-0.376	-0.261	-0.432	0.6294
	M100	-0.338	-0.222	-0.382	0.5567
	M100	-0.338	-0.222	-0.382	0.5567
PMKR10-9B	NRM	-3.31	-4.3	2.95	6.172
	M5	-2.23	-3.57	1.77	4.569
	M10	-1.476	-1.785	0.093	2.318
	M15	-1.21	-0.877	-0.602	1.611
	M20	-1.053	-0.45	-0.802	1.398
	M25	-0.912	-0.228	-0.826	1.252
	M30	-0.805	-0.103	-0.798	1.138
	M40	-0.618	0.001	-0.682	0.9205
	M60	-0.435	0.1	-0.521	0.686
	M80	-0.324	0.064	-0.412	0.5279
	M100	-0.296	0.072	-0.356	0.4687

	M100	-0.296	0.072	-0.356	0.4687
PMKR10-7A	NRM	-3.24	-4.04	2.35	5.689
	M5	-2.3	-3.18	1.12	4.077
	M10	-1.911	-1.497	-0.412	2.462
	M15	-1.673	-0.706	-0.984	2.065
	M20	-1.471	-0.272	-1.132	1.877
	M25	-1.282	-0.075	-1.132	1.712
	M30	-1.13	0.02	-1.051	1.543
	M40	-0.902	0.143	-0.895	1.282
	M60	-0.684	0.152	-0.719	1.004
	M80	-0.562	0.127	-0.616	0.8433
	M100	-0.523	0.124	-0.551	0.77
	M100	-0.523	0.124	-0.551	0.77
PMKR02-10B	NRM	-3.2	1.69	-1.2	3.813
	M5	-2.78	1.32	-1.26	3.326
	M10	-1.747	0.41	-1.056	2.082
	M15	-1.053	-0.349	-0.69	1.306
	M20	-0.535	-0.896	-0.34	1.098
	M25	-0.316	-1.105	-0.143	1.158
	M30	-0.177	-1.239	-0.028	1.252
	M40	-0.098	-1.209	0.09	1.216
	M60	-0.03	-1.026	0.132	1.035
	M80	-0.009	-0.869	0.137	0.8799
	M100	0.032	-0.752	0.14	0.765
	M100	0.032	-0.752	0.14	0.765
PMKR02-5B	NRM	-3.93	1.43	-2.58	4.916
	M5	-3.32	1.17	-2.23	4.171
	M10	-1.784	0.002	-0.939	2.016
	M15	-0.84	-0.904	0.029	1.235
	M20	-0.417	-1.388	0.474	1.525
	M25	-0.24	-1.589	0.68	1.745
	M30	-0.113	-1.74	0.802	1.919
	M40	0.031	-1.704	0.831	1.896
	M60	0.083	-1.493	0.783	1.688
	M80	0.059	-1.3	0.694	1.475
	M100	0.04	-1.179	0.612	1.329
	M100	0.04	-1.179	0.612	1.329
PMKR02-6B	NRM	-5.61	4.99	-4.28	8.643
	M5	-4.55	4.12	-3.83	7.233
	M10	-2.56	1.9	-2.22	3.884
	M15	-1.45	-0.224	-0.882	1.712
	M20	-0.935	-0.682	-0.174	1.17
	M25	-0.656	-1.241	0.206	1.419
	M30	-0.475	-1.461	0.389	1.585
	M40	-0.332	-1.648	0.55	1.769
	M60	-0.282	-1.633	0.603	1.763
	M80	-0.241	-1.516	0.593	1.645
	M100	-0.226	-1.388	0.552	1.51
	M100	-0.226	-1.388	0.552	1.51
PMKR02-9B	NRM	-1.64	1.146	-0.165	2.007
	M5	-1.525	0.834	-0.27	1.759
	M10	-1.073	0.219	-0.312	1.139
	M15	-0.724	-0.373	-0.222	0.8438
	M20	-0.489	-0.747	-0.088	0.8974
	M25	-0.342	-0.932	0.013	0.993
	M30	-0.26	-0.969	0.074	1.006
	M40	-0.148	-0.942	0.131	0.9629
	M60	-0.11	-0.746	0.126	0.7644
	M80	-0.063	-0.586	0.123	0.6024
	M100	-0.025	-0.514	0.112	0.5263
	M100	-0.025	-0.514	0.112	0.5263
PMKR18-1C	NRM	-5.2	-11.59	5.36	13.79
	M5	-4.88	-4.04	8.49	10.6
	M10	-4.58	1.89	3.89	6.295
	M15	-3.92	3.75	1.47	5.62
	M20	-3.26	3.99	0.62	5.188
	M25	-2.87	3.88	0.24	4.835
	M30	-2.29	3.46	0.06	4.146
	M40	-1.76	2.83	-0.07	3.328
	M60	-1.092	1.787	-0.136	2.099
	M80	-0.686	1.278	-0.095	1.454
	M100	-0.596	1.01	-0.088	1.177
	M100	-0.596	1.01	-0.088	1.177
PMKR18-3B	NRM	-9.44	-11.44	0.05	14.83
	M5	-8.8	-4.92	3.11	10.55
	M10	-5.65	1.08	0.15	5.754
	M15	-3.94	2.89	-1.17	5.026
	M20	-3.05	3.06	-1.38	4.533
	M25	-2.36	2.74	-1.28	3.84
	M30	-1.82	2.43	-1.09	3.226
	M40	-1.267	1.849	-0.847	2.396
	M60	-0.832	1.143	-0.627	1.547
	M80	-0.568	0.83	-0.428	1.093
	M100	-0.453	0.644	-0.354	0.8634

	M100	-0.453	0.644	-0.354	0.8634
PMKR18-8B	NRM	-6.6	-28.9	13.3	32.5
	M5	-3.47	-17.89	16.86	24.82
	M10	-3.5	-4.27	8.37	10.03
	M15	-3.39	1.15	3.92	5.305
	M20	-2.83	2.71	2.2	4.491
	M25	-2.4	3.16	1.38	4.2
	M30	-2.26	3.13	0.85	3.952
	M40	-1.81	2.81	0.56	3.392
	M60	-1.35	2.21	0.33	2.609
	M80	-1.034	1.71	0.216	2.01
	M100	-0.715	1.353	0.111	1.535
	M100	-0.715	1.353	0.111	1.535
PMKR18-2B	NRM	-11.25	-14.71	3.05	18.77
	M5	-7.89	-5.64	6.65	11.76
	M10	-4.54	0.89	1.96	5.024
	M15	-3.3	2.79	0.11	4.318
	M20	-2.32	3.18	-0.58	3.976
	M25	-1.78	2.88	-0.61	3.446
	M30	-1.42	2.63	-0.68	3.071
	M40	-1.02	2.1	-0.61	2.412
	M60	-0.754	1.458	-0.397	1.689
	M80	-0.584	1.126	-0.274	1.298
	M100	-0.478	0.953	-0.314	1.111
	M100	-0.478	0.953	-0.314	1.111
PMKR13-8B	NRM	-5	38	48	61.48
	M5	-6.4	35.2	43.6	56.34
	M10	-4.2	25.1	29.4	38.83
	M15	-2.28	14.82	14.27	20.69
	M20	-1.22	7.77	5.79	9.769
	M25	-0.73	4.57	2.72	5.371
	M30	-0.48	3.12	1.63	3.552
	M40	-0.267	1.908	-0.87	2.114
	M60	-0.239	1.171	0.472	1.285
	M80	-0.194	0.835	0.363	0.9315
	M100	-0.13	0.685	0.262	0.7449
	M100	-0.13	0.685	0.262	0.7449
PMKR13-2B	NRM	126.1	-3.3	-142.5	190.3
	M5	117.6	3.1	-134.3	178.5
	M10	91.7	5.9	-100.83	142
	M15	60.8	11.2	-75.9	97.88
	M20	35	14.7	-48.3	61.46
	M25	19.7	13	-30	38.2
	M30	12.15	10.66	-18.65	24.68
	M40	4.28	6.17	-7.38	10.53
	M60	0.93	2.31	-1.52	2.914
	M80	0.398	1.24	-0.444	1.376
	M100	0.279	0.835	-0.151	0.8935
	M100	0.279	0.835	-0.151	0.8935
PMKR13-5B	NRM	192.8	33.4	-113.7	226.3
	M5	181.3	38.6	-106.7	213.9
	M10	146	37.2	-89.6	175.3
	M15	104	38.2	-68.7	130.4
	M20	65.8	35.8	-49.3	89.7
	M25	39.8	25.1	-32.8	57.34
NEW	M30	27.4	20.9	-23	41.41
	M40	10.55	13	-11.03	20.05
	M60	2.48	4.56	-2.78	5.889
	M80	0.87	2.07	-0.82	2.388
	M100	0.493	1.234	-0.29	1.36
	M100	0.493	1.234	-0.29	1.36
PMKR13-6B	NRM	129.7	155.1	89	220.9
	M5	120	144.8	85.3	206.5
	M10	98.3	125	66.7	172.4
	M15	67.9	101.8	42.5	129.5
	M20	43.3	75.1	24.4	90.03
	M25	27.4	52.6	11.6	60.44
	M30	17.5	37.5	5.7	41.74
	M40	6.26	19.29	0.98	20.3
	M60	1.38	6.21	-0.12	6.362
	M80	0.49	2.95	0.04	2.993
	M100	0.235	1.605	0.201	1.635
	M100	0.235	1.605	0.201	1.635
PMSH03-2B	NRM	0.041	-1.781	1.082	2.084
	M5	0.19	-1.502	0.854	1.738
	M10	0.183	-1.101	0.605	1.27
	M15	0.222	-0.917	0.473	1.056
	M20	0.214	-0.77	0.421	0.9035
	M25	0.181	-0.686	0.361	0.7961
	M30	0.17	-0.635	0.323	0.7324
	M40	0.095	-0.546	0.25	0.6082
	M60	0.076	-0.4	0.192	0.45
	M80	0.075	-0.309	0.173	0.3619
	M100	0.068	-0.247	0.149	0.2968

	M100	0.068	-0.247	0.149	0.2968
PMSH03-6B	NRM	-0.374	-1.906	1.08	2.222
	M5	-0.022	-1.489	0.776	1.679
	M10	0.069	-1.122	0.58	1.265
	M15	0.042	-0.919	0.461	1.029
	M20	0.047	-0.801	0.378	0.8867
	M25	0.059	-0.714	0.354	0.7989
	M30	0.062	-0.635	0.332	0.7195
	M40	0.018	-0.518	0.245	0.5733
	M60	0.101	-0.403	0.18	0.4532
	M80	0.08	-0.296	0.155	0.3434
	M100	0.044	-0.258	0.099	0.2802
	M100	0.044	-0.258	0.099	0.2802
PMSH03-7B	NRM	-0.036	-1.728	1.491	2.282
	M5	0.168	-1.493	0.76	1.684
	M10	0.224	-1.147	0.556	1.294
	M15	0.173	-0.931	0.457	1.052
	M20	0.15	-0.817	0.358	0.9047
	M25	0.129	-0.732	0.33	0.8126
	M30	0.103	-0.66	0.286	0.7271
	M40	0.095	-0.572	0.25	0.6315
	M60	0.096	-0.425	0.159	0.464
	M80	0.057	-0.337	0.107	0.3583
	M100	0.051	-0.268	0.075	0.2828
	M100	0.051	-0.268	0.075	0.2828
PMSH03-10B	NRM	-0.16	-1.774	1.449	2.296
	M5	0.032	-1.566	0.707	1.718
	M10	0.15	-1.231	0.575	1.367
	M15	0.071	-0.986	0.436	1.081
	M20	0.09	-0.887	0.353	0.9587
	M25	0.085	-0.793	0.355	0.8733
	M30	0.091	-0.728	0.31	0.7965
	M40	0.088	-0.612	0.219	0.656
	M60	-0.018	-0.471	0.208	0.515
	M80	0.068	-0.345	0.144	0.3798
	M100	0.044	-0.304	0.105	0.3245
	M100	0.044	-0.304	0.105	0.3245
PMKR03-2B	NRM	-0.616	0.814	-0.266	1.055
	M5	-0.6	0.754	-0.284	1.004
	M10	-0.531	0.677	-0.265	0.8996
	M15	-0.424	0.612	-0.232	0.7796
	M20	-0.357	0.517	-0.201	0.6597
	M25	-0.295	0.424	-0.178	0.5463
	M30	-0.233	0.348	-0.131	0.439
	M40	-0.148	0.238	-0.097	0.2964
	M60	-0.107	0.0992	-0.0567	0.1565
	M80	-0.0589	0.0321	-0.0123	0.06821
	M100	-0.0714	0.0217	-0.0103	0.07534
	M100	-0.0714	0.0217	-0.0103	0.07534
PMKR03-4B	NRM	-0.603	0.735	-0.114	0.9575
	M5	-0.564	0.695	-0.122	0.9037
	M10	-0.482	0.608	-0.119	0.7852
	M15	-0.46	0.565	-0.122	0.7387
	M20	-0.361	0.488	-0.094	0.6137
	M25	-0.316	0.411	-0.114	0.5309
	M30	-0.253	0.341	-0.085	0.4332
	M40	-0.181	0.258	-0.072	0.3231
	M60	-0.1162	0.1513	-0.0321	0.1934
	M80	-0.0973	0.0897	-0.0314	0.136
	M100	-0.1036	0.064	0.0037	0.1231
	M100	-0.1036	0.064	0.0037	0.1231
PMAF06-3B	NRM	0.382	-1.834	-0.666	1.988
	M5	0.27	-1.91	-0.354	1.961
	M10	0.206	-1.931	-0.17	1.95
	M15	0.186	-1.817	-0.079	1.828
	M20	0.241	-1.667	-0.065	1.686
	M25	0.137	-1.523	-0.041	1.53
	M30	0.187	-1.405	-0.026	1.418
	M40	0.149	-1.22	-0.019	1.229
	M60	0.097	-0.976	-0.01	0.9807
	M80	0.055	-0.841	0.009	0.8425
	M100	0.091	-0.74	0.0011	0.7457
	M100	0.091	-0.74	0.0011	0.7457
PMAF06-6B	NRM	0.036	-1.781	-1.132	2.111
	M5	-0.194	-1.928	-0.614	2.032
	M10	-0.3	-2.01	-0.34	2.063
	M15	-0.275	-1.899	-0.25	1.933
	M20	-0.149	-1.743	-0.175	1.758
	M25	-0.151	-1.601	-0.14	1.615
	M30	-0.166	-1.481	-0.118	1.495
	M40	-0.123	-1.279	-0.084	1.287
	M60	-0.101	-1.034	-0.061	1.041
	M80	-0.118	-0.874	-0.044	0.8826
	M100	-0.08	-0.77	-0.037	0.7816

	M100	-0.08	-0.77	-0.037	0.7816
PMAF06-10B	NRM	0.474	-1.725	-1.02	2.06
	M5	0.24	-1.826	-0.411	1.887
	M10	0.157	-1.903	-0.105	1.912
	M15	0.11	-1.821	-0.004	1.824
	M20	0.159	-1.69	0.004	1.697
	M25	0.064	-1.574	0.029	1.576
	M30	0.066	-1.459	0.047	1.462
	M40	0.094	-1.266	0.061	1.271
	M60	0.05	-1.04	0.056	1.043
	M80	0.047	-0.897	0.054	0.9001
	M100	0.045	-0.773	0.034	0.7754
	M100	0.045	-0.773	0.034	0.7754
PMAF06-1B	NRM	0.464	-1.863	-1.038	2.182
	M5	0.23	-2.04	-0.6	2.14
	M10	0.15	-2.07	-0.37	2.109
	M15	0.169	-1.927	-0.277	1.954
	M20	0.154	-1.775	-0.225	1.796
	M25	0.14	-1.606	-0.184	1.622
	M30	0.163	-1.463	-0.154	1.48
	M40	0.135	-1.275	-0.112	1.287
	M60	0.097	-1.032	-0.099	1.041
	M80	0.092	-0.881	-0.081	0.8897
	M100	0.059	-0.786	-0.068	0.7907
	M100	0.059	-0.786	-0.068	0.7907
PMKR12-6B	NRM	-1.14	-10.91	12.22	16.42
	M5	-1.08	-10.93	10.7	15.33
	M10	-1.9	-10.04	6.57	12.15
	M15	-2.1	-8.68	4.11	9.835
	M20	-2.27	-7.73	2.98	8.588
	M25	-2.03	-6.88	2.45	7.583
	M30	-1.71	-6.25	2.09	6.805
	M40	-1.39	-5.17	1.67	5.607
	M60	-0.95	-3.66	1.17	3.96
	M80	-0.65	-2.56	0.85	2.775
	M100	-0.493	-1.922	0.603	2.074
	M100	-0.493	-1.922	0.603	2.074
PMKR12-7B	NRM	-3.3	-14.4	20	24.85
	M5	-3.13	-13.82	17.79	22.75
	M10	-2.62	-12.43	10.57	16.53
	M15	-2.43	-10.2	5.97	12.07
	M20	-1.09	-8.59	4.09	9.58
	M25	-1.54	-7.52	2.94	8.221
	M30	-1.72	-6.67	2.33	7.276
	M40	-1.22	-5.58	1.71	5.965
	M60	-0.89	-4.04	1.21	4.309
	M80	-0.53	-2.94	0.86	3.11
	M100	-0.49	-2.25	0.68	2.399
	M100	-0.49	-2.25	0.68	2.399
PMKR12-9B	NRM	-1.71	-12.84	11.24	17.14
	M5	-2.37	-12.36	9.78	15.94
	M10	-2.3	-10.33	6.23	12.28
	M15	-2.57	-8.48	4.07	9.756
	M20	-2.53	-7.26	3.07	8.283
	M25	-2.12	-6.45	2.52	7.246
	M30	-2.38	-5.88	2.2	6.713
	M40	-2	-5.1	1.86	5.784
	M60	-1.54	-3.97	1.45	4.497
	M80	-1.17	-3.01	1.05	3.399
	M100	-0.86	-2.38	0.92	2.691
	M100	-0.86	-2.38	0.92	2.691
PMKR12-2B	NRM	-14.3	-44.8	1.5	47.01
	M5	-11.1	-40.8	2.8	42.37
	M10	-7.4	-30.3	3.7	31.39
	M15	-3.9	-20.6	3.3	21.26
	M20	-2.76	-14.24	2.35	14.69
	M25	-2.18	-10.11	1.58	10.47
	M30	-2.09	-7.75	1.03	8.091
	M40	-1.48	-5.17	0.3	5.388
	M60	-1.09	-3.15	-0.13	3.335
	M80	-0.87	-2.39	-0.18	2.553
	M100	-0.676	-1.888	-0.17	2.013
	M100	-0.676	-1.888	-0.17	2.013
PMSL02-2B	NRM	-2.4	30	25.2	39.3
	M5	-5.07	16.5	9.49	19.49
	M10	-3.3	1.35	-0.73	3.637
	M15	-2.66	-2.59	-1.56	4.029
	M20	-2.19	-3.1	-1.49	4.072
	M25	-1.94	-3.07	-1.24	3.839
	M30	-1.62	-2.9	-1.14	3.509
	M40	-1.25	-2.5	-0.86	2.926
	M60	-0.988	-1.727	-0.496	2.05
	M80	-0.791	-1.3815	-0.4385	1.6515
	M100	-0.594	-1.036	-0.381	1.253

	M100	-0.594	-1.036	-0.381	1.253
PMSL02-5B	NRM	9.4	20.7	28.6	36.56
	M5	-1.7	9.89	12.02	15.66
	M10	-4.94	-0.83	-1.06	5.121
	M15	-4.14	-2.38	-1.83	5.113
	M20	-3.47	-2.52	-1.61	4.579
	M25	-2.94	-2.36	-1.41	4.022
	M30	-2.64	-2.05	-1.34	3.601
	M40	-2.04	-1.71	-0.9	2.804
	M60	-1.345	-1.182	-0.597	1.887
	M80	-0.986	-0.921	-0.374	1.4
	M100	-0.75	-0.731	-0.327	1.097
	M100	-0.75	-0.731	-0.327	1.097
PMSL02-10B	NRM	1.1	21.5	14.2	25.77
	M5	-7.37	8.25	3.24	11.53
	M10	-5.56	-3.06	-0.88	6.404
	M15	-3.87	-4.29	-0.73	5.821
	M20	-2.89	-4.17	-0.48	5.101
	M25	-2.27	-3.71	-0.29	4.358
	M30	-2	-3.35	-0.26	3.908
	M40	-1.44	-2.73	-0.12	3.083
	M60	-0.86	-1.887	0.046	2.074
	M80	-0.72	-1.387	0.028	1.563
	M100	-0.466	-1.069	-0.055	1.167
	M100	-0.466	-1.069	-0.055	1.167
PMSL02-3B	NRM	-10	29.3	24.8	39.67
	M5	-10.57	16.05	8.43	20.99
	M10	-4.91	2.16	-2.05	5.745
	M15	-3.33	-1.9	-2.12	4.378
	M20	-2.62	-2.64	-1.8	4.134
	M25	-2.31	-2.71	-1.56	3.887
	M30	-1.98	-2.56	-1.33	3.504
	M40	-1.52	-2.3	-1.02	2.937
	M60	-1.153	-1.67	-0.629	2.125
	M80	-0.838	-1.35	-0.512	1.669
	M100	-0.653	-1.094	-0.384	1.331
	M100	-0.653	-1.094	-0.384	1.331
PMKR15-1B	NRM	-14.03	16.87	-15.9	27.1
	M5	-7.3	12.94	-8.75	17.24
	M10	-1.44	5.55	-1.55	5.939
	M15	-0.63	2.87	0.42	2.971
	M20	-0.095	1.674	1.097	2.004
	M25	-0.03	1.136	1.319	1.741
	M30	0.032	0.826	1.32	1.557
	M40	0.099	0.541	1.31	1.421
	M60	0.145	0.303	1.121	1.17
	M80	0.143	0.151	0.92	0.9438
	M100	0.116	0.113	0.782	0.7985
	M100	0.116	0.113	0.782	0.7985
PMKR15-5B	NRM	-4.54	3.23	-2.3	6.028
	M5	-0.785	1.939	1.192	2.407
	M10	0.22	1.03	2.02	2.279
	M15	0.37	0.774	1.962	2.142
	M20	0.427	0.635	1.85	2.002
	M25	0.413	0.606	1.671	1.825
	M30	0.423	0.527	1.617	1.753
	M40	0.39	0.441	1.439	1.555
	M60	0.287	0.382	1.138	1.234
	M80	0.299	0.269	0.964	1.045
	M100	0.244	0.166	0.88	0.9283
	M100	0.244	0.166	0.88	0.9283
PMKR15-9B	NRM	-4.04	3.39	-1.54	5.492
	M5	-0.978	1.96	1.206	2.5
	M10	0.04	0.82	2.15	2.298
	M15	0.23	0.5	2.12	2.189
	M20	0.297	0.346	1.991	2.043
	M25	0.256	0.324	1.898	1.942
	M30	0.295	0.27	1.742	1.787
	M40	0.285	0.228	1.531	1.574
	M60	0.26	0.148	1.298	1.332
	M80	0.211	0.088	1.167	1.189
	M100	0.182	0.054	0.953	0.9717
	M100	0.182	0.054	0.953	0.9717
PMKR15-2B	NRM	-12.3	8.9	-8.59	17.45
	M5	-4.75	6.41	-2.66	8.41
	M10	-0.51	2.78	1.68	3.288
	M15	0.31	1.6	2.38	2.884
	M20	0.48	1.18	2.41	2.73
	M25	0.51	0.98	2.39	2.631
	M30	0.54	0.84	2.26	2.472
	M40	0.5	0.69	2.06	2.229
	M60	0.427	0.476	1.686	1.801
	M80	0.403	0.371	1.461	1.56
	M100	0.291	0.225	1.226	1.28

	M100	0.291	0.225	1.226	1.28
PMSL04-5C	NRM	-1.17	-3.07	-3.11	4.526
	M5	-1.69	-3.24	-3.56	5.103
	M10	-1.67	-3.06	-3.41	4.874
	M15	-1.65	-2.86	-3.12	4.546
	M20	-1.51	-2.63	-2.86	4.169
	M25	-1.48	-2.41	-2.58	3.827
	M30	-1.32	-2.2	-2.45	3.544
	M40	-1.19	-1.92	-2.13	3.105
	M60	-0.891	-1.509	-1.673	2.423
	M80	-0.75	-1.14	-1.325	1.902
	M100	-0.563	-0.926	-1.127	1.557
	M100	-0.563	-0.926	-1.127	1.557
PMSL04-8B	NRM	-4.8	-26.5	4.9	27.35
	M5	-4.7	-27	4.7	27.8
	M10	-6	-26.8	4.9	27.94
	M15	-5.3	-26.1	4.5	26.99
	M20	-4.9	-25.2	4.6	26.13
	M25	-4.7	-23.8	4.4	24.63
	M30	-4.1	-22.1	4.4	22.91
	M40	-3.86	-18.2	3.86	19
	M60	-1.66	-9.94	2.75	10.45
	M80	-1.12	-5.41	1.31	5.676
	M100	-0.75	-2.94	0.41	3.062
	M100	-0.75	-2.94	0.41	3.062
PMSL04-6B	NRM	-4.8	-24.6	5.9	25.7
	M5	-5.4	-25.1	5.6	26.32
	M10	-4.9	-24.9	5.7	26
	M15	-6.2	-24.4	5.6	25.77
	M20	-5.8	-23.4	5.5	24.74
	M25	-4.8	-22.2	5.3	23.34
	M30	-4.6	-20.7	4.9	21.77
	M40	-3.81	-17.13	4.42	18.09
	M60	-1.57	-9.25	2.53	9.716
	M80	-0.99	-4.86	1.27	5.123
	M100	-0.68	-2.76	0.6	2.903
	M100	-0.68	-2.76	0.6	2.903
PMSL04-4B	NRM	-0.91	-2.96	-2.96	4.099
	M5	-1.56	-3.1	-3.08	4.643
	M10	-1.53	-2.97	-2.95	4.455
	M15	-1.43	-2.75	-2.67	4.089
	M20	-1.31	-2.51	-2.43	3.728
	M25	-1.1	-2.34	-2.19	3.388
	M30	-1.08	-2.14	-2.04	3.147
	M40	-0.892	-1.806	-1.78	2.688
	M60	-0.754	-1.413	-1.385	2.117
	M80	-0.588	-1.103	-1.108	1.67
	M100	-0.503	-0.944	-0.916	1.408
	M100	-0.503	-0.944	-0.916	1.408
PMAF05-10B	NRM	-1.37	-7.73	3.24	8.495
	M5	-1.32	-7.63	3.05	8.324
	M10	-1	-6.79	2.84	7.43
	M15	-0.86	-5.83	2.47	6.391
	M20	-0.75	-4.91	2.14	5.409
	M25	-0.46	-4.26	1.83	4.657
	M30	-0.46	-3.62	1.53	3.953
	M40	-0.27	-2.87	1.22	3.134
	M60	-0.2	-1.97	0.795	2.134
	M80	-0.144	-1.459	0.629	1.595
	M100	-0.126	-1.131	0.494	1.24
	M100	-0.126	-1.131	0.494	1.24
PMAF05-8B	NRM	0.82	-7.26	3.42	8.062
	M5	1.35	-7.14	3.25	7.955
	M10	0.78	-6.37	3.02	7.093
	M15	1.04	-5.52	2.59	6.188
	M20	0.76	-4.71	2.22	5.265
	M25	0.37	-3.98	1.9	4.421
	M30	0.45	-3.41	1.67	3.82
	M40	0.3	-2.7	1.29	3.006
	M60	0.232	-1.87	0.915	2.095
	M80	0.199	-1.371	0.646	1.529
	M100	0.118	-1.11	0.551	1.245
	M100	0.118	-1.11	0.551	1.245
PMAF05-7B	NRM	1.75	-3.41	3.63	5.284
	M5	1.53	-3.56	3.5	5.217
	M10	1.22	-3.63	3.23	4.824
	M15	1.04	-3.03	2.8	4.251
	M20	0.85	-2.67	2.27	3.606
	M25	0.72	-2.26	1.89	3.034
	M30	0.655	-1.875	1.637	2.574
	M40	0.441	-1.437	1.208	1.928
	M60	0.337	-0.993	0.89	1.376
	M80	0.266	-0.775	0.678	1.063
	M100	0.192	-0.634	0.534	0.8509

	M100	0.192	-0.634	0.534	0.8509
PMAF05-2B	NRM	-3.11	-6.59	1.08	7.366
	M5	-2.64	-6.69	1.11	7.274
	M10	-1.87	-5.87	1.11	6.264
	M15	-1.48	-4.89	1.06	5.22
	M20	-1.22	-4.08	0.98	4.369
	M25	-0.82	-3.32	0.84	3.52
	M30	-0.55	-2.85	0.76	2.997
	M40	-0.46	-2.11	0.57	2.237
	M60	-0.275	-1.451	0.327	1.513
	M80	-0.265	-1.107	0.252	1.166
	M100	-0.152	-0.899	0.231	0.9403
	M100	-0.152	-0.899	0.231	0.9403
PMKR07-8B	NRM	-3.25	2.86	-4.48	6.233
	M5	-2.09	3.05	-2.65	4.551
	M10	-1.46	2.54	-1.31	3.213
	M15	-1.32	2.16	-1.07	2.749
	M20	-1.211	1.905	-0.932	2.442
	M25	-1.1	1.727	-0.812	2.203
	M30	-0.985	1.559	-0.75	1.991
	M40	-0.772	1.329	-0.617	1.656
	M60	-0.648	1.031	-0.497	1.315
	M80	-0.459	0.838	-0.388	1.031
	M100	-0.422	0.708	-0.348	0.8948
	M100	-0.422	0.708	-0.348	0.8948
PMKR07-5B	NRM	-1.53	-0.16	5.84	6.039
	M5	-0.75	-0.97	5.39	5.526
	M10	-0.41	-0.24	3.18	3.211
	M15	-0.418	0.781	1.662	1.883
	M20	-0.376	1.259	0.973	1.635
	M25	-0.353	1.445	0.607	1.606
	M30	-0.331	1.469	0.435	1.567
	M40	-0.372	1.389	0.268	1.463
	M60	-0.251	1.169	0.113	1.201
	M80	-0.209	0.987	0.068	1.011
	M100	-0.18	0.834	0.028	0.8532
	M100	-0.18	0.834	0.028	0.8532
PMKR05-5B	NRM	-1.54	4	-2.37	4.903
	M5	-1.68	3.92	-2.48	4.935
	M10	-1.51	3.73	-2.33	4.65
	M15	-1.23	3.36	-2.11	4.156
	M20	-1.14	2.96	-1.87	3.683
	M25	-0.91	2.6	-1.59	3.182
	M30	-0.85	2.29	-1.42	2.826
	M40	-0.636	1.843	-1.133	2.255
	M60	-0.427	1.271	-0.802	1.562
	M80	-0.311	0.958	-0.617	1.182
	M100	-0.298	0.781	-0.486	0.9668
	M100	-0.298	0.781	-0.486	0.9668
PMKR05-3B	NRM	-1.03	5.17	0.35	5.284
	M5	-1.49	5.06	0.05	5.273
	M10	-1.37	4.76	-0.19	4.952
	M15	-1.14	4.23	-0.29	4.392
	M20	-0.97	3.73	-0.36	3.869
	M25	-0.74	3.27	-0.34	3.364
	M30	-0.73	2.91	-0.33	3.014
	M40	-0.55	2.33	-0.32	2.418
	M60	-0.344	1.625	-0.236	1.678
	M80	-0.225	1.239	-0.165	1.27
	M100	-0.254	0.972	-0.119	1.011
	M100	-0.254	0.972	-0.119	1.011
PMSL01-10B	NRM	-4.59	-4.9	-1.92	6.983
	M5	-2.83	-2.54	-0.24	3.808
	M10	-1.358	0.797	0.326	1.608
	M15	-1.053	1.478	0.014	1.815
	M20	-0.854	1.492	-0.127	1.724
	M25	-0.728	1.411	-0.153	1.595
	M30	-0.642	1.285	-0.174	1.447
	M40	-0.534	1.047	-0.161	1.186
	M60	-0.362	0.78	-0.132	0.8696
	M80	-0.314	0.62	-0.097	0.7016
	M100	-0.268	0.533	-0.07	0.6008
	M100	-0.268	0.533	-0.07	0.6008
PMSL01-4B	NRM	-0.15	-9.64	9.24	13.35
	M5	0.15	-7.36	9.57	12.07
	M10	-0.45	-3.03	4.82	5.707
	M15	-0.809	-0.826	1.794	2.134
	M20	-0.731	0.043	0.716	1.024
	M25	-0.664	0.36	0.237	0.7916
	M30	-0.547	0.509	0.03	0.7478
	M40	-0.385	0.506	-0.104	0.6438
	M60	-0.256	0.393	-0.115	0.4828
	M80	-0.187	0.311	-0.082	0.3724
	M100	-0.162	0.248	-0.067	0.3032

	M100	-0.162	0.248	-0.067	0.3032
PMSL01-5B	NRM	-2.92	-6.96	-2.77	8.043
	M5	-2.08	-3.92	-0.39	4.454
	M10	-1.381	0.328	0.315	1.454
	M15	-1.179	1.301	-0.081	1.757
	M20	-1.035	1.424	-0.208	1.773
	M25	-0.873	1.382	-0.248	1.653
	M30	-0.729	1.2295	-0.237	1.4495
	M40	-0.585	1.077	-0.226	1.246
	M60	-0.403	0.786	-0.167	0.899
	M80	-0.338	0.628	-0.117	0.7224
	M100	-0.276	0.552	-0.12	0.6286
	M100	-0.276	0.552	-0.12	0.6286
PMSL01-3B	NRM	1.2	-25.4	36.6	44.61
	M5	1.1	-23.7	36	43.09
	M10	1.5	-17.5	25.1	30.66
	M15	0.785	-12.47	16.715	20.915
	M20	0.07	-7.44	8.33	11.17
	M25	-0.21	-4.46	4.9	6.631
	M30	-0.31	-2.73	2.99	4.061
	M40	-0.359	-0.943	1.251	1.607
	M60	-0.23	0.076	0.216	0.3247
	M80	-0.182	0.233	0.047	0.2992
	M100	-0.151	0.268	-0.016	0.3082
	M100	-0.151	0.268	-0.016	0.3082
PMKR06-7B	NRM	-0.14	2.35	2.32	3.3
	M5	-0.34	2.21	1.84	2.901
	M10	-0.5	2.1	0.83	2.313
	M15	-0.51	2.15	0.41	2.252
	M20	-0.52	2.14	0.28	2.216
	M25	-0.45	2.09	0.21	2.152
	M30	-0.52	2.03	0.15	2.105
	M40	-0.448	1.883	0.068	1.937
	M60	-0.384	1.579	0	1.625
	M80	-0.305	1.345	-0.029	1.38
	M100	-0.269	1.183	-0.048	1.214
	M100	-0.269	1.183	-0.048	1.214
PMKR06-5B	NRM	-0.32	1.51	2.07	2.577
	M5	-0.367	1.496	1.64	2.25
	M10	-0.347	1.653	0.955	1.94
	M15	-0.298	1.754	-0.685	1.906
	M20	-0.315	1.778	0.564	1.892
	M25	-0.33	1.768	0.462	1.857
	M30	-0.257	1.715	0.394	1.778
	M40	-0.285	1.578	0.299	1.631
	M60	-0.129	1.319	0.163	1.335
	M80	-0.137	1.123	0.118	1.137
	M100	-0.138	0.965	0.079	0.978
	M100	-0.138	0.965	0.079	0.978
PMSH01-9B	NRM	-2.8	5.81	5.18	8.275
	M5	-3.06	5.17	4.68	7.615
	M10	-2.73	4.58	3.87	6.586
	M15	-2.16	3.91	3.24	5.513
	M20	-2.04	3.35	2.75	4.788
	M25	-1.76	3.06	2.45	4.298
	M30	-1.52	2.75	2.18	3.824
	M40	-1.4	2.3	1.85	3.269
	M60	-1.003	1.692	1.317	2.367
	M80	-0.771	1.348	0.913	1.802
	M100	-0.6	1.1	0.711	1.44
	M100	-0.6	1.1	0.711	1.44
PMSH01-8B	NRM	-3.81	2.74	18.2	18.79
	M5	-3.12	1.5	15.06	15.45
	M10	-2.1	0.86	8.72	9.013
	M15	-1.47	0.77	5.6	5.843
	M20	-1.18	0.75	4.1	4.332
	M25	-1.02	0.74	3.31	3.536
	M30	-0.94	0.69	2.8	3.031
	M40	-0.76	0.63	2.2	2.416
	M60	-0.591	0.481	1.565	1.741
	M80	-0.444	0.412	1.225	1.367
	M100	-0.326	0.335	0.93	1.041
	M100	-0.326	0.335	0.93	1.041
PMSH01-1B	NRM	-1.71	2.84	5.02	6.016
	M5	-1.73	2.33	4.46	5.322
	M10	-1.39	1.92	3.69	4.39
	M15	-1.3	1.57	3.01	3.631
	M20	-1.09	1.3	2.54	3.057
	M25	-0.85	1.15	2.22	2.635
	M30	-0.702	1.031	1.936	2.303
	M40	-0.642	0.837	1.589	1.908
	M60	-0.425	0.613	1.221	1.431
	M80	-0.35	0.475	0.944	1.113
	M100	-0.291	0.387	0.746	0.8894

	M100	-0.291	0.387	0.746	0.8894
PMKR11-9B	NRM	-4.16	3.06	-3.37	6.166
	M5	-4.08	3.46	-3.78	6.549
	M10	-3.9	3.46	-3.81	6.462
	M15	-3.55	3.35	-3.65	6.097
	M20	-3.4	3.15	-3.54	5.829
	M25	-3.23	3.01	-3.38	5.558
	M30	-3.02	3.09	-3.24	5.401
	M40	-2.81	2.92	-3.02	5.055
	M60	-2.4	2.58	-2.69	4.434
	M80	-2	2.37	-2.28	3.853
	M100	-1.62	2.07	-1.92	3.26
	M100	-1.62	2.07	-1.92	3.26
PMKR11-10B	NRM	-3.46	3.03	-2.95	5.463
	M5	-3.48	3.34	-3.39	5.898
	M10	-3.21	3.35	-3.39	5.747
	M15	-2.83	3.17	-3.22	5.338
	M20	-2.8	3.05	-3	5.118
	M25	-2.51	2.92	-2.88	4.81
	M30	-2.57	2.8	-2.75	4.691
	M40	-2.22	2.65	-2.54	4.285
	M60	-1.88	2.31	-2.23	3.721
	M80	-1.61	2.08	-1.97	3.287
	M100	-1.302	1.869	-1.707	2.846
	M100	-1.302	1.869	-1.707	2.846
PMKR11-3B	NRM	-1.91	-4.27	0.14	4.68
	M5	-1.4	-4.63	-0.02	4.835
	M10	-1.33	-4.67	0.07	4.856
	M15	-1.1	-4.46	0.11	4.592
	M20	-0.97	-4.24	0.13	4.348
	M25	-0.98	-3.97	0.12	4.095
	M30	-0.92	-3.83	0.11	3.938
	M40	-0.92	-3.51	0.09	3.632
	M60	-0.77	-2.98	0.11	3.083
	M80	-0.64	-2.5	0.12	2.588
	M100	-0.66	-2.13	0.11	2.23
	M100	-0.66	-2.13	0.11	2.23
PMKR11-1B	NRM	-2.41	-5.23	0.4	5.771
	M5	-1.84	-5.57	0.21	5.871
	M10	-1.68	-5.67	0.34	5.926
	M15	-1.51	-5.41	0.44	5.638
	M20	-1.29	-5.12	0.43	5.296
	M25	-1.17	-4.85	0.43	5.005
	M30	-1.37	-4.64	0.39	4.855
	M40	-1.16	-4.19	0.4	4.369
	M60	-0.9	-3.55	0.35	3.676
	M80	-0.86	-2.95	0.36	3.096
	M100	-0.54	-2.48	0.33	2.556
	M100	-0.54	-2.48	0.33	2.556
PMSH01-3B	NRM	-2.04	-3.73	6.2	7.518
	M5	-1.87	-3.68	5.64	6.988
	M10	-1.67	-3.44	4.99	6.285
	M15	-1.42	-3.03	4.28	5.434
	M20	-1.32	-2.77	3.71	4.818
	M25	-1.08	-2.49	3.26	4.243
	M30	-0.97	-2.22	2.92	3.797
	M40	-0.8	-1.91	2.44	3.202
	M60	-0.463	-1.389	1.793	2.315
	M80	-0.489	-1.094	1.311	1.777
	M100	-0.351	-0.887	1.063	1.428
	M100	-0.351	-0.887	1.063	1.428
PMKR17-2B	NRM	-26.4	11.1	-23.2	36.85
	M5	-12.32	6.64	-10.37	17.42
	M10	-3.33	0	-1.85	3.811
	M15	-1.477	-1.712	-0.147	2.266
	M20	-0.977	-1.961	0.013	2.191
	M25	-0.746	-1.941	0.13	2.084
	M30	-0.72	-1.804	0.113	1.946
	M40	-0.505	-1.492	0.034	1.576
	M60	-0.336	-1.156	0.001	1.203
	M80	-0.271	-0.921	-0.032	0.9603
	M100	-0.267	-0.814	-0.027	0.8568
	M100	-0.267	-0.814	-0.027	0.8568
PMAF04-1B	NRM	-2.89	-7.92	1.96	8.655
	M5	-2.56	-7.33	1.9	7.99
	M10	-2.36	-6.63	1.71	7.239
	M15	-2.03	-5.78	1.59	6.326
	M20	-1.65	-5.07	1.45	5.523
	M25	-1.55	-4.46	1.29	4.895
	M30	-1.21	-3.96	1.15	4.295
	M40	-1.05	-3.18	0.88	3.462
	M60	-0.75	-2.53	0.77	2.751
	M80	-0.618	-1.937	0.517	2.098
	M100	-0.552	-1.844	0.588	2.013

	M100	-0.552	-1.844	0.588	2.013
PMAF04-5B	NRM	-1.57	-5	-0.06	5.24
	M5	-1.51	-4.81	-0.01	5.043
	M10	-1.38	-4.48	0.04	4.693
	M15	-1.16	-4.11	0.08	4.274
	M20	-1.01	-3.62	0.14	3.766
	M25	-0.94	-3.23	0.17	3.37
	M30	-0.79	-2.93	0.17	3.036
	M40	-0.67	-2.34	0.21	2.444
	M60	-0.437	-1.652	0.135	1.714
	M80	-0.306	-1.303	0.084	1.341
	M100	-0.332	-1.044	0.098	1.099
	M100	-0.332	-1.044	0.098	1.099
PMSL06-2B	NRM	-0.005	1.072	-0.313	1.117
	M5	0.013	1.076	-0.314	1.121
	M10	0.029	1.073	-0.313	1.119
	M15	0.02	1.049	-0.313	1.095
	M20	0.004	1.01	-0.308	1.056
	M25	0.043	0.956	-0.3	1.003
	M30	0.013	0.901	-0.285	0.9454
	M40	-0.014	0.8	-0.264	0.8426
	M60	0.016	0.669	-0.226	0.7067
	M80	-0.008	0.601	-0.207	0.6359
	M100	-0.016	0.569	-0.197	0.6023
	M100	-0.016	0.569	-0.197	0.6023
PMSL06-6C	NRM	0.376	0.815	0.783	1.191
	M5	0.379	0.818	0.779	1.192
	M10	0.365	0.823	0.776	1.189
	M15	0.355	0.807	0.749	1.157
	M20	0.348	0.778	0.706	1.107
	M25	0.329	0.713	0.659	1.026
	M30	0.273	0.684	0.603	0.9515
	M40	0.259	0.599	0.491	0.8167
	M60	0.154	0.498	0.337	0.6208
	M80	0.15	0.479	0.244	0.5585
	M100	0.097	0.478	0.173	0.5178
	M100	0.097	0.478	0.173	0.5178
PMKR09-5A	NRM	9.4	-11.6	27.1	30.88
	M5	8.7	-12.1	25.8	29.84
	M10	4.94	-11.58	18.65	22.5
	M15	1.65	-9.38	10.76	14.37
	M20	-0.1	-6.92	5.89	9.084
	M25	-0.29	-5.43	3.79	6.631
	M30	-0.52	-4.22	2.5	4.928
	M40	-0.45	-3.03	1.48	3.405
	M60	-0.424	-1.789	0.669	1.956
	M80	-0.364	-1.272	0.391	1.38
	M100	-0.235	-0.981	0.26	1.042
	M100	-0.235	-0.981	0.26	1.042
PMKR08-8A	NRM	-7.93	-5.99	-7.19	12.27
	M5	-7.04	-5.49	-6.63	11.12
	M10	-4.18	-3.63	-3.68	6.648
	M15	-2.57	-2.45	-2.05	4.099
	M20	-1.967	-1.94	-1.477	3.133
	M25	-1.589	-1.667	-1.134	2.567
	M30	-1.366	-1.438	-0.934	2.193
	M40	-1.054	-1.137	-0.689	1.696
	M60	-0.701	-0.793	-0.442	1.147
	M80	-0.564	-0.633	-0.34	0.9133
	M100	-0.446	-0.506	-0.246	0.7203
	M100	-0.446	-0.506	-0.246	0.7203
PMKR08-6A	NRM	-5.27	-7.54	-7.08	11.61
	M5	-5.02	-6.98	-6.63	10.86
	M10	-3.06	-4.87	-3.66	6.818
	M15	-1.89	-3.22	-2.05	4.257
	M20	-1.34	-2.45	-1.4	3.13
	M25	-1.13	-2.02	-1.06	2.546
	M30	-0.97	-1.694	-0.859	2.133
	M40	-0.742	-1.314	-0.616	1.63
	M60	-0.513	-0.921	-0.382	1.121
	M80	-0.408	-0.703	-0.301	0.8664
	M100	-0.273	-0.557	-0.214	0.656
	M100	-0.273	-0.557	-0.214	0.656
PMKR01-4A	NRM	-2.78	-7.93	-5.78	10.2
	M5	-2.22	-4.94	-4.13	6.814
	M10	-2.07	-2.6	-3.3	4.682
	M15	-2.06	-2.08	-3.11	4.265
	M20	-1.96	-1.76	-3.04	4.017
	M25	-1.87	-1.7	-2.95	3.879
	M30	-1.87	-1.58	-2.94	3.822
	M40	-1.9	-1.53	-2.77	3.688
	M60	-1.72	-1.4	-2.57	3.389
	M80	-1.65	-1.34	-2.4	3.21
	M100	-1.52	-1.27	-2.22	2.976

	M100	-1.52	-1.27	-2.22	2.976
PMKR07-2A	NRM	-7.25	-7.32	-6.43	12.14
	M5	-6.28	-6.66	-4.55	10.22
	M10	-3.06	-2.37	-1.4	4.119
	M15	-1.701	0.073	-0.512	1.778
	M20	-1.148	0.953	-0.338	1.53
	M25	-0.895	1.207	-0.283	1.53
	M30	-0.769	1.263	-0.286	1.506
	M40	-0.52	1.206	-0.248	1.337
	M60	-0.395	0.95	-0.203	1.049
	M80	-0.331	0.758	-0.147	0.8403
	M100	-0.267	0.643	-0.119	0.7068
	M100	-0.267	0.643	-0.119	0.7068
PMAF04-2A	NRM	-2.12	-4.58	-0.64	5.089
	M5	-1.8	-4.48	-0.56	4.857
	M10	-1.65	-4.14	-0.5	4.487
	M15	-1.43	-3.76	-0.39	4.04
	M20	-1.23	-3.37	-0.22	3.59
	M25	-1.05	-3	-0.15	3.183
	M30	-0.97	-2.64	-0.13	2.819
	M40	-0.76	-2.2	-0.05	2.326
	M60	-0.515	-1.501	0.011	1.587
	M80	-0.394	-1.167	0.027	1.229
	M100	-0.299	-0.912	-0.042	0.9606
	M100	-0.299	-0.912	-0.042	0.9606
PMAF05-1A	NRM	-2.02	-7.03	1.96	7.572
	M5	-1.39	-7.05	2.01	7.458
	M10	-1.06	-6.15	1.84	6.503
	M15	-0.8	-5.06	1.59	5.365
	M20	-0.59	-4.19	1.35	4.44
	M25	-0.58	-3.51	1.18	3.751
	M30	-0.39	-3.02	0.98	3.201
	M40	-0.39	-2.36	0.78	2.519
	M60	-0.193	-1.667	0.543	1.764
	M80	-0.136	-1.282	0.413	1.353
	M100	-0.152	-1.046	0.309	1.101
	M100	-0.152	-1.046	0.309	1.101
PMSL01-9A	NRM	-2.35	-5.36	4.56	7.418
	M5	-1.53	-3.61	5.1	6.429
	M10	-1.33	-0.4	2.32	2.703
	M15	-1.23	0.817	0.714	1.64
	M20	-1.102	1.248	0.104	1.668
	M25	-0.971	1.331	-0.158	1.655
	M30	-0.775	1.281	-0.259	1.52
	M40	-0.563	1.071	-0.284	1.243
	M60	-0.334	0.742	-0.237	0.8474
	M80	-0.223	0.53	-0.183	0.6036
	M100	-0.182	0.411	-0.149	0.4738
	M100	-0.182	0.411	-0.149	0.4738
PMSL01-1B	NRM	7	-17.6	-26.4	32.54
	M5	5.47	-12.42	-19.68	23.9
	M10	1.26	-3.01	-7.24	7.944
	M15	-0.33	0.33	-2.73	2.77
	M20	-0.525	1.05	-1.683	2.052
	M25	-0.446	1.148	-1.219	1.733
	M30	-0.444	1.081	-0.985	1.529
	M40	-0.344	0.853	-0.653	1.128
	M60	-0.174	0.592	-0.362	0.7151
	M80	-0.167	0.39	-0.208	0.4727
	M100	-0.065	0.362	-0.202	0.4198
	M100	-0.065	0.362	-0.202	0.4198
PMKR11-9A	NRM	-4.05	1.58	-4.08	5.957
	M5	-3.95	1.82	-4.51	6.269
	M10	-3.8	1.91	-4.49	6.178
	M15	-3.54	1.74	-4.3	5.834
	M20	-3.32	1.79	-4.1	5.571
	M25	-3.2	1.76	-3.94	5.372
	M30	-3.11	1.65	-3.78	5.164
	M40	-2.81	1.6	-3.48	4.752
	M60	-2.38	1.53	-3.04	4.148
	M80	-1.9	1.43	-2.56	3.492
	M100	-1.62	1.27	-2.19	3.006
	M100	-1.62	1.27	-2.19	3.006
PMKR11-5A	NRM	-2.5	-6.36	-0.63	6.864
	M5	-2.42	-6.87	-0.87	7.341
	M10	-1.89	-6.88	-0.7	7.175
	M15	-1.81	-6.69	-0.61	6.952
	M20	-1.43	-6.33	-0.49	6.504
	M25	-1.5	-6.11	-0.52	6.316
	M30	-1.65	-5.87	-0.49	6.12
	M40	-1.39	-5.48	-0.43	5.669
	M60	-1.06	-4.71	-0.27	4.832
	M80	-0.95	-3.97	-0.12	4.082
	M100	-0.91	-3.38	-0.07	3.497

	M100	-0.91	-3.38	-0.07	3.497
PMSL04-7A	NRM	-10.7	-29.3	6.5	31.81
	M5	-11.1	-29.7	6.3	32.32
	M10	-12.4	-29.3	6.3	32.41
	M15	-10.8	-26.9	6.3	31.54
	M20	-10.8	-26.9	6.3	29.61
	M25	-9.1	-24.6	6.1	26.93
	M30	-7.8	-21.6	5.7	23.63
	M40	-4.39	-14.77	4.34	16.01
	M60	-1.96	-6.4	1.74	6.914
	M80	-1.28	-3.28	0.36	4.5
	M100	-0.97	-1.603	-0.21	1.885
	M100	-0.97	-1.603	-0.21	1.885
PMSL04-1A	NRM	-1.18	-2.42	-2.63	3.768
	M5	-1.56	-2.5	-3	4.205
	M10	-1.69	-2.31	-2.86	4.046
	M15	-1.5	-2.09	-2.52	3.602
	M20	-1.41	-1.9	-2.23	3.252
	M25	-1.15	-1.74	-1.98	2.878
	M30	-1.129	-1.537	-1.77	2.602
	M40	-0.928	-1.297	-1.494	2.185
	M60	-0.689	-1.009	-1.159	1.684
	M80	-0.581	-0.83	-0.95	1.389
	M100	-0.47	-0.726	-0.819	1.191
	M100	-0.47	-0.726	-0.819	1.191
PMKR03-1A	NRM	-0.645	0.607	-0.338	0.948
	M5	-0.617	0.571	-0.371	0.9206
	M10	-0.529	0.511	-0.326	0.8046
	M15	-0.481	0.451	-0.286	0.7191
	M20	-0.398	0.401	-0.249	0.6176
	M25	-0.334	0.334	-0.222	0.5222
	M30	-0.276	0.27	-0.171	0.4218
	M40	-0.1772	0.179	-0.0127	0.2819
	M60	-0.1213	0.0882	-0.0877	0.1737
	M80	-0.0646	0.0327	-0.0558	0.09144
	M100	-0.0591	0.0039	0.0247	0.06423
	M100	-0.0591	0.0039	0.0247	0.06423
PMSH03-1A	NRM	0.05	-1.406	1.675	2.188
	M5	0.268	-1.427	0.94	1.73
	M10	0.172	-1.081	0.641	1.269
	M15	0.15	-0.86	0.509	1.01
	M20	0.112	-0.74	0.44	0.8678
	M25	0.166	-0.641	0.403	0.7751
	M30	0.123	-0.594	0.339	0.6948
	M40	0.136	-0.511	0.269	0.5934
	M60	0.066	-0.494	0.187	0.5322
	M80	0.079	-0.284	0.187	0.349
	M100	0.106	-0.248	0.153	0.3099
	M100	0.106	-0.248	0.153	0.3099
PMSH03-4A	NRM	-0.164	-1.941	1.553	2.491
	M5	0.212	-1.481	0.896	1.744
	M10	0.208	-1.094	0.643	1.286
	M15	0.148	-0.944	0.511	1.083
	M20	0.206	-0.762	0.443	0.9053
	M25	0.2	-0.702	0.379	0.8223
	M30	0.158	-0.628	0.345	0.7339
	M40	0.092	-0.512	0.295	0.5976
	M60	0.128	-0.41	0.157	0.4571
	M80	0.09	-0.319	0.144	0.3615
	M100	0.069	-0.268	0.138	0.3094
	M100	0.069	-0.268	0.138	0.3094
PMSL07-4A	NRM	-1.23	-5.96	-1.39	6.237
	M5	-0.94	-5.76	-1.4	6.007
	M10	-1.1	-5.45	-1.23	5.692
	M15	-0.99	-5.05	-1.06	5.249
	M20	-0.82	-4.65	-0.91	4.807
	M25	-0.67	-4.21	-0.74	4.332
	M30	-0.55	-3.87	-0.71	3.973
	M40	-0.42	-3.3	-0.53	3.37
	M60	-0.42	-2.55	-0.38	2.616
	M80	-0.294	-1.977	-0.353	2.029
	M100	-0.253	-1.709	-0.253	1.746
	M100	-0.253	-1.709	-0.253	1.746
PMSL07-9A	NRM	-1.98	-5.15	-2.07	5.898
	M5	-2	-5.05	-2.01	5.794
	M10	-1.69	-4.8	-1.82	5.404
	M15	-1.46	-4.45	-1.61	4.95
	M20	-1.42	-4.07	-1.41	4.536
	M25	-1.42	-3.7	-1.25	4.159
	M30	-1.09	-3.36	-1.11	3.703
	M40	-0.9	-2.88	-0.92	3.152
	M60	-0.68	-2.25	-0.7	2.452
	M80	-0.618	-1.84	-0.553	2.018
	M100	-0.484	-1.532	-0.421	1.66

	M100	-0.484	-1.532	-0.421	1.66
PMKR13-9A	NRM	-3.02	5.84	6.01	8.911
	M5	-1.98	5	5.22	7.493
	M10	-0.19	3.69	3.2	4.886
	M15	0.05	3.03	2.37	3.845
	M20	0.19	2.46	1.79	3.051
	M25	0.24	2	1.35	2.426
	M30	0.242	1.715	1.105	2.055
	M40	0.133	1.26	0.84	1.521
	M60	0.109	0.854	0.596	1.047
	M80	0.081	0.672	0.393	0.7824
	M100	0.088	0.559	0.338	0.6586
	M100	0.088	0.559	0.338	0.6586
PMKR13-11B	NRM	-13.2	50.3	60.4	79.69
	M5	-13	46.3	55.2	73.2
	M10	-11.1	35.9	40.2	55.02
	M15	-6.3	23	22.9	33.02
	M20	-2.74	12.54	10.61	16.66
	M25	-1.21	7.07	4.94	8.711
	M30	-0.52	4.43	2.81	5.273
	M40	-0.18	2.35	1.35	2.715
	M60	0.018	1.245	0.729	1.443
	M80	0.033	0.886	0.536	1.036
	M100	0.046	0.711	0.407	0.8203
	M100	0.046	0.711	0.407	0.8203
PMAF03-4A	NRM	-0.299	-1.602	0.19	1.64
	M5	-0.376	-1.51	0.189	1.568
	M10	-0.35	-1.576	0.191	1.625
	M15	-0.293	-1.541	0.191	1.58
	M20	-0.308	-1.511	0.199	1.555
	M25	-0.323	-1.461	0.19	1.508
	M30	-0.293	-1.416	0.209	1.461
	M40	-0.273	-1.315	0.21	1.359
	M60	-0.198	-1.111	0.197	1.146
	M80	-0.204	-0.954	0.187	0.9931
	M100	-0.152	-0.832	0.17	0.8625
	M100	-0.152	-0.832	0.17	0.8625
PMAF03-6A	NRM	-0.515	-1.531	0.398	1.664
	M5	-0.511	-1.548	0.377	1.673
	M10	-0.463	-1.521	0.386	1.636
	M15	-0.448	-1.5	0.38	1.611
	M20	-0.462	-1.465	0.391	1.585
	M25	-0.356	-1.429	0.37	1.519
	M30	-0.449	-1.368	0.371	1.487
	M40	-0.374	-1.27	0.367	1.373
	M60	-0.271	-1.107	0.319	1.183
	M80	-0.299	-0.969	0.283	1.052
	M100	-0.207	-0.84	0.261	0.904
	M100	-0.207	-0.84	0.261	0.904
PMKR14-8A	NRM	1.1	-7.57	-5.27	9.288
	M5	0.69	-6.98	-4.49	8.329
	M10	0.33	-5.89	-3.19	6.705
	M15	0.01	-5.19	-2.57	5.787
	M20	0.26	-4.64	-2.06	5.084
	M25	-0.12	-4.1	-1.66	4.43
	M30	-0.12	-3.69	-1.41	3.949
	M40	-0.19	-3.01	-0.93	3.157
	M60	-0.08	-2.06	-0.78	2.206
	M80	-0.066	-1.557	-0.667	1.695
	M100	0.044	-1.282	-0.539	1.392
	M100	0.044	-1.282	-0.539	1.392
PMKR14-5A	NRM	0.51	-7.8	-6.04	9.879
	M5	0.31	-7.28	-5.16	8.927
	M10	-0.63	-5.98	-3.66	7.041
	M15	-0.69	-5.21	-2.92	6.011
	M20	-0.57	-4.61	-2.32	5.196
	M25	-0.57	-3.99	-1.9	4.453
	M30	-0.53	-3.53	-1.54	3.886
	M40	-0.3	-2.7	-1.18	2.959
	M60	-0.307	-1.8	-0.698	1.955
	M80	-0.206	-1.305	-0.582	1.444
	M100	-0.171	-1.025	-0.439	1.128
	M100	-0.171	-1.025	-0.439	1.128
PMKR16-1A	NRM	-12.96	5.45	-16.39	21.59
	M5	-9.16	5.93	-10.59	15.21
	M10	-5.89	3.18	-6.09	9.052
	M15	-4.35	1.52	-4.15	6.201
	M20	-3.58	0.63	-3.11	4.78
	M25	-3.12	0.28	-2.45	3.982
	M30	-2.73	-0.11	-2.03	3.401
	M40	-2.25	-0.39	-1.5	2.729
	M60	-1.629	-0.639	-0.908	1.971
	M80	-1.365	-0.665	-0.62	1.639
	M100	-1.221	-0.761	-0.489	1.519

	M100	-1.221	-0.761	-0.489	1.519
PMSL03-8A	NRM	-1.615	-1.763	-0.725	2.499
	M5	-1.456	-1.775	-0.722	2.406
	M10	-1.49	-1.64	-0.677	2.317
	M15	-1.288	-1.579	-0.598	2.124
	M20	-1.225	-1.436	-0.508	1.954
	M25	-0.987	-1.292	-0.418	1.679
	M30	-0.892	-1.135	-0.335	1.428
	M40	-0.693	-0.883	-0.254	1.151
	M60	-0.499	-0.607	-0.207	0.8125
	M80	-0.375	-0.457	-0.189	0.6212
	M100	-0.36	-0.367	-0.179	0.5448
	M100	-0.36	-0.367	-0.179	0.5448
PMSL03-4A	NRM	-1.65	-2.59	-0.71	3.152
	M5	-1.51	-2.53	-0.68	3.028
	M10	-1.41	-2.49	-0.67	2.94
	M15	-1.38	-2.35	-0.59	2.784
	M20	-1.26	-2.25	-0.53	2.633
	M25	-1.15	-2.03	-0.43	2.375
	M30	-0.991	-1.849	-0.354	2.127
	M40	-0.756	-1.574	-0.266	1.766
	M60	-0.56	-1.081	-0.192	1.233
	M80	-0.441	-0.813	-0.191	0.9442
	M100	-0.407	-0.646	-0.158	0.7796
	M100	-0.407	-0.646	-0.158	0.7796
PMKR15-7A	NRM	-33.2	15.1	-21.7	42.41
	M5	-18.37	12.48	-11.79	25.14
	M10	-4.01	5.43	-0.51	6.765
	M15	-1.25	2.82	2.13	3.749
	M20	-0.3	1.67	2.93	3.39
	M25	0.06	1.12	3.1	3.292
	M30	0.25	0.84	3.12	3.241
	M40	0.33	0.49	2.96	3.024
	M60	0.36	0.29	2.51	2.548
	M80	0.33	0.11	2.09	2.117
	M100	0.344	0	1.763	1.797
	M100	0.344	0	1.763	1.797
PMKR15-4A	NRM	-1.31	4.59	2.68	5.47
	M5	0.81	3.21	5.43	6.363
	M10	1.73	1.86	6.6	7.07
	M15	1.89	1.33	6.49	6.887
	M20	1.74	1.15	6.21	6.551
	M25	1.67	0.97	5.89	6.203
	M30	1.57	0.86	5.64	5.92
	M40	1.48	0.79	5.14	5.403
	M60	1.32	0.6	4.43	4.661
	M80	1.15	0.43	3.86	4.045
	M100	1	0.3	3.29	3.455
	M100	1	0.3	3.29	3.455
PMAF02-4A	NRM	-0.1	-9.5	-26.4	28.04
	M5	-0.3	-9.6	-23.6	25.53
	M10	-0.68	-8.76	-15.13	17.49
	M15	-0.48	-6.62	-6.17	9.057
	M20	-0.3	-5.1	-1.25	5.263
	M25	-0.22	-4.06	0.64	4.118
	M30	-0.15	-3.4	1.17	3.597
	M40	-0.03	-2.42	1.23	2.715
	M60	-0.064	-1.437	0.874	1.683
	M80	-0.088	-1.02	0.63	1.202
	M100	-0.002	-0.734	0.518	0.9894
	M100	-0.002	-0.734	0.518	0.9894
PMAF02-7A	NRM	-79.1	-107.5	62.4	147.3
	M5	-80.9	-104.3	67.5	148.3
	M10	-68.9	-98.5	76.2	142.3
	M15	-50.9	-85.7	71.4	122.6
	M20	-33.2	-70.6	58.7	97.62
	M25	-26.5	-56.5	45.9	77.51
	M30	-16	-45.1	35.2	59.4
	M40	-9.5	-28.7	21.6	37.1
	M60	-2.55	-13.03	8.55	15.8
	M80	-0.83	-6.36	4.11	7.615
	M100	-0.46	-3.64	2.12	4.236
	M100	-0.46	-3.64	2.12	4.236
PMSL02-7A	NRM	-5.5	20.2	13.5	24.9
	M5	-10.28	7.71	-0.73	12.87
	M10	-6.46	-3.06	-5.2	8.84
	M15	-3.75	-3.9	-3.13	6.252
	M20	-2.8	-3.51	-2.22	5.008
	M25	-2.34	-3.17	-1.65	4.274
	M30	-2.09	-2.92	-1.37	3.843
	M40	-1.43	-2.32	-0.98	2.894
	M60	-1.005	-1.739	-0.601	2.097
	M80	-0.704	-1.259	-0.37	1.489
	M100	-0.589	-1.051	-0.3	1.241

	M100	-0.589	-1.051	-0.3	1.241
PMSL02-4A	NRM	5.3	87.8	8.4	88.35
	M5	1.3	74.1	-5.3	74.26
	M10	-4	41.3	-11.5	43.06
	M15	-3.3	20.9	-8.4	22.83
	M20	-3.67	11.27	-6.1	13.33
	M25	-2.37	6.18	-4.56	8.044
	M30	-2.36	3.42	-3.39	5.365
	M40	-1.89	0.98	-2.2	3.066
	M60	-1.265	-0.342	-1.232	1.799
	M80	-0.97	-0.63	-0.759	1.383
	M100	-0.709	-0.615	-0.548	1.087
	M100	-0.709	-0.615	-0.548	1.087
PMSL06-1A	NRM	0.241	1.062	-0.387	1.156
	M5	0.189	1.056	-0.398	1.144
	M10	0.206	1.055	-0.392	1.144
	M15	0.188	1.04	-0.393	1.128
	M20	0.22	0.993	-0.382	1.086
	M25	0.151	0.937	-0.369	1.018
	M30	0.171	0.886	-0.346	0.9669
	M40	0.126	0.786	-0.32	0.8581
	M60	0.101	0.651	-0.272	0.7132
	M80	0.031	0.572	-0.262	0.6298
	M100	0.029	0.55	-0.235	0.599
	M100	0.029	0.55	-0.235	0.599
PMSL06-9A	NRM	0.385	0.914	1.148	1.517
	M5	0.383	0.917	1.147	1.518
	M10	0.352	0.903	1.148	1.502
	M15	0.35	0.885	1.124	1.473
	M20	0.322	0.861	1.098	1.432
	M25	0.289	0.843	1.041	1.37
	M30	0.292	0.795	0.974	1.291
	M40	0.239	0.672	0.847	1.108
	M60	0.162	0.489	0.611	0.7997
	M80	0.131	0.333	0.413	0.5467
	M100	0.095	0.231	0.269	0.3668
	M100	0.095	0.231	0.269	0.3668
PMAF01-1A	NRM	75.6	22.6	-26.3	83.15
	M5	71.3	21.3	-33.9	81.81
	M10	55.5	22	-44.2	74.3
	M15	33.3	24.2	-38.8	56.56
	M20	19.1	22.6	-27.2	40.18
	M25	9.15	18.29	-17.09	26.65
	M30	4.19	14.28	-10.6	18.27
	M40	0.71	9.7	-4.92	10.9
	M60	-0.53	5.96	-2.13	6.354
	M80	-0.44	4.39	-1.47	4.647
	M100	-0.43	3.47	-1.08	3.664
	M100	-0.43	3.47	-1.08	3.664
PMSH02-4A	NRM	-2.06	-1.1	7.11	7.487
	M5	-1.19	-0.78	6.13	6.295
	M10	-0.7	-0.47	5.43	5.495
	M15	-0.48	-0.43	4.75	4.794
	M20	-0.38	-0.56	4.02	4.075
	M25	-0.25	-0.5	3.33	3.374
	M30	-0.21	-0.45	2.66	2.706
	M40	-0.144	-0.432	1.912	1.966
	M60	-0.009	-0.319	1.237	1.277
	M80	-0.064	-0.224	0.872	0.9027
	M100	0.023	-0.221	0.847	0.8759
	M100	0.023	-0.221	0.847	0.8759
PMSH02-5A	NRM	-6.41	-7.22	6.21	11.48
	M5	-3.6	-5.78	5.75	8.91
	M10	-1.65	-3.96	5.11	6.673
	M15	-0.82	-2.95	4.46	5.412
	M20	-0.45	-2.34	3.9	4.572
	M25	-0.27	-1.97	3.27	3.825
	M30	-0.12	-1.7	2.7	3.195
	M40	-0.032	-1.238	1.926	2.29
	M60	0.012	-0.816	1.149	1.41
	M80	0.038	-0.598	0.942	1.117
	M100	0.008	-0.516	0.735	0.8978
	M100	0.008	-0.516	0.735	0.8978
PMKR12-4A	NRM	-5.4	-21.3	23.2	31.93
	M5	-4.6	-20.8	20.9	29.86
	M10	-3.69	-17.7	13.79	22.74
	M15	-3.06	-14.21	8.17	16.67
	M20	-2.22	-11.43	4.94	12.65
	M25	-2.05	-9.34	3.07	10.04
	M30	-1.38	-7.96	2.06	8.342
	M40	-1.58	-6.18	1.07	6.47
	M60	-0.91	-4.23	0.5	4.36
	M80	-0.7	-3.05	0.36	3.145
	M100	-0.46	-2.26	0.24	2.316

	M100	-0.46	-2.26	0.24	2.316
PMKR12-5A	NRM	0.3	-11	20.7	23.49
	M5	-0.71	-11.27	18.28	21.49
	M10	-0.93	-10.56	11.29	15.48
	M15	-0.96	-9.28	6.56	11.4
	M20	-1.31	-8.03	4.32	9.217
	M25	-1.27	-7.11	3.31	7.947
	M30	-1.35	-6.39	2.65	7.049
	M40	-1.12	-5.4	2.02	5.875
	M60	-0.77	-3.93	1.38	4.239
	M80	-0.49	-2.86	1.01	3.073
	M100	-0.39	-2.19	0.75	2.349
	M100	-0.39	-2.19	0.75	2.349
PMAF06-4A	NRM	0.053	-1.855	-0.937	2.079
	M5	-0.1	-1.965	-0.491	2.028
	M10	-0.108	-1.988	-0.27	2.009
	M15	-0.097	-1.863	-0.18	1.874
	M20	-0.059	-1.696	-0.139	1.702
	M25	-0.04	-1.532	-0.102	1.536
	M30	-0.048	-1.408	-0.097	1.413
	M40	-0.067	-1.235	-0.073	1.239
	M60	-0.01	-0.974	-0.055	0.9756
	M80	-0.042	-0.849	-0.041	0.8511
	M100	-0.046	-0.742	-0.033	0.7446
	M100	-0.046	-0.742	-0.033	0.7446
PMAF06-5A	NRM	0.301	-1.886	-1.009	2.16
	M5	0.23	-2.01	-0.48	2.076
	M10	0.26	-2.06	-0.21	2.085
	M15	0.201	-1.928	-0.128	1.942
	M20	0.19	-1.779	-0.083	1.791
	M25	0.131	-1.629	-0.064	1.636
	M30	0.1	-1.507	-0.039	1.511
	M40	0.112	-1.299	-0.027	1.304
	M60	0.087	-1.054	-0.016	1.057
	M80	0.099	-0.899	-0.009	0.9049
	M100	0.079	-0.776	-0.002	0.7797
	M100	0.079	-0.776	-0.002	0.7797
PMKR10-5A	NRM	-3.62	-5.04	4.12	7.446
	M5	-2.53	-4.32	2.64	5.66
	M10	-1.5	-2.42	0.29	2.858
	M15	-1.233	-1.325	-0.513	1.882
	M20	-1.031	-0.894	-0.756	1.56
	M25	-0.84	-0.627	-0.826	1.334
	M30	-0.727	-0.454	-0.793	1.167
	M40	-0.544	-0.265	-0.712	0.934
	M60	-0.372	-0.093	-0.519	0.6453
	M80	-0.299	-0.048	-0.397	0.4995
	M100	-0.225	-0.04	-0.352	0.4196
	M100	-0.225	-0.04	-0.352	0.4196
PMKR18-9A	NRM	8.7	-27.9	17.5	34.05
	M5	3.1	-18.2	20.2	27.34
	M10	-3.85	-5.24	8.89	11.01
	M15	-4.55	0.41	3.52	5.77
	M20	-4.39	2.22	1.61	5.174
	M25	-3.88	2.73	0.63	4.789
	M30	-3.69	3.01	0.11	4.76
	M40	-2.79	2.59	-0.22	3.813
	M60	-2.02	2.15	-0.37	2.97
	M80	-1.461	1.511	-0.31	2.124
	M100	-1.25	1.211	-0.275	1.762
	M100	-1.25	1.211	-0.275	1.762
PMSL05-7A	NRM	4.33	7.34	8.44	12
	M5	3.76	7.1	8.4	11.62
	M10	3.51	6.84	7.65	10.85
	M15	3.15	6.41	6.85	9.894
	M20	3	6.11	6.3	9.275
	M25	2.66	5.76	5.87	8.642
	M30	2.54	5.42	5.51	8.138
	M40	2.51	4.89	4.96	7.403
	M60	1.88	4.03	4.11	6.06
	M80	1.75	3.45	3.45	5.181
	M100	1.47	2.97	2.94	4.429
	M100	1.47	2.97	2.94	4.429
PMSL05-1A	NRM	-0.34	8.11	-15.99	17.93
	M5	-0.86	7.98	-15.94	17.85
	M10	-1.11	7.73	-15.29	17.17
	M15	-1.26	7.34	-14.64	16.43
	M20	-1	6.92	-14.12	15.76
	M25	-0.88	6.74	-13.51	15.12
	M30	-0.89	6.55	-13.12	14.69
	M40	-0.68	6.04	-12.26	13.69
	M60	-0.73	5.77	-10.61	12.1
	M80	-0.65	5.1	-9.24	10.57
	M100	-0.68	4.43	-8.25	9.387

	M100	-0.68	4.43	-8.25	9.387
PMKR17-3A	NRM	-41.1	41.9	-31.3	66.5
	M5	-27.8	30.4	-23.7	47.6
	M10	-13.79	16.89	-13.61	25.71
	M15	-7.05	9.13	-8.12	14.11
	M20	-4.38	4.97	-4.99	8.297
	M25	-2.87	3.03	-3.39	5.372
	M30	-1.94	1.49	-2.27	3.339
	M40	-1.184	0.296	-1.226	1.73
	M60	-0.665	-0.356	-0.515	0.9132
	M80	-0.516	-0.547	-0.285	0.8039
	M100	-0.415	-0.551	-0.284	0.7458
	M100	-0.415	-0.551	-0.284	0.7458
PMKR05-7A	NRM	-1.02	3.52	-2.73	4.567
	M5	-0.96	3.45	-2.87	4.593
	M10	-0.79	3.32	-2.71	4.357
	M15	-0.79	3.06	-2.44	3.991
	M20	-0.62	2.75	-2.13	3.533
	M25	-0.52	2.41	-1.87	3.096
	M30	-0.39	2.13	-1.63	2.706
	M40	-0.428	1.707	-1.275	2.173
	M60	-0.273	1.201	-0.903	1.527
	M80	-0.205	0.911	-0.69	1.161
	M100	-0.147	0.733	-0.552	0.9298
	M100	-0.147	0.733	-0.552	0.9298
PMKR06-1A	NRM	-0.19	4.89	1.55	5.132
	M5	-0.76	4.63	0.68	4.746
	M10	-1.15	4.62	-0.36	4.775
	M15	-1.24	4.56	-0.62	4.761
	M20	-0.99	4.36	-0.67	4.524
	M25	-1.04	4.08	-0.73	4.273
	M30	-0.88	3.84	-0.68	4.002
	M40	-0.66	3.4	-0.63	3.524
	M60	-0.54	2.73	-0.56	2.836
	M80	-0.41	2.27	-0.51	2.359
	M100	-0.322	1.948	-0.457	2.027
	M100	-0.322	1.948	-0.457	2.027
PMSH01-7A	NRM	2.9	-31.5	-61.3	69.03
	M5	5	-29	-55.9	63.14
	M10	2.4	-17.4	-34.2	38.46
	M15	1.52	-8.69	-16.78	18.96
	M20	0.8	-4.03	-7.58	8.624
	M25	0.05	-2.26	-3.65	4.289
	M30	0.173	-1.383	-1.713	2.208
	M40	0.064	-0.659	-0.211	0.6954
	M60	-0.001	-0.268	0.451	0.5246
	M80	0.077	-0.024	0.453	0.4599
	M100	-0.007	-0.028	0.45	0.4506
	M100	-0.007	-0.028	0.45	0.4506
PMSH01-10A	NRM	-1.15	0.89	7.18	7.329
	M5	-1.12	0.34	6.65	6.752
	M10	-0.99	0.11	5.8	5.886
	M15	-0.85	-0.04	5.01	5.083
	M20	-0.83	-0.07	4.45	4.53
	M25	-0.7	-0.1	4.07	4.128
	M30	-0.65	-0.05	3.71	3.768
	M40	-0.58	-0.03	3.24	3.293
	M60	-0.46	-0.02	2.47	2.516
	M80	-0.399	-0.001	1.892	1.934
	M100	-0.284	0.041	1.514	1.541
	M100	-0.284	0.041	1.514	1.541
PMKR02-2A	NRM	-3.81	-1.82	-2.47	4.89
	M5	-3.22	-1.75	-1.97	4.158
	M10	-1.73	-2.23	-0.21	2.829
	M15	-0.67	-2.68	1.05	2.959
	M20	-0.33	-2.91	1.58	3.328
	M25	-0.11	-2.94	1.84	3.473
	M30	-0.02	-2.95	1.89	3.504
	M40	0.11	-2.71	1.8	3.258
	M60	0.12	-2.16	1.47	2.615
	M80	0.139	-1.733	1.217	2.122
	M100	0.081	-1.492	1.012	1.804
	M100	0.081	-1.492	1.012	1.804
PMKR02-8A	NRM	-2.85	1.78	-1.42	3.646
	M5	-2.53	1.42	-1.36	3.205
	M10	-1.615	0.451	-0.708	1.821
	M15	-0.9	-0.349	-0.101	0.9703
	M20	-0.589	-0.844	0.249	1.059
	M25	-0.426	-1.043	0.422	1.203
	M30	-0.295	-1.155	0.515	1.298
	M40	-0.232	-1.156	0.55	1.301
	M60	-0.153	-1.008	0.48	1.127
	M80	-0.132	-0.859	0.424	0.9674
	M100	-0.149	-0.757	0.383	0.8611

	M100	-0.149	-0.757	0.383	0.8611
PMKR04-4A	NRM	-2.02	-6.93	14.05	15.8
	M5	-2.4	-1.46	6.26	6.856
	M10	-2.54	1.36	2.86	4.059
	M15	-2.18	1.83	2	3.475
	M20	-2.04	1.87	1.62	3.211
	M25	-1.823	1.736	1.373	2.867
	M30	-1.51	1.605	1.157	2.577
	M40	-1.225	1.384	0.934	2.069
	M60	-0.91	0.962	0.628	1.465
	M80	-0.72	0.777	0.436	1.145
	M100	-0.504	0.654	0.309	0.8815
	M100	-0.504	0.654	0.309	0.8815

Acknowledgment

I am very much grateful to my advisor, Dr. Tesfaye Kidane, for a clear and precise training in the field sampling and sample treatment and data analysis back in the laboratory and for his continuous support via out the study. I also thank the Department of Earth Sciences, especially Dr. Balemwal Atnafu, for letting me use the facility of paleomagnetic laboratory for free.

I am also grateful to Dr. Julie Rowland for allowing me to take part in the Afar field excursion and use the paleomagnetic data for this study. Likewise, I thank everybody in the field excursion, especially, David, Charlotte and Katherine.

I would like to thank Dr. Bekele Abebe, Dr. Mulugeta Alene, Dr. Abera Alemu, Dr. Gezhagne Yirgu, Dr. Tilahun Mamo and Ato Beniam for providing the necessary materials for this study. Eden, Roman, Aynalem and Worku are also greatly acknowledged. Many thanks to Ato Wolde; for helping us in the field sampling and thin section preparation.

I wish to thank colleagues and friends from Geological Survey of Ethiopia, Ato Bayessa, Dr. Meseret, Tesfaye, Bereket, Getachew, Leta, Matebe, Samuel and especial acknowledgment goes to (Yohannes) Jhon and Dr. Jiri Sima, thanks for everything.

Anteneh, Aymiro, Esayas, Tenbit, Betseha, Elisa, Azeb, Asalfew; thank you guys, your help and encouragement is so much appreciated.

I am very much grateful to my family; Dad, Mom, Hiwot, Merima, Emu and Etu.

Finally, I would like to say thank you to Shalom; thank you very much for being there for me whenever I need you.

References

Acocella, V., Abebe, B., Korme, T. & Barberi, F. (2008). Structure of the Tendaho Graben and Manda Hararo rift: Implication for the evolution of the southern Red Sea propagator in the central Afar. *Tectonics,* **27**, doi: 10.1029/2007TC002236.

Acton, G.D. & S. Stein (1991). Block rotation and continental extension in Afar: a comparison to oceanic microplate systems. *Tectonics,* **10**, 501–526.

Acton, G., Tessema, A., Jackson, M. & Bilham, R. (2000). The tectonic and geomagnetic significance of paleomagnetic observations from volcanic rocks from central Afar: *Earth and Planetary Science Letters*, **180**, 225–241.

Almond, D.C. (1986). Geological evolution of the Afro-Arabian dome. *Tectonophysics* **331**, 302–333.

Aquater S.P.A. (1979). Geothermal resource exploration project, Tendaho Area, Prefeasibility study.

Audin, L., X. Quidelleur, E. Coulie, V. Courtillot, S. Gilder, I. Manighetti, P.Y. Gillot, P. Tapponnier and T. Kidane (2004). Paleomagnetism and K-Ar and 40Ar/39Ar ages in Ali Sabieh area (Republic of Djibouti and Ethiopia): Constraints on the mechanism of Aden ridge propagation into south eastern Afar during the last 10Myr. *Geophysical Journal International*, **158**, 327-345.

Baker, J., Snee, L., & Menzies, M., (1996). A brief Oligocene period of flood volcanism in Yemen, *Earth and Planetary Science Letters*, **138**, 39–49.

Barberi, F. & Varet, J., (1970). The Erta `Ale volcanic range. *Bulletin Volcanologique*, **34**, 848- 917.

Barberi, F. Barberi, E. Bonati, G. Marinelli and J. Varet. (1974) Transverse tectonic during the split of continent: Data from the Afar rift. *Tectonophysics* **23**, 17–19.

Barberi, F., G. Ferrara, R. Santacroce, M. Treuil & J. Varet, (1975). A transitional basalt-pantellerite sequence of fractional crystallization, the Boina centre (Afar rift, Ethiopia). *Journal of Petrology,* **16**, 22–56.

Bayer, R., Shabanian, E., Rgard, V., Doerfilnger, E., Abbassi, M., Chery, J., Niforoushan, F., Tatar, M., Vernant, P. & Bellier, O. (2003). Active deformation in the Zagros-Marakn transition zone from GPS measurements in the interval 2000-2002. *Geophysical Research Abstract*, **5**, 0589.

Berhe, S.M., B. Desta, M. Nicoletti and M. Teferra. (1987). Geology, geochronology and geodynamic implications of Cenozoic magmatic province in W and SE Ethiopia. *Journal of Geological Society of London,* **144**, 213–226.

Berhe, S.M. (1990) Ophiolites in northeast and east Africa: implication for Proterozoic crustal growth. *Journal of Geological Society London,* **147**, 41–57.

Besse, J. & Courtillot, V. (1991). Revised and synthetic apparent polar wander paths of the African, Eurasian, North American and Indian plates, and a true polar wander since 200Ma. *Journal Geophysical Research,* **96**, 4029-4050.

Beyene, A. & Abdelsalam, M. (2005). Tectonics of the Afar Depression: A review and synthesis. *Journal of African Earth Science*, **41**, 41-59.

Bilham, R., Bendick, R., Larson, K., Braun, J., Tesfaye, S., Mohr, P., & Asfaw, L., (1999), Secular and tidal strain across the Ethiopian rift. *Geophysical Research Letters*, **27**, 2789–2984.

Black, W.H., R. Black, W.H. Morton & T. Hailu (1974). Early structure around the Afar triple junction. *Nature,* **248**, 496–497.

Bohannon, R., Naeser, C., Schmidt, D., & Zimmermann, R., (1989). The timing of uplift, volcanism and rifting peripheral to the Red Sea: A case for passive rifting: *Journal of Geophysical Research*, **94**, 1683–1701.

Butler, R.F. (1992). Paleomagnetisum: magnetic domains to geologic terrains. *Oxford, Blackwell scientific publications*, Ltd., 319p.

Cande, S.C. & Kent, D.V. (1995). Revised caliberation of the geomagnetic polarity time scale for the late cretaceous and Cenozoic. *Journal of geophysical Research,* **100**, 6093-6095.

Chadima, M. & Hrouda, F. (2009). Remasoft, paleomagnetic data browser and analyzer for windows. Version **3.0**. *AGICO Inc*. (www.agico.com).

Chazot, G. & Bertrand, H. (1993). Mantle sources and magma controlled crust interactions during early Red Sea-Gulf of Aden rifting in southern Yemen; elemental and Sr, Nd, Pb isotope evidence. *Journal of Geophysical Research*, **98**, 1819-1835.

Chessex, R., Delaloye, M., Muller, J. & Weidmann, M. (1975). Evolution of the volcanic region of Ali Sabeh, in light of the K/Ar age determination in Afar depression of Ethiopia, In: A.Pilger and A. Rosler, (eds), *Afar Depression of Ethiopia proceedings of an international symposium on the Afar region and rift related problems*, Schweizerbart, Stuttgart, **1** .221-227.

Christiansen, T.B., H.-U. Schaefer & M. Schoenfeld, (1975). Geology of southern and central Afar, Ethiopia. In: A. Pilger and A. Rosler, (eds), *Afar depression of Ethiopia, proceedings of*

an international symposium on the Afar region and rift related problems, Bad Bergzabren, Germany, **1**, E. Schweizerbart'sche Verlagsbuchhandlung, Stuttgart, Germany, pp. 259–277.

Chu, D. & Gordon, R.G. (1998). Current plate motions across the Red Sea. *Geophysical Journal International*, **135**, 313–328.

Civetta, L., M. DeFino, P. Gasparini, M.R. Ghiara, L. LaVolpe & L. Lirer (1974). Geology of central-eastern Afar (Ethiopia). In: A. Pilger and A. Rosler, (eds), *Afar depression of Ethiopia, proceedings of an international symposium on the Afar region and rift related problems.* Bad Bergzabren, Germany, E. Schweizerbart'sche Verlagsbuchhandlung, Stuttgart, F.R. Germany, **1**, 259–277.

CNR - CNRS Afar team, (1973). Geology of northern Afar (Ethiopia). *Revue de Geographie Physique et de Geologie Dynamique*, **15**, 443- 490.

Cogne, J.P. (2003). Paleomac, a mackintosh application for treating paleomagnetic data and making plate reconstructions. *Geochemistry, Geophysices, Geosystem*, **4**,1007, doi:101029/2001GC000227.

Collet, B., H. Taud, J.F. Parrot, F. Bonavia & J. Chorowicz, (2000). New kinematic approaches for the Danakil block using a Digital Elevation Model representation. *Tectonophysics*, **316**, 343–357.

Courtillot, V. (1982). Propagating rifts and continental break up. *Tectonics*, **1**, 239-250.

Courtillot, V., Achache, J., Landre, F., Bonhommet, N., Montigny, R. & Feraud, G., (1984). Episodic spreading and rift propagation – new Paleomagnetic and geochronological data from the Afar nascent passive margin. *Journal of geophysical Research*, **89**, 3315–3333.

Courtillot, V., R. Armijo, & P. Tapponnier (1987). Kinematics of the Sinai Triple Junction and a two-phase model of Arabia-Africa rifting. In: M. P. Coward, J. F. Dewey, and P. L. Hancock , (eds), 1987. *Continental Extensional Tectonics*, Geological Society of London. Special Publication, **28**, 559– 573.

Crane, K & Bonatti, E. (1987). The role of fracture zones during early Red Sea rifting. Structural analysis using space shuttle radar and Landsat imagery, *Journal of the Geological Society London*, **144,** 407–420.

Dauteuil, O., P. Huchon, F. Quemeneur & T. Souriot, (2001). Propagation of an oblique spreading center; the western Gulf of Aden. *Tectonophysics*, **332**, 423–442.

Debayle, E., Léveque, J.-J., & Cara, M., (2001). Seismic evidence for a deeply rooted low-velocity anomaly in the upper mantle beneath the northeastern Afro-Arabian continent. *Earth and Planetary Science Letters*. **193**, 423–436.

Daniel, C., Vidal, P., Coulon, C., & Vellutini, P.J. & Piguet, P. (1994). Temporal evolution of mantle sources during continental rifting—the volcanism of Djibouti (Afar): *Journal of Geophysical Research*, **99**, 2853–2869.

Dunlop, D. & Ozdemir, O. (1997). Rock magnetism: Fundamentals and frontiers. *Cambridge university press*, 573pp.

Eagles, G., Gloaguen, R. & Ebinger, C., (2002). A model for the creation of a microplate: kinematics of the Danakil microplate. *Earth and planetary Science Letters*, **203**, 607–620.

Ebinger, C.J., Yemane, T., WoldeGabriel, G., Aronson, J.L.& WalterR.C., (1993). Late Eocene–Recent volcanism and faulting in the southern main Ethiopian rift. *Journal of Geological Society of London*, **150**, 99–108.

Ebinger, C. J., & N. J. Hayward (1996), Soft plates and hot spots: Views from Afar. *Journal of Geophysical Research*, **101**, 21,859– 21, 876.

Ebinger, C. & Sleep, N. (1998). Cenozoic magmatism throughout East Africa resulting from impact of a single plume: *Nature*, **395**, pp. 788.

Fischer, R.A. (1953). Dispersion on sphere. *Proceedings of the Royal society of London series A*, **217**, 295-305.

Furman, T., Bryce, J.G., Karson, J. & Iotti, A. (2004). East Africa Rift System (EARS) plume structure: insights from Quaternary mafic lavas of Turkana, Kenya. *Journal of Petrology*, **45**, 1069-1088.

Furman, T., Bryce, J., Rooney, T., Hanan, B., Yirgu, G. & Ayalew, D., (2006). Heads and tails: 30 million years of the Afar plume. In: Yirgu, G., Ebinger, C.J.& Maguire, P.K.H.(eds) 2006. *The Afar Volcanic Province within the East African Rift System*. Geological Society of London. Special Publication. **259**, 95–119.

Gass, I.G. (1970). The evolution of volcanism in the junction area of the Red Sea, Gulf Aden and Ethiopian Rifts. *Philosophical Transactions Royal Society of London*, **267**, 369–381.

George, R., Rogers, N., Kelley, S., (1998). Earliest magmatism in Ethiopia: Evidence for two mantle plumes in one flood basalt province: *Geology*, **26**, 923–926.

Halls, H.C. (1976). A least square method to find a remenance direction from converging remagnetization circles. *Geophysical Journal of Royal Astronomical society*, **45**, 297-304.

Halls, H.C. (1978). The use of converging remagnetization circles in paleomagnetisum. *Physics of the earth and planetary interiors*, **16**, 1-11.

Hart, W., WoldeGabriel, G., Walter, R., & Mertzman, S., (1989). Basaltic volcanism in Ethiopia: Constraints on continental rifting and mantle interactions: *Journal of Geophysical Research*, **94**, 7731–7748.

Hayward, N.J. (1997). A quantitative comparison of oceanic and continental rift segmentation. Unpublished *PhD thesis*, University of Leeds, United Kingdom.

Hempton, M.R. (1987). Constraints on Arabian Plate motion and extensional history of the Red Sea. *Tectonics*, **6**, 687–705.

Hofman, C., Courtillot, V., Feraud, G., Rochette, P., Yirgu, G., Ketefo, E.& Pik, R., (1997). Timing of the Ethiopian flood basalt event and implications for plume birth and global change. *Nature*, **389**(6653), 838–841.

Holt, J.W., J.L. Kirschvink and F. Garner (1996). Geomagnetic field inclinations for the past 400kyr from the 1km core of Hawaii Scientific Drilling Project. *Journal Geophysical Research*, 101, 11,655-11,664.

Joffe, S. & Garfunkel, Z., (1987). Plate kinematics of the circum Red Sea—a re-evaluation, *Tectonophysics*, **141**, 5–22.

Kazmin V.G. &. Byakov, A.F (2000). Magmatism and crustal accretion in continental rifts.*Journal of African Earth Sciences*, **30**, 555–568.

Kidane, T., Carlut, J., Courtillot, V., Gallet, Y., Quidelleur, X., Gillot, P.Y. & Haile, T. (1999). Paleomagnetic and geochronological identification of the Reunion subchron in Ethiopian Afar. *Journal of Geophysical Research*, **104**, 10405-10419.

Kidane, T., V. Courtillot, I. Manighetti, L. Audin, P. Lahitte, X. Quidelleur, P.-Y. Gillot, Y. Gallet, J. Carlut & T. Haile, (2003). New paleomagnetic and geochronologic results from Ethiopian Afar: Block rotations linked to rift overlap and propagation and determination of 2 Ma reference pole for stable Africa. *Journal of Geophysical Research*, **108**, 1–32.

Kieffer, B., & Arndt. N. (2004). Flood and shield basalts from Ethiopia: Magmas from the African Superswell, *Journal of Petrology*. **45**, 793-834.

Kirschvink, J.L. (1980). The least square line and plane and the analysis of paleomagnetic data. *Geophysical Journal of the Royal Astronomical Society*, **62**, 699-718.

Lahitte, P., Gillot, P.-Y.& Courtillot, V., (2003). Silicic central volcanoes as precursors to rift propagation: the Afar case. *Earth and Planetary Science Letters*, **207**, 103–116.

Langeries, C., Dekkers, M.J., De Lange, G.J., Paterne, M. and Van Santvoort P.J.M. (1997). Mangetostratigraphy & astronomical calibration of the last 1.1Myr from an eastern

Mediterranean piston core and dating of short events in Brunhes. *Geophysical Journal International*, **129**: 75-94.

Le Pichon, X. & J. Francheteau, (1978). A plate-tectonic analysis of the Red Sea–Gulf of Aden area. *Tectonophysics*, **46**, 369–406.

Lund, S.P., Acton, G., Hastedt, M & Wlliams, T. (1998). Geomagnetic field excursions occurred often during the last million years. *EOS*, **79(14)**, 178-179.

Makris, J., & A. Ginzburg (1987). The Afar Depression: Transition between continental rifting and sea-floor spreading. *Tectonophysics*, **141**, 199– 214.

Manighetti, I., P. Tapponnier, V. Courtillot, S. Gruszow, & P.-Y. Gillot, (1997). Propagation of rifting along the Arabia-Somalia plate boundary: The gulfs of Aden and Tadjoura, *Journal of Geophysical Research*, **102**, 2681– 2710.

Manighetti, I., P. Tapponnier, P.-Y. Gillot, E. Jacques, V. Courtillot, R. Armijo, J.-C. Ruegg, & G. King, (1998). Propagation of rifting along the Arabia-Somalia plate boundary: Into Afar, *Journal of Geophysical Research*, **103**, 4947–4974.

Manighetti, I., G. C. P. King, Y. Gaudemer, C. H. Scholtz, & C. Doubre, (2001a), Slip accumulation and lateral propagation of active normal faults in Afar. *Journal of Geophysical Research*, **106**, 13,667– 13,696.

Manighetti, I., P. Tapponnier, V. Courtillot, Y. Gallet, E. Jacques, & Y. Gillot, (2001b), Strain transfer between disconnected, propagating rifts in Afar. *Journal of Geophysical Research*, **106**, 13,613– 13,665.

McFadden, P.L., Merill, R.T., McElhinny, M.W. & Lee, S. (1991). Reversals of the earth's magnetic field and temporal variations of the dynamo families. *Journal of Geophysical Research*, **96**, 3923-3933.

Menzies, M.A., Baker, J., Bosence, D., Dart, C., Davison, I., Hurford, A., Al-kadasi, M., McClay, K., Nichols, G., Al-subbary, A. & Yalland, A. (1992). In: Storey, B.C., Alabaster, T. & Pankhrust, R.J. (eds), Magmatisum and causes of continental break up. *Geological Society special publications,* **68**, 293-304.

Mohr, P.A. (1975). Structural setting and evolution of Afar. In: A. Pilger and A. Rosler, (eds), *Afar depression of Ethiopia, proceedings of an international symposium on the Afar region and rift related problems*. Bad Bergzabren, Germany, **1**, E.Schweizerbart'sche Verlagsbuchhandlung, Stuttgart, Germany, pp. 27–37.

Morgan, W.J. (1970). Convection plumes in the lower mantle. *Nature*, **230**, 42-43.

Nowaczyk, N.R., Frederichs, T.W., Eisenhauer, A. & Gard, G. (1994). Magneto-stratigraphic data from late quaternary sediments from the yermak plateau, Arctic Ocean: evidence for four geomagnetic polarity events within the last 170ka of Brunhes chron. *Geophysical Journal International*, **117**: 453-471.

Nowaczyk, N.R. & Frederichs, T.W. (1999). Geomagnetic events and relative paleointensity variations during the past 300ka as recorded in Kolbeinsey ridge sediments, Iceland sea: indications for a strongly variable geomagnetic field. *International Journal Earth sciences*, **88**: 116-131.

Nyblade, A., Owens, T.J., Gurrola, H., Ritsema, J. & Langston, C.A. (2000). Seismic evidence for a deep upper mantle thermal anomaly beneath east Africa. *Geology*, **28**, 599-602.

Pik, R., Deniel, C., Coulon, C., Yirgu, G. & Marty, B. (1999). Isotopic and trace element signatures of Ethiopian flood basalts; evidence for plume-lithosphere interactions. *Geochimica et Cosmochimica Acta*, **63**, 2263-2279.

Rogers, N.W. (2006). Basaltic magmatism and the geodynamics of the East African Rift System. In: Yirgu, G., Ebinger, C.J. & Maguire, P.K.H. (eds) 2006. *The Afar Volcanic Province within the East African Rift System*. Geological Society of London, Special Pub. **259**, 77-94.

Rogers, N., Macdonald, R., Fitton, J.G., George, R., Smith, M. & Barreiro, B. (2000). Two mantle plumes beneath the East African rift system: Sr, Nd and Pb isotope evidence from Kenya rift basalts. *Earth and planetary science letters*, **176**, 387-400.

Rognon, P. (1975). Tectonic deformation in central Afar basins in the upper Pleistocene and Holocene periods, from the study of lacustrine deposits. In: A. Pilger and A. Rosler, (eds), 1975. *Afar depression of Ethiopia, proceedings of an international symposium on the Afar region and rift related proble.* Bad Bergzabren, Germany, **1**, E. Schweizerbart'sche Verlagsbuchhandlung, Stuttgart, Germany, pp. 198–200.

Rowland, J. V., E. Baker, C. J. Ebinger, D. Keir, T. Kidane, J. Biggs, N. Hayward & T. J. Wright, (2007). Fault growth at a nascent slow-spreading ridge: 2005 Dabbahu rifting episode, Afar. *Geophysical Journal International*, **171**, doi: 10.1111/j.1365-246X.2007.03584.x

Schilling, J. G. (1973), Afar mantle plume: Rare earth evidence. *Nature*, **242**, 2–5.

Schilling, J.-G., Kingsley, R., Hanan, B. & McCully, B. (1992). Nd-Sr-Os isotopic variations along the Gulf of Aden: evidence for mantle-plume lithosphere interaction. Journal of geophysical Research. **97**, 10927–10966.

Sengor, A.M.C. & Burke, K. (1978). Relative timing of rifting and volcanism on earth and its tectonic implications. *Geophysical Research Letters*, **5**, 419-421.

Sengor, A.M.C., (2001). Elevation as mantle plume activity. *Geological Society of America*, **352**, 183-225.

Sigmundsson, F., (1992). Tectonic implications of the 1989 Afar earthquake sequence, Geophysical Research Letters, **19**, 877–880.

Sigmundsson, F.,(2006). *Iceland Geodynamics: Crustal deformation and divergent plate tectonics.* Springer-Praxis, Chichester, U.K. p228.

Souriot T. & J.-P. Brun, (1992). Faulting and block rotation in the Afar triangle, East Africa: the Danakil crank-arm model. *Geology*, **20**, 911–924.

Stern, R.J. (1994). Arc assembly and continental collision in the Neoproterizoic East African Orogen—implication for the consolidation of Gondwanaland. *Annual Review Earth Planetary Science*, **22**, 319–351.

Sultan, M., R. Becker, R.E. Arvidson, P. Shore, R.J. Stern, Z. El Alfy and E.A. Guinness, (1992).Nature of the Red Sea crust: a controversy revisited. *Geology* **20**, 593–596.

Tapponnier, P., R. Armijo, I. Manighetti, & V. Courtillot (1990). Bookshelf faulting and horizontal block rotations between overlapping rift zones in southern Afar. *Geophysical Research Letters,* **17**, 1–4.

Tazieff, H. & J. Varet, (1972). Tectonic significance of the Afar (or Danakil) Depression. *Nature*, **235**, 144–147.

Tefera, M., Chernet, T., & Haro, W., (1996). Geological Map of Ethiopia. *Ethiopian Institute of Geological Surveys*. scale 1:2,000,000.

Tesfaye, S., Kusky, T.T. & Harding, D., (2003). Early Continental breakup boundary and migration of the Afar triple junction, Ethiopia. Geological Society of America Bulletin, **115**, 1053–1067.

Vail, J.R. (1985). Pan-African (late Precambrian) tectonic terranes and reconstruction of the Arabian–Nubian Shield. *Geology*, **13**, 839–842.

Varet, J. & Gasse, F. (1978). Geology of central and southern Afar (Ethiopia and Djibouti Republic): Paris, *Editions du centres National de la Recherché Scientifique,* report, 124p. Map, scale 1:500,000.

Vellutini, P. (1990) The Manda-Inakir Rift, Republic of Djibouti: a comparison with the Asal Rift and its geodynamic interpretation, *Tectonophysics* **172**, 141–153.

Vidal, P., Deniel, C., Vellutini, P.J., Piguet, P., Coulon, C., Vincent, J. & Audin, J. (1991). Changes of mantle sources in the course of a rift evolution: the Afar case. *Geophysical Research Letters*, **18**, 1913-1916.

Vigny, C., P. Huchon, J.C. Ruegg, K. Khanbari & L. Asfaw, (2006a). New GPS data in Yemen confirm slow Arabia plate motion. *Journal of Geophysical Research*, **111**,. B02402.

Vigny, C., P. Huchon, J.-C. Ruegg, K. Khanbari, & L. M. Asfaw (2006b). Confirmation of Arabia plate slow motion by new GPS data in Yemen. *Journal of Geophysical Research*, **111**, B02402.

Walker, K., Nyblade, A. A., Klemperer, S. L., Bokelmann, G. H. R. & Owens, T. J. (2003). On the relationship between extension and anisotropy: Constraints from shear wave splitting across the East Africa Plateau. *Journal of Geophysical Research*. **109**, doi: 10.1029/2003JB002866.

Weeraratne, D.S., Forsyth, D.W., Fisher, K.M. & Nyblade, A.A. (2003). Evidance for an upper mantle beneath the Tanzanian craton from Rayleigh wave tomography. *Journal of Geophysical Research*, 108.

White, R. & McKenzie, D. (1989). Magmatisum at rift zones: The generation of volcanic continental margins and flood basalts. *Journal of Geophysical Research*, **94**, 7685-7729.

Wright, T. J., Ebinger, C.J., Biggs, Ayele, A., Yirgu, G., Keir, D. & Stork, A. (2006). Magma-maintained rift segmentation at continental rupture in the 2005 Afar dyking episode, *Nature*, **442**, 291 – 294.

Yirgu, G., Ayele, A. & Ayalew, D. (2006a). Recent seismo-volcanic crisis in Northern Afar, Ethiopia, *Eos*, **87(33),** 325–336.

Yirgu, G., Ebinger, C.J., & Maguire, P.K.H. (2006b). The Afar volcanic province wthin the East African Rift System: introduction. In: Yirgu, G., Ebinger, C.J., & Maguire, P.K.H. (eds). The Afar Volcanic Province within the East African Rift System, *Geological Society of London, Special Publication*. **259**, 1-6.